HEMILARYNX PRESSURE DISTRIBUTIONS ACROSS GLOTTAL ANGLES AND
GLOTTAL DIAMETERS

Joshua L. Mewhinney

A Thesis

Submitted to the Graduate College of Bowling Green
State University in partial fulfillment of
the requirements for the degree of

MASTER OF SCIENCE

August 2016

Committee:

Lewis P. Fulcher, Advisor

Marco Nardone

Ronald C. Scherer

ABSTRACT

Lewis P. Fulcher, Advisor

Using the Plexiglas Model M5, a static hemilarynx condition was produced using vocal fold pieces housed within a wind tunnel to collect pressure distributions throughout the glottis under constant flow conditions. In order to make the hemilarynx condition, one vocal fold piece was always kept vertical within the glottis, while the other spanned three different glottal angles, one converging, one uniform, and one diverging. The variability of glottal diameter was also introduced and data was collected at 0.01, 0.04, and 0.16 cm diameters. Pressure distributions and flow rates for such configurations are of interest for the analysis of phonation in patients for whom one vocal fold has been immobilized.

Flow bistability was introduced at each of the glottal diameters for each glottal angle. Observations regarding the effect that flow bistability had on the pressure distributions showed that a bistable condition of flow produced noticeably less prominent changes in the pressure values intraglottally than the changes in pressures related to the asymmetric angles themselves. The flow bistability therefore created the greatest differences in larger diameter cases. From these pressure distributions, the data can be used in other multimass models to provide insight into the asymmetric forces that may occur within the larynx during phonation.

To my father Edward, mother Barbara, sister Kara, and late cousin Squid

ACKNOWLEDGMENTS

I would like to thank my advisor, Dr. Fulcher, Dr. Scherer, Dr. Nardone and the rest of the physics department at Bowling Green State University for their guidance throughout the entire masters program. Dr. Fulcher and Dr. Scherer's influence in the scope of this project allowed me to collect a great deal of data that hopefully will help the voice community. I would also like to thank Dr. Scherer for his guidance in the lab throughout the data collection process and his insight into the physiological processes of the vocal mechanisms. Everyone in Bowling Green welcomed me with open arms and helped me learn a great deal throughout my studies, as well as learn a great deal about myself.

TABLE OF CONTENTS

LIST OF FIGURES

LIST OF EQUATIONS

1.1 $\quad P + \frac{1}{2}\rho v^2 = constant$

1.2 $\quad R = P_g / v \ (dyne \ s/cm^5)$

1.3 $\quad P_s - P_{11} = 1.37 \ \frac{\rho}{2} \left(\frac{U_g}{A_{g1}} \right)^2 + \int_0^{l_c} \frac{\rho}{A_c(x)} \ \frac{dU_g}{dt} \ dx$

1.4 $\quad P_{11} - P_{12} = 12 \ \frac{\mu \ l_g^2 d_1}{A_{g1}^3} \ U_g + \rho \ \frac{d_1}{A_{g1}} \frac{dU_g}{dt}$

1.5 $\quad P_{12} - P_{21} = \frac{\rho}{2} (\frac{1}{A_{g2}^2} - \frac{1}{A_{g1}^2}) \ U_g^2$

1.6 $\quad P_{21} - P_{22} = 12 \frac{\mu \ l_g^2 d_2}{A_{g2}^3} U_g + \frac{\rho \ d_2}{A_{g2}} \frac{dU_g}{dt}$

1.7 $\quad P_{22} - P_1 = - \ \rho \ \frac{U_g^2}{A_{g2} A_1} (1 - \frac{A_{g2}}{A_1})$

1.8 $\quad A_{g1} = A_{g01} + 2 \ l_g \ x_1$

1.9 $\quad A_{g2} = A_{g02} + 2 \ l_g \ x_2$

1.10 $\quad P_s - P_{11} = 1.37 \frac{\rho}{2} \left(\frac{U_g}{A_{g1}} \right)^2$

1.11 $\quad P_{11} - P_{12} = 12 \frac{\mu \ l_g^2 d_1}{A_{g1}^3} \ U_g$

1.12 $\quad P_{12} - P_{21} = \frac{\rho}{2} (\frac{1}{A_{g2}^2} - \frac{1}{A_{g1}^2}) \ U_g^2$

1.13 $\quad P_{21} - P_{22} = 12 \frac{\mu \ l_g^2 d_2}{A_{g2}^3} U_g$

1.14 $\quad P_{22} - P_1 = - \rho \dfrac{U_g^2}{A_{g2} \, A_1}(1 - \dfrac{A_{g2}}{A_1})$

CHAPTER 1. VOCAL FOLD OSCILLATIONS WITHIN A HEMILARYNX CONDITION

1.1 Aerodynamic Forces and the Bernoulli Effect within the Larynx

Communication is fundamental to human existence. People communicate every day in order to complete tasks of all kinds. By taking advantage of the properties of sound, individuals are able to create as well as interpret acoustic signals. Speech and hearing are thus extremely beneficial and effective ways of communication. Speech includes sequencing of sounds both phonated (using the laryngeal sound source – vowels such as /a/ and /i/ and consonants such as /z/ and /v/) and unphonated (voiceless sounds such as /s/ and /f/ and whisper). What about those who have great difficulty in phonating during speech? Abnormal phonation can lead to significant quality of life issues for an individual. It is therefore of particular interest to understand both normal and abnormal phonation from a physical point of view, and to determine how to help individuals with voice concerns with this information.

Phonation begins with the process of setting the vocal folds are set into oscillation by sufficient transglottal pressure (generated from an air pressure increase in the lungs), and the resulting motion produces pulsatile airflow cycles above the glottis. The airflow cycles are responsible for creating the laryngeal acoustic sound source. This source (in time and in frequency content) excites and is modified by resonance characteristics of the respiratory airway and the supraglottal vocal tract. Of special interest in the current study are the intraglottal pressures that force the vocal folds into vibration and allow the continuation of the phonation cycles as determined by the vocal fold tissue characteristics. During the outward motion of the vocal folds, the glottis (the space between the vocal folds) has a convergent shape. A consequence of this shape is an intraglottal pressure above that of the vocal tract. This positive air pressure pushes the tissue of the vocal folds away from the midline. Due to the viscoelastic

properties of the vocal fold mucosa and muscle tissue, there are also medial forces acting inward (toward the midline) as the tissue is displaced (a recoil effect). After the vocal folds separate during the opening phase of the cycle, these forces will require that they move toward each other. The glottis typically takes on a divergent shape for this closing phase of the cycle. Recoil pulls the vocal folds back toward each other, and this motion is augmented by a negative intraglottal air pressure, created partly by a small Bernoulli effect and also by rarefaction in the supraglottal region. Self-sustaining oscillations result when the energy gained from the aerodynamic forces is balanced by the loss of energy due to the viscous forces in the tissue (Titze 1993).

The first attempt at modeling the aerodynamic forces present in the larynx was conducted by van den Berg (van den Berg *et al*. 1957). In an ideal case, the larynx is subject to Bernoulli's equation,

$$P + \frac{1}{2}\rho v^2 = constant, \tag{1.1}$$

where the sum of the static pressure P and the kinetic pressure $\frac{1}{2}\rho v^2$ is a constant at each separate region in a duct of moving fluid with changing cross sectional area. A diagram of the model van den Berg and colleagues created from a plaster cast of an excised human larynx is shown in **Figure 1.1**. Pressure taps were used to measure the pressures within the glottis (which had parallel sides), and past the glottis, using six pressure taps in all.

The subglottal pressure could be measured up to 64 centimeters of water (cm H_2O), while the volume velocities were simultaneously recorded up to a rate of 2 L/s. From the subglottal pressure and the volume velocity, the resistance of the glottis R can be determined from the equation,

$$R = P_s/v \; (dyne \; s/cm^5), \tag{1.2}$$
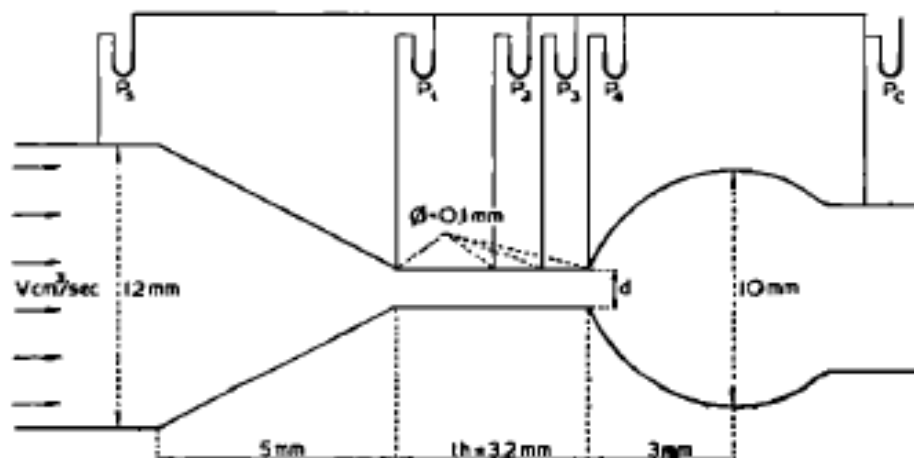
Figure 1.1 Diagram of the van den Berg *et al.* model used to study the pressures and flow resistance of the larynx. Dimensions of the model and locations of the pressure taps connected to manometers are shown (van den Berg *et al.* 1957).

where P_s is the subglottal pressure and v is the volume velocity. The total resistance could then be expressed as the sum of three different resistances experienced in the different geometrical regions of the model: subglottal $R_1 = (P_s - P_1)/v$, intraglottal $R_2 = (P_1 - P_4)/v$, and supraglottal $R_3 = P_4/v$ (van den Berg *et al.* 1957). van den Berg then used both the presumed resistance due to friction during laminar flow and the presumed resistance due to turbulent flow to account for corrections to the Bernoulli equation. The authors found that at smaller diameters and lower volume velocities, corrections to frictional losses dominated the resistive aspects, while at larger diameters and larger volume velocities, corrections due to a turbulent term were the primary resistive aspects of the model.

1.2 Ishizaka and Flanagan's Two Mass Model

Another model of historical importance in understanding vocal fold oscillation is the two mass model designed by Ishizaka and Flanagan (1972). The key motivation behind this model was to be able to look at physical properties of the vocal folds when treating a single vocal fold as a two mass and a three spring coupled system (Ishizaka and Flanagan 1972). In **Figure 1.2**, the first mass represents the lower portion of the vocal fold and the second mass represents the

upper part of the tissue when flow occurs in the direction from left to right. The opposing vocal

fold would simply be a mirror image in a symmetric case (an important observation for the

purposes of the current study, which will keep one side vertical while the other side varies in its

angle). Based on the physiology of the larynx, the observation that the two separate masses (the

lower and the upper mass) oscillate out of phase with each other yields both convergent and
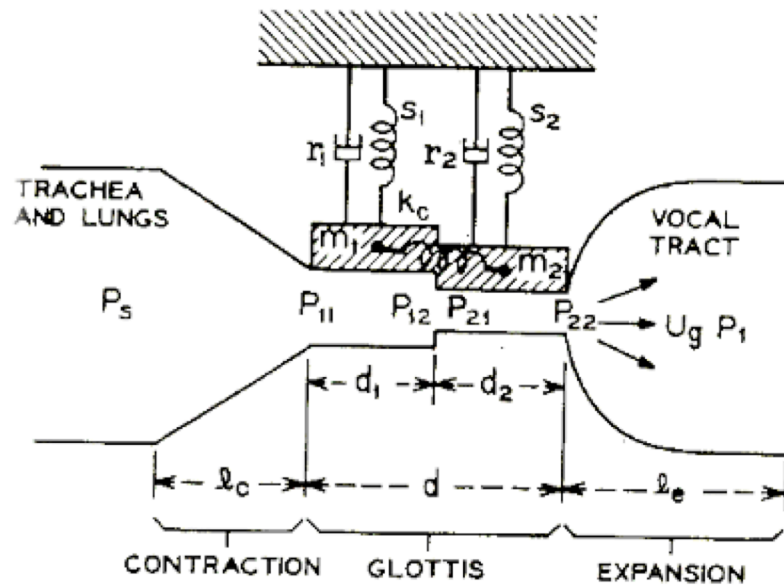
Figure 1.2 Schematic drawing of the two mass model
(Ishizaka and Flanagan 1972).

divergent glottal shapes (assuming mirror-image motion of the other side), presenting a very

good analogy of how sustained oscillation occurs.

"The masses m_1 and m_2 are coupled by a spring with a spring constant k_c and are allowed

to oscillate laterally by the springs s_1 and s_2, whose damping constants r_1 and r_2 correspond to the

equivalent viscous resistances of the tissues of vocal folds. The intraglottal pressures at different

locations of the vocal folds are denoted by the following symbols: P_s = subglottal pressure, P_{11} =

pressure at the end of the subglottis, P_{12} = pressure at the trailing edge of the mass m_1, P_{21} =

pressure at the leading edge of mass m_2, P_{22} = pressure at the beginning of the supraglottis, and

P_1 = pressure in the vocal tract. The quantity U_g denotes the glottal flow rate (in cm^3/s)"

(Thapa 2005). During oscillation, the two masses can oscillate with up to a 55 degree phase

difference, creating two distinctly different rectangular ducts within the glottis. The pressures at

the end of the first rectangular duct (P_{12}) and at the beginning of the second rectangular duct

(P_{21}) are not the same. **Figure 1.3** shows the pressure distributions throughout a convergent

glottis. Due to area reduction, the pressure drops from the higher subglottal pressure P_s towards

atmospheric pressure P_0. In the first portion of the glottis, the pressures are shown to drop below

atmospheric pressure, and then after exiting the glottis there is a region in the illustration in

which the pressure recovers to be greater than atmospheric pressure. The pressure drops that

occur within each rectangular duct are a result of viscous losses in the system, and are

represented by the expression $12\mu d l_g{}^2/A_g{}^3$ where d is the vertical (axial) length of the

rectangular duct, μ is the shear viscosity coefficient, l_g is the anterior-posterior length of the vocal
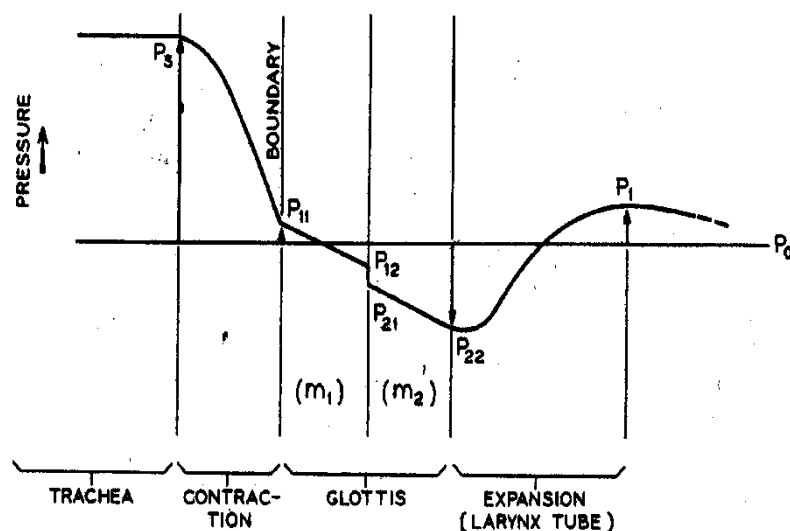
Figure 1.3 Converging glottis pressure distribution within the
two mass model (Ishizaka and Flanagan 1972).

folds, and A_g is the cross-sectional area of the glottal duct. Similar to the resistances that van den Berg *et al*. had expressed, Ishizaka and Flanagan developed the following equations to describe these changes in pressure related to the geometry of the ducts and their relationship with airflow:

$$P_s - P_{11} = 1.37 \frac{\rho}{2} \left(\frac{U_g}{A_{g1}} \right)^2 + \int_0^{l_c} \frac{\rho}{A_c(x)} \frac{dU_g}{dt} \, dx, \tag{1.3}$$

$$P_{11} - P_{12} = 12 \frac{\mu \, l_g^2 d_1}{A_{g1}^3} U_g + \rho \frac{d_1}{A_{g1}} \frac{dU_g}{dt}, \tag{1.4}$$

$$P_{12} - P_{21} = \frac{\rho}{2} \left(\frac{1}{A_{g2}^2} - \frac{1}{A_{g1}^2} \right) U_g^2, \tag{1.5}$$

$$P_{21} - P_{22} = 12 \frac{\mu \, l_g^2 d_2}{A_{g2}^3} U_g + \frac{\rho \, d_2}{A_{g2}} \frac{dU_g}{dt}, \tag{1.6}$$

$$P_{22} - P_1 = - \rho \frac{U_g^2}{A_{g2} A_1} \left(1 - \frac{A_{g2}}{A_1} \right). \tag{1.7}$$

The dynamic cross sectional area of the lower and upper glottal areas are given by:

$$A_{g1} = A_{g01} + 2 \, l_g \, x_1, \tag{1.8}$$

$$A_{g2} = A_{g02} + 2 \, l_g \, x_2, \tag{1.9}$$

where A_{g01} and A_{g02} are the prephonatory (equilibrium) cross sectional areas of the glottis, and x_1 and x_2 are lateral displacements of the two masses. Ishizaka and Matsudaira (1972) simplified these equations using the assumption that fluid flow within the model is quasi-steady incompressible flow. Under these circumstances, the volume flow through the model is time independent, and the inertive terms with time derivatives (Equations 1.3, 1.4, and 1.6) can be omitted. The previous equations then simplify to the following:

$$P_s - P_{11} = 1.37 \frac{\rho}{2} \left(\frac{U_g}{A_{g1}} \right)^2, \tag{1.10}$$

$$P_{11} - P_{12} = 12 \frac{\mu \, l_g^2 d_1}{A_{g1}^3} U_g, \tag{1.11}$$

$$P_{12} - P_{21} = \frac{\rho}{2} \left(\frac{1}{A_{g2}^2} - \frac{1}{A_{g1}^2} \right) U_g^2, \tag{1.12}$$

$$P_{21} - P_{22} = 12 \frac{\mu \, l_g^2 d_2}{A_{g2}^3} U_g, \tag{1.13}$$

$$P_{22} - P_1 = -\rho \, \frac{U_g^2}{A_{g2} \, A_1} \left(1 - \frac{A_{g2}}{A_1} \right). \tag{1.14}$$

1.3 The Hemilarynx Condition and Model M5

A hemilarynx is a specific anatomical case of the human larynx after a medical procedure called a hemilaryngectomy. The primary reason an individual would have a hemilaryngectomy is the presence of carcinoma (cancer) within one of the vocal folds. In some cases, only a partial hemilaryngectomy is required, and part of the vocal fold can be reconstructed using a bipedicle muscle flap with the sternohyoid, sternothyroid, or thyroid muscles (Bailey *et al.*, 1985). "The flap is created by making parallel vertical incisions and undermining the entire muscle. The sternohyoid muscle flap is sutured at the level of the true vocal cord anteriorly" (Thapa 2005).

The hemilarynx condition can be modeled by straightening one side of the Ishizaka and Flanagan model. **Figure 1.4** shows the two mass model altered to have one vocal fold composed of the two mass coupled system and the opposing wall being a flat surface. It is no longer a mirror image of the opposing two masses. The cross sectional areas of the original two mass model would then be half the value of the full larynx, potentially altering the pressure distributions and flows. By knowing the pressure distributions of both a full larynx and hemilarynx and their relationships with fluid flow, the phonatory consequences of this

configuration and their relation to potential techniques in phonosurgery could then be developed to optimize the quality of phonation within a patient.
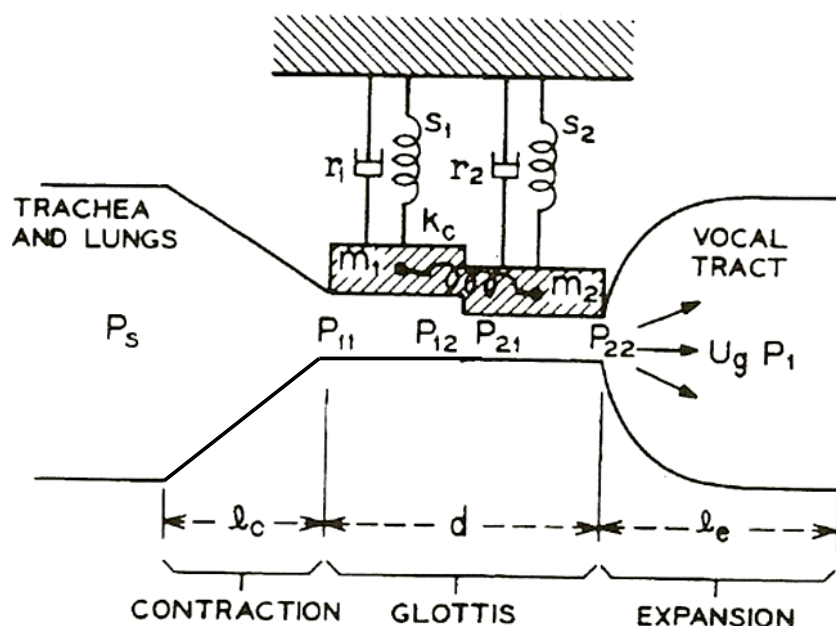
Figure 1.4 A hemilarynx representation of the two mass model
(Ishizaka and Flanagan 1972).

In addition to physical models such as the two mass model and the HM5 model which will be discussed later, there has also been a great deal of work in understanding asymmetric forces present within a hemilarynx using excised models. In Jiang and Titze's (1993) study, excised canine larynges were used to make a hemilarynx by removing one vocal fold and replacing it with a Plexiglas plate. They claimed there was a functional similarity between the hemilarynx and the full larynx with regards to the pressure dependence of the amplitude, the frequency of vocal fold vibrations of the hemilarynx, and their rates of change. The only key difference was that the flow required to obtain similar pressure dependences was about half that of the full larynx (Thapa 2005). Along with these lesser flows through the glottis of a hemilarynx, it was also suspected that even though normal phonation could be obtained, it would be roughly about 6 decibels lower in intensity.

In another use of excised canine hemilarynges conducted by Alipour and Scherer (2000), miniature pressure transducers were used to collect information about the pressure distributions along a Plexiglas wall. The study showed that pressures on the Plexiglas surface varied both longitudinally and vertically, and the flow resistance within the hemilarynx containing the Plexiglas wall was about half the resistance of a normal full larynx comprised of real vocal fold tissue (Alipour and Scherer 2000). Following this study, Alipour and Scherer (2002) also used a static hemilarynx model in which pressures were measured on both sides throughout a rectangular glottis containing a vocal fold structure across from a long Plexiglas vertical wall. Pressure distributions were taken at glottal diameters of 0.04 cm, 0.08 cm, and 0.16 cm, and the pressures along the vocal fold wall were found to be greater than the pressures on the opposing wall. This is a consequence of the fact that airflow along the long vertical wall is faster than the flow along the vocal fold wall (Alipour and Scherer 2002). This study was limited in that the glottis was always a rectangular duct and the model did not apply converging and diverging glottal shapes, but rather only a uniform symmetric case.

Model M5 is a Plexiglas model that has been used in efforts to give a more precise picture of the pressure distributions and fluid flows that occur during phonation. Due to the large range of different geometrical configurations that M5 is capable of modeling, a great deal of data has been collected in the past, although there is a great deal more data that still can be collected. Scherer *et al.* (2001) have used M5 to collect empirical data in relation to a symmetric full larynx as well as a diverging glottal configuration having an obliquity of 10 degrees. Initially in an effort to use M5 to describe the pressure distributions present in a hemilarynx, Thapa (2005) used what he referred to as HM5 to collect pressure distributions using model M5, with one side being vertical across all conditions, and the other varying in angle, both converging and
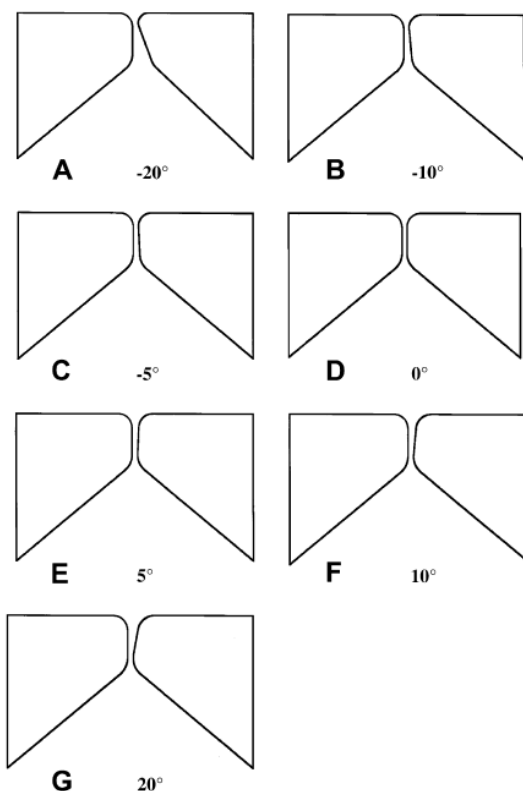
Figure 1.5 Converging glottal shapes (A-C), symmetric glottis, and diverging
glottal shapes (E-G) used in Model M5 are shown (Fulcher *et al* 2010).

diverging angles of 5, 10, and 20 degrees. These can be seen in **Figure 1.5** (Fulcher *et al.* 2005).

For each of these respective geometries, Thapa reported pressure distributions representing five

different transglottal pressure drops (cm H_2O) and simultaneously recorded the volume flows

(cm^3/s) through the model. During data collection, Thapa also attended to the fact that the flow

throughout the glottis was bistable, similar to the flow found in the static hemilarynx work of

Alipour and Scherer (Fulcher *et al.* 2010). Because the flow experienced this bistablity, it was

then necessary to measure pressures along both the flow wall (FW) and the non-flow wall

(NFW) to ensure that any differences in pressures on the vocal fold wall and the vertical wall

would be accounted for. These pressure distributions consistently showed that pressures along

the FW were lower than pressures along the NFW due to faster fluid flows along the FW. The

intraglottal pressures measured using a converging laryngeal shape were also consistently above

the supraglottal pressures, and intraglottal pressures measured using a diverging hemilaryngeal shape were consistently below the supraglottal pressures.

Following the measurements collected by Thapa, the physical data from Model M5 was then compared with results from a computational package called FLUENT. FLUENT is a commercial computation code used to consider the laminar flow of a Newtonian fluid governed by the Navier-Stokes equations (Fulcher *et al.*, 2010). Bo (2010) used the geometric dimensions of a two dimensional model of M5 to adjust the mesh size and the boundary conditions necessary to produce bistable behavior of fluid flow, providing a numerical understanding of the flows that are present in M5. **Figure 1.6** shows some examples of the similarities between the physical data from M5 and the computational data from FLUENT, lending support to the usefulness of FLUENT.
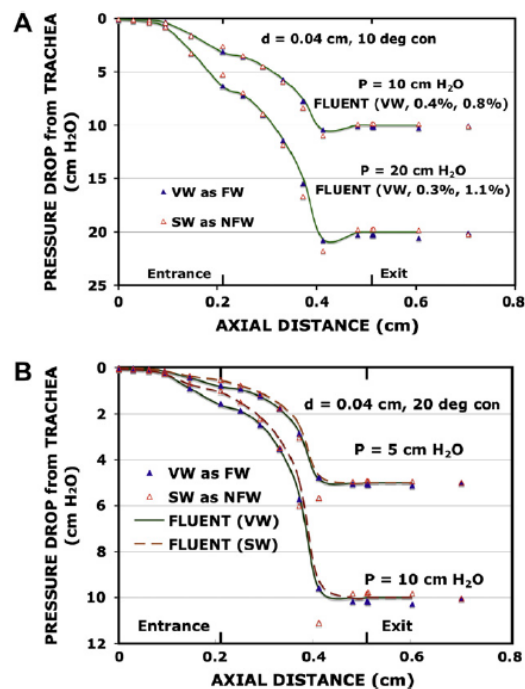
Figure 1.6 Comparison of the physical M5 data and FLUENT's computational data for a 10º convergent glottis (A) and a 20º convergent glottis in a hemilarynx (Fulcher *et al.* 2010).

The present study is to some extent a continuation of Thapa's research; however, the variability of glottal diameter has been introduced in an effort to understand how the glottal diameter may affect the pressure distributions during phonation. All of Thapa's geometric configurations had the same glottal diameter of 0.04 cm. This study obtains data for diameters of 0.01, 0.04, and 0.16 cm, as well as two additional transglottal pressures (1 and 15 cm H_2O) to complement those used by Thapa (3, 5, 10, 20, 40 cm H_2O). Three glottal angles were chosen, converging and diverging angles of 10 degrees as well as the uniform case of 0 degrees; the angles chosen depict three distinct snapshots of the phonatory cycle. This work extends the hemilarynx condition to a wider range of glottal diameters and glottal angles, necessary information in considering the effects of having one vocal fold fixed in a vertical position (as well as mimicking moments of asymmetric motion in which one side is vertical).

CHAPTER 2. MODEL M5 GEOMETRY, EXPERIMENTAL SETUP, AND DATA

COLLECTION

2.1 Plexiglas Model M5

As previously stated, the physical static model of the vocal folds and airway, model M5, has been used to collect data regarding the pressures and airflows present during a wide range of glottal configurations expected during human phonation. The model has been used for both symmetric and asymmetric glottal configurations. The model is 7.5 times the size of an average human male larynx for the convenience of obtaining intraglottal pressures over much of the axial surface of the vocal folds. Through this 7.5 factor of similitude, pressures within the model are 7.5^2 less than in real life, and volume flows are 7.5 times real life, and thus real life pressures and flows can be obtained using model M5 (Thapa 2005). M5 has Plexiglas slabs making a wind tunnel in which vocal fold pieces are housed. The wind tunnel represents part of both the trachea and the vocal tract, and the dimensions can be seen in **Figure 2.1**. In this diagram, air is pulled
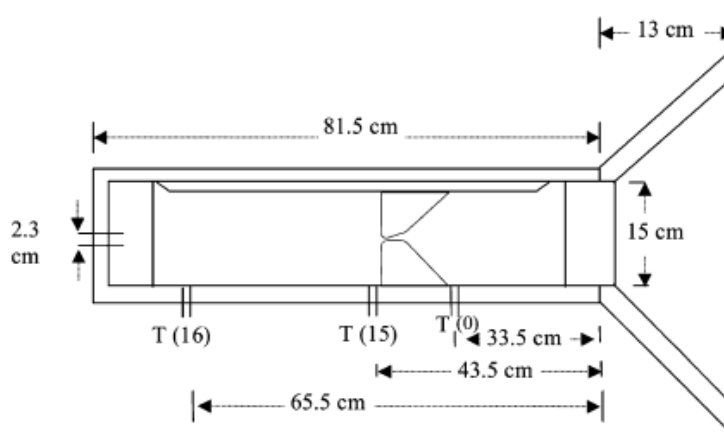
Figure 2.1 Schematic diagram of the dimensions of the M5
wind tunnel (Scherer *et al.* 2001).

through the system from right to left by a vacuum source. In addition to vocal folds placed in the tunnel, in **Figure 2.1** along the top edge there is a separation shim. Different shims placed on the side behind the right vocal fold are used to approximate glottal diameters of 0.01, 0.04, and 0.16

cm in this study. Using screws that vary the tightness of the vocal folds against the shim, the

glottal diameter can be finely adjusted and then measured using feeler gauges. The feeler gauges

allow for a diameter measure with a high degree of accuracy, where the thinnest feeler gauge

used was 0.001 inches.

When model M5 was milled, 9 pairs of vocal fold pieces were made. There are four pairs

of converging vocal folds (2.5, 5, 10, 20 degrees for each vocal fold), four pairs of diverging

vocal folds having the same angles, and one pair of 0 degree vocal fold pieces (the uniform

glottis). Each pair has one vocal fold piece that does not have pressure taps while the other vocal

fold piece has 14 pressure taps drilled into the surface. As shown in **Figure 2.2**, pressure taps 1

through 5 are along the inferior vocal fold surface, tap 6 is positioned at the glottal entrance, taps

7 through 11 are located along the straight medial surface of the folds, tap 12 is located at the

rounded portion of the glottal exit region, and taps 13 and 14 are located along the surface on top

of the vocal fold past the glottal exit. Tap 15 is located in the side of the wind tunnel in the
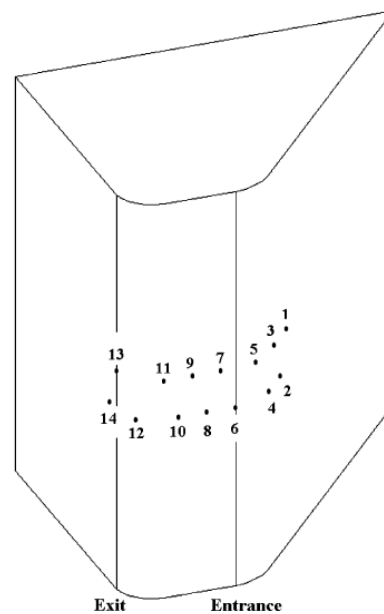
Figure 2.2 Schematic diagram of the pressure tap
locations on a vocal fold piece (Scherer *et al.* 2001).

location expected for the side wall ventricle. Tap 16 is downstream, and it is used to establish the transglottal pressure drop desired for each run. Each of the taps was drilled to be normal (perpendicular) to the surface of the vocal fold.

During data collection, in order to create a hemilarynx, one of the vocal fold pieces used was always 0 degrees ("vertical"). Within the physical model, only the "left" vocal fold piece has the pressure taps. Also, there is bistability of flow exiting the glottis, wherein the flow will tend to exit either to the right or to the left, creating different pressures on the vocal fold pieces within the glottis. This bistability has been explored in other model M5 work (Scherer 2001, Thapa 2005, Whitfield 2010). It is a natural phenomenon due to the glottal flow exiting into a rectangular downstream duct, and has been seen in phonation. Due to the bistability of the airflow, pressures were recorded when the vocal fold with pressures taps was the side that had the flow moving close to it, thus being the flow wall (FW), and then as the non-flow wall
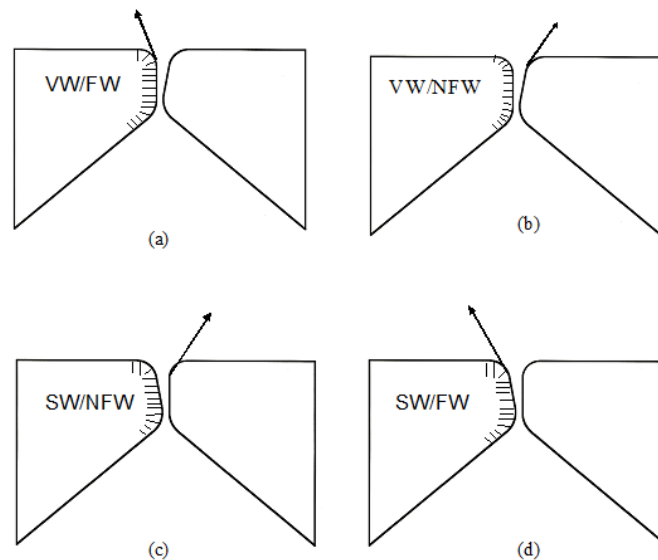
Figure 2.3 Schematic diagram showing (a) the vertical wall (VW) as the FW, (b) the VW as the NFW, (c) the slanted wall (SW) as the NFW, and (d) the SW as the FW (Thapa 2005).

(NFW), when the flow was moving along the medial surface of the other vocal fold. The flow direction was determined by physically placing a piece of paper in the glottis while the air was moving, forcing the flow to the one or the other side. **Figure 2.3** shows that each specific geometry requires pressures of the "mirror" image, or the reverse configuration with the pressure taps present on the opposing vocal fold.

2.2 Experimental Setup and Equipment Calibration

While conducting experimental research using model M5, data were obtained through the use of various mechanical and electrical devices. The accuracy of measurements is highly dependent on the experimental apparatus being used. It is necessary to conduct relatively frequent calibrations of equipment for the purpose of collecting valid physical measurements over time and experimental runs. Throughout this project numerous calibrations were performed on the flowmeters, pressure transducers, and pneumotachographs used to collect data. Following a description of the experimental setup, calibration procedures of these devices will be briefly discussed.

Figure 2.4 shows the experimental setup used to collect pressure and flow data from model M5. The 16 pressure taps within the model are connected to a Scanivalve pressure scanner (Model W0602/IP-24T) which is also connected to a Validyne pressure transducer (DP-103). The pressure scanner opens one specific port related to a specific pressure tap by the use of a solenoid controller, and the pressure is allowed to quickly build up through the line and apply force to the diaphragm of the DP-103 pressure transducer. The pressure transducer and its signal conditioner with the appropriate gain setting then converts the associated pressure applied to the diaphragm into a voltage output. Similarly another Validyne pressure transducer (MP45-16) and its signal conditioner and gain setting are connected to a pneumotach downstream from the

model, which creates voltages representing the volume flow pulled through the system by the

wet/dry vacuum. Digital multimeters (DM) are also connected to the signal conditioner to

monitor the voltages created by the pressure transducers being sent to the computer through a

data translation box. The multimeters are very important in the conduct of the measurements,

specifically in monitoring the volume flow since the flow is kept constant to maintain the

prescribed transglottal pressure drop throughout an entire run of measuring pressures at the 16

individual pressure taps.
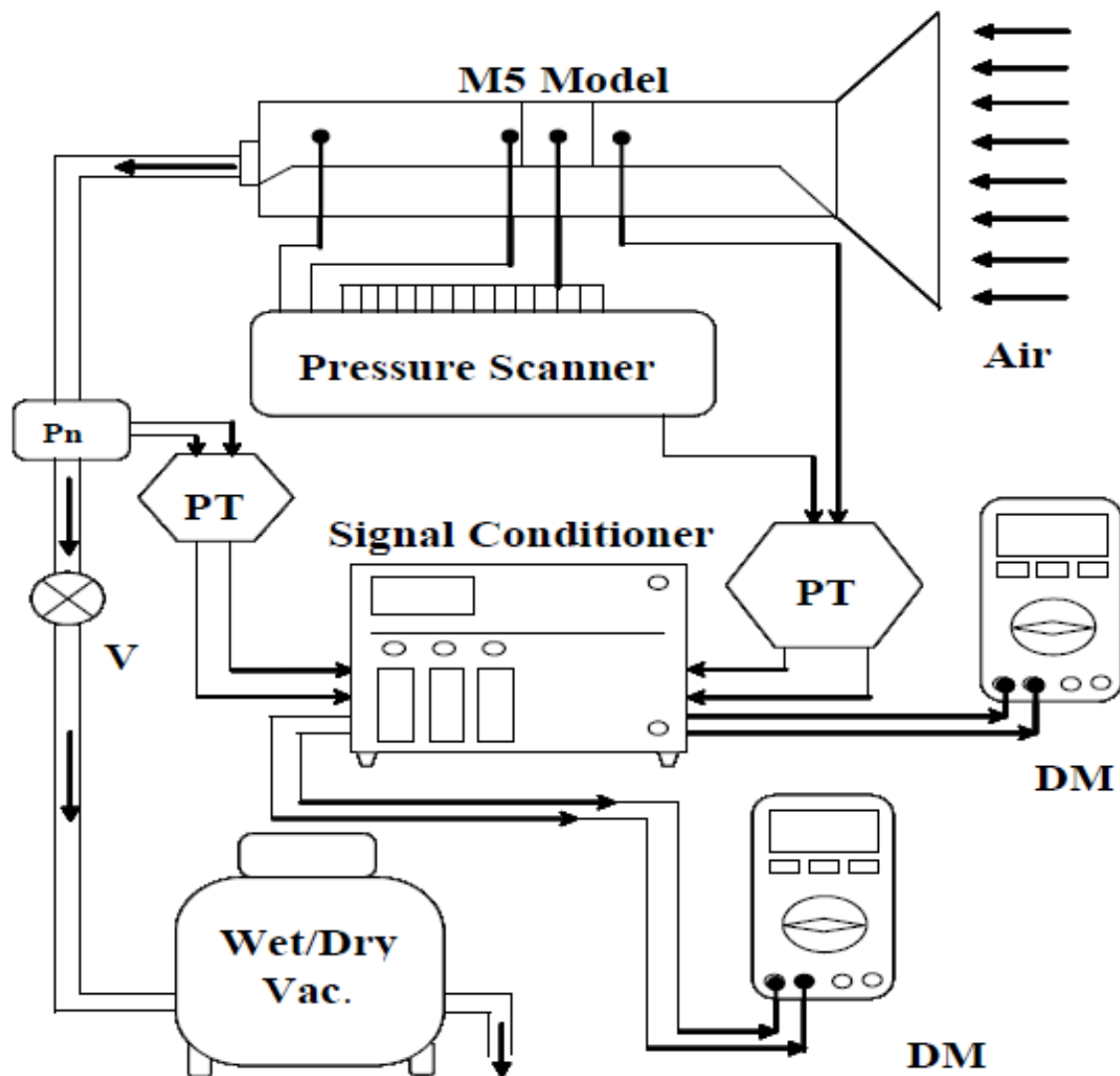
Figure 2.4 Schematic drawing of the experimental setup of model M5 (Scherer *et al.* 2001).

2.2.1 Flowmeters

In this study, Gilmont #4 and Gilmont #5 vertical variable area flowmeters were used to calibrate both the Hans Rudolph Inc. 4700 series and Model 4813 pneumotachographs. The height of the float within the flowmeter corresponds to the airflow through the device and is read by eye. Prior to each of these flowmeters being used in calibration of the pneumotachographs, it was necessary to validate the manufacturer's given calibration equations for the flowmeters by way of cross-calibration. Each of the flowmeters was connected in line with the vacuum system and as flow was pulled through the system, the floats in each flowmeter would simultaneously rise in accordance with the respective amount of fluid flow measured in liters per minute. The flowmeters were placed in line with each other, and also reversed in line with each other for the cross-calibration. This process resulted in validating the calibration equation provided by the manufacturer.

2.2.2 Pressure Transducers

The Validyne DP-103 and MP45-16 pressure transducers must also be calibrated. Each of the pressure transducers was calibrated using a Dwyer micromanometer by connecting both sides of the pressure transducer to the micromanometer using plastic tubing. The micromanometer range is one inch of water with an accuracy of better than $(1/2000)^{th}$ of an inch (0.00127 cm H2O), and has a metal inner spear with a sharp point suspended above the fluid in a u-tube-shaped tank. The height of the point is adjusted by turning the barrel of the micrometer. The micromanometer has an analog meter which will spike when the point makes contact with the fluid's surface, closing an electrical circuit. The physical pressure difference observed in inches of H_2O can then be associated with the respective voltage of the pressure transducer that is simultaneously recorded using a digital multimeter. Calibration measurements were made at all

six of the gain settings of the signal conditioner, each one representing a different range of

pressures; the gain settings are 1, 2.5, 5, 10, 25, and 50 mV/V. From the physical measurements,

graphs of voltage versus pressure were created and linear trendlines were fit to the data (using

Microsoft Excel) to obtain equations representing the voltage and pressure relationships for each

particular gain setting (the "calibrations"). The equations produced were compared with the

previous calibrations made by Whitfield (2010). For the DP-103 transducer, the largest percent

difference between the current calibration equations and those made in 2010 was a 5.77%

difference at the 1 mV/V gain setting, which is the most sensitive gain setting. Likewise, the 1

mV/V gain setting for the MP45-16 showed the greatest percent difference from Whitfield's

calibration equations at a value of 5.82%. To view a table of the current calibration equations and

figures of the voltage versus pressure graphs, please see Appendix B.

2.2.3 Pneumotachographs

Pneumotachographs are devices with internal flow resistance elements used to measure

the volume flow traveling through them. The two pneumotachographs used in this study, the

Hans Rudolph Inc. 4700 series and Model 4813, have multiple screens acting as the flow

resistance elements for the appropriate ranges of the flows for this study. For each pneumotach,

the MP45-16 pressure transducer ports were connected to the upstream and downstream ports of

the pneumotach screens. When flow is pulled through the system, the pneumotach then allows

the pressure drop across the flow resistance element to be measured by the pressure transducer,

creating a voltage output. During pneumotach calibration, flow is also simultaneously pulled

through the flowmeters and the float readings are recorded and used with the equations

representing the flow to determine the volume flows. The pneumotachographs need to be

calibrated frequently due to dust particulates appearing on the windscreen resistance elements.

Simply cleaning and rinsing the windscreens with alcohol after several flow runs and

recalibrating the pneumotachographs ensured that the flow data remain accurate (within

approximately 2%). Figures of these calibrations can be seen in Appendix C.

2.3 Data Collection Procedure

Once all of the appropriate calibrations were completed, experimental runs were carried

out. The appropriate voltages necessary to achieve the desired transglottal pressure values were

calculated under conditions of similitude. Based on the calibrations, a gain control setting was

chosen for both pressure transducers. The solenoid controller was then positioned at tap 16 to set

the desired transglottal pressure voltage for a specific experimental run. Data were recorded into

a Microsoft Excel file using software called Measure Foundry, which allows the analog voltages

supplied from the signal conditioner to be transmitted digitally to the computer using a DT9834

Series data acquisition module. The sampling rate used to collect data from each pressure tap as

well as the pneumotach was 5000 Hz, and 65535 measures for both the pressure and flow were

recorded. These measures were then used to create an average, standard deviation, and

coefficient of variation for both the pressures at each tap and the flow, for the given transglottal

pressure and glottal configuration. Upon the initial completion of data collection for tap 16 (to

establish the desired transglottal pressure and the specific dependent flow that the given

condition required), the solenoid controller was then positioned to record measures from taps 1

through 15. After collecting these data, measurements were also repeated for tap 16 to verify that

the flow and pressure voltages were relatively consistent. After measurements were collected for

all of the pressure taps at one particular transglottal pressure, pressure distributions were then

created from the averages in relation to their axial distance to show the intraglottal pressures

present during the given geometric setting of the hemilarynx vocal fold condition.

CHAPTER 3. RESULTS: GLOTTAL CONFIGURATIONS AND PRESSURE

DISTRIBUTIONS

3.1 Symmetric Glottal Configurations

For the zero degree included angle case, the vocal folds were parallel for three different

diameters (0.01 cm, 0.04 cm, and 0.16 cm, real life values). Each of the diameters was measured

by hand at four different positions within the glottis, two positions above and two positions

below the pressure taps, using feeler gauges. The position of the vocal fold was adjusted until the

average measure was extremely close to the prescribed diameter. The 0.04 cm diameter

symmetric case measurements were used specifically to test for the consistency of model M5

pressure and flow measurements against those obtained by Thapa in 2005. In addition, 0.01 cm

diameter symmetric case measures were obtained to test the consistency of model M5

measurements taken by Scherer in 2001. Previously collected data for the uniform zero degree

case at a diameter of 0.16 cm by Scherer was also used for comparison.

3.1.1 Pressure Distributions of a 0.04 cm Diameter Symmetric Glottis

For the first flow runs conducted, it was of great importance to verify that the data being

collected would be consistent with the previously collected hemilarynx data. Two new

transglottal pressures were measured in addition to the five pressures that Thapa had measured.

Figure 3.1 shows a comparison of Thapa's 0.04 cm uniform pressure distributions (in red) and

the repeated 0.04 cm uniform pressure distributions (in black) measured when flow was directed

along the side with pressure taps. The recorded average minimal diameter for the new measure

resembles a real life human value of 0.039963 cm, varying slightly from the 0.040217 cm

diameter recorded by Thapa (0.6% difference in diameters). From **Figure 3.1** it can be observed

that given the current calibration of equipment, the new pressure values recorded share almost

Figure 3.1 Comparison of Mewhinney and Thapa's flow wall pressure distributions for multiple transglottal pressure drops for the symmetric uniform glottis of 0.04 cm diameter.

identical pressure curves with previous data at the 3, 5, 10, and 20 cm H_2O. Upon observation of

the 40 cm H_2O transglottal pressure drop, however, Thapa's pressure distribution seems to be

noticeably higher than the newly collected measures. This is not a mistake, however: the last

points represented in the pressure distributions indicate that Thapa's pressure distribution simply

did not have a transglottal pressure drop exactly equal to 40 cm of H_2O, where the new data

more accurately targets this desired pressure drop. The comparison of the non flow wall pressure

distributions in **Figure 3.2** also indicate highly similar pressure distributions for the 3, 5, 10, and

20 cm H_2O conditions, and again a slight variation in the 40 cm H_2O pressure drop. However,

paying attention to the last points of each of the 40 cm H_2O pressure distributions, the measures

are both nearly equal while intraglottally the pressures measured by Thapa are higher. A possible

explanation for this difference may be a slight variation of the fluid flow during one of the flow

Figure 3.2 Comparison of Mewhinney and Thapa's non flow wall pressure distributions for multiple transglottal pressure drops for the symmetric uniform glottis of 0.04 cm diameter.

runs; however, these differences do not appear to be greater than about 1.2 cm of H_2O, so they still share a high degree of consistency. Following these comparisons, the bistable nature of the fluid flow through model M5 is examined in **Figure 3.3**. As previously reported in hemilarynx work by Alipour and Scherer (2001) and Thapa (2005), the transglottal pressure distributions show that when flow is directed along the wall with pressure taps, a greater pressure drop would be observed than when the flow is directed along the opposite wall. **Figure 3.3** supports this notion for the comparison of the flow and non flow wall in the symmetric glottis since the medial surface air pressures are slightly lower on the flow wall side.

The new measurements in this study were within roughly 3% of those Thapa reported. This result suggests high reliability of pressure distribution results over time for the same glottal

configurations. Further verifications of the accuracy of the pressure distributions follow in the

next section.

Figure 3.3 Pressure distributions of both flow wall and non flow wall intraglottal pressures for a uniform symmetric glottis with a 0.04 cm glottal diameter.

3.1.2 Pressure Distributions of a 0.01 cm Diameter Symmetric Glottis

A validation for the pressure and flow values previously collected by Scherer and

colleagues using model M5 ("Scherer" for short in this thesis) was performed for the 0.01 cm

diameter symmetric glottis. Scherer obtained pressure distributions at this diameter for

transglottal pressure drops equal to 3, 5, 10, 15, and 25 cm H_2O in 2012. Four of Scherer's

recorded pressure distributions are compared to those collected in **Figure 3.4**. During the present

data collection at the 0.01 cm diameter, it was observed that the flow did not seem to have

bistable characteristics. This is most likely due to the geometry of the glottis, in that the diameter

is so small that the fluid flow remains very low. For example, at the largest transglottal pressure

drop of 40 cm H_2O, the required flow to achieve this pressure drop was measured at only a value

of 62.15 cm^3/s (real life). The fluid flows did compare very well with those reported by Scherer

also, with the largest difference being roughly 3 cm^3/sec at the 15 cm H_2O pressure drop

(Scherer recorded 27.28 cm^3/sec, Mewhinney recorded 24.87 cm^3/sec). Dealing with volume

flows this low, it is likely that the flow will remain laminar, and will not create any sort of flow

jets or vortices in either direction. The largest percent differences from the values of pressure

recorded by Scherer were less than 1%.

Figure 3.4 Comparison of Mewhinney and Scherer's pressure distributions at a glottal
diameter of 0.01 cm for multiple transglottal pressure drops for the uniform symmetric glottis.

3.1.3 Scherer's Supplemented 0.16 cm Pressure Distributions

For the larger glottal diameter of the 0.16 uniform symmetric glottis, it was observed that
there was again a bistable condition present in the fluid flow. Unpublished data collected by
Scherer representing the pressure differences for the flow wall and the non flow wall are shown
in **Figure 3.5** for transglottal pressure drops of 3, 5, 10, and 15 cm H_2O. The intraglottal
pressures downstream of the glottal entrance tend to be lower along the flow wall than the non
flow wall.

Figure 3.5 Scherer's pressure distributions of a symmetric uniform 0.16 cm diameter
glottis (Scherer unpublished data 2012) showing the pressure distributions for both the
flow wall and the non flow wall sides of the glottis.

3.1.4 Comparison of Pressure Distributions for Different Glottal Diameters for the Symmetric

Uniform Glottis

As phonation occurs, the opening of the glottis varies based on the sounds being

produced. In order to understand the asymmetric forces of the vocal folds in a hemilarynx

condition, it is important to compare the pressures present at different locations of the vocal fold

at different diameters. It is also of significant interest to look for differences between several

different transglottal pressure drops, since larger transglottal pressures produce larger intensities

of the acoustic signals. How do the pressure distributions vary for the same transglottal pressures

but different diameters for the symmetric uniform glottis? The flow direction must be accounted

for in this comparison. For flow directed along the vertical wall containing the pressure taps, the

pressure distributions for transglottal pressures of 3 cm H_2O (**Figure 3.6**), 5 cm H_2O (**Figure

3.7**), 10 cm H_2O (**Figure 3.8**), and 15 cm H_2O (**Figure 3.9**) are shown in the figures below.

There is a significant change in the intraglottal pressures as diameter increases, shown by all four

figures; the pressure at glottal entrance decreases as diameter increases, significantly lowering

the intraglottal pressures when the glottal diameter is larger. The pressures are positive

(indicating outward force on the vocal folds) except for the largest diameter of 0.16 cm, where

the pressures become negative at the glottal entry. Also, as the glottal diameter increases, the

pressure distributions tend to reach or surpass the desired transglottal pressure drop more

upstream in the glottis. For example, this value is reached at tap 11 for the 0.01 cm diameter, tap

9 for the 0.04 cm diameter, and tap 6 for the 0.16 cm diameter (for reference, tap number 6 is at

the glottal entrance). It is noted that the pressure distributions alter only because of a change in

glottal diameter, not the glottal configuration *per se*, or the shape of the vocal fold surface *per se*.

One similarity due to the vocal fold contour being the same is that for all conditions shown, the

minimum pressure occurs at tap 11 where the curvature of the vocal fold begins (that is, the

glottal exit radius that creates the rounded exit curvature to the vocal fold). This is typically

attributed to the increase in air particle velocity at that rounding. The intraglottal pressures

change relatively linearly for the 0.01 cm and 0.04 cm diameters, whereas for the largest

diameter, 0.16 cm, the intraglottal pressures show two local minima, at glottal entrance (tap 6)

and near tap 11, where the pressure is lowest for all cases. A nearly linear decrease in intraglottal

pressure suggests that the pressures are following a viscous-based decrease in pressure between

parallel plates (as suggested by the Poiseuille expression in fluid mechanics), but for the 0.16 cm

case, the diameter is too wide and glottal length too short (0.3 cm) for the required viscous-based

conditions to develop in the glottis. It is observed that after tap 11 for all three diameters for

these flow wall cases, the pressures remain below or approximately equal to the downstream

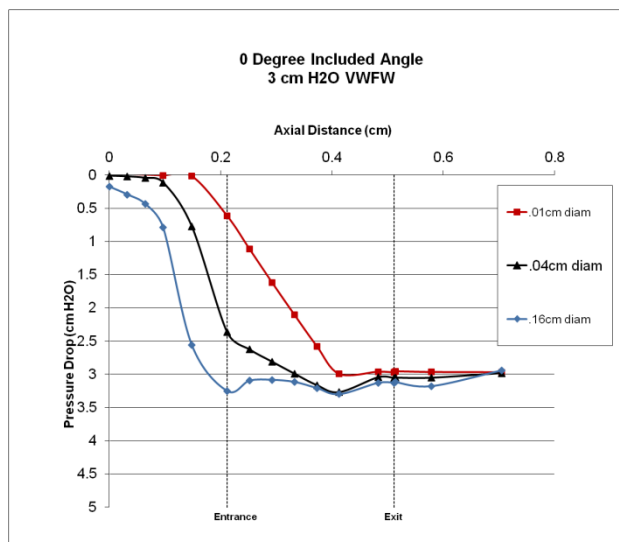pressure (measured at tap 16, furthest to the right in the figures).

Figure 3.6 Comparison of pressure distributions for three glottal diameters for the symmetric uniform glottis for a transglottal pressure drop of 3 cm H_2O when flow is directed along the vertical wall with the pressure taps.
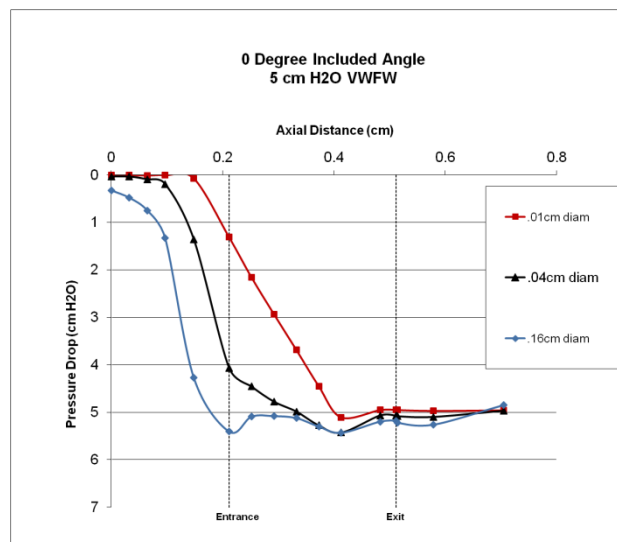

Figure 3.7 Comparison of pressure distributions for three glottal diameters for the symmetric uniform glottis for a transglottal pressure drop of 5 cm H_2O when flow is directed along the vertical wall with the pressure taps.
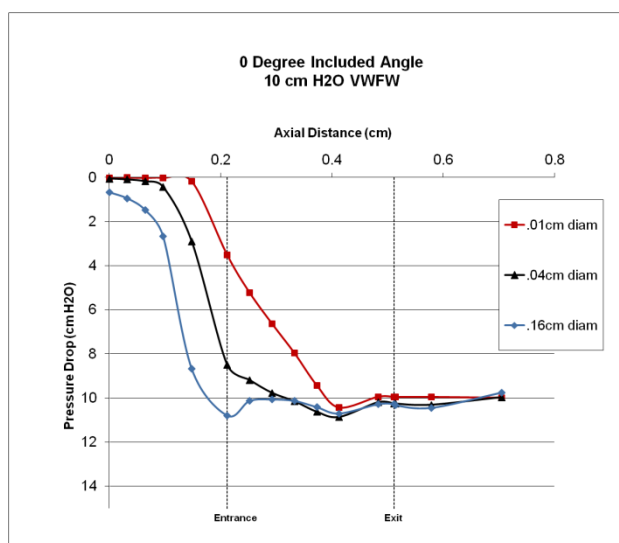

Figure 3.8 Comparison of pressure distributions for three glottal diameters for the symmetric uniform glottis for a transglottal pressure drop of 10 cm H_2O when flow is directed along the vertical wall with the pressure taps.
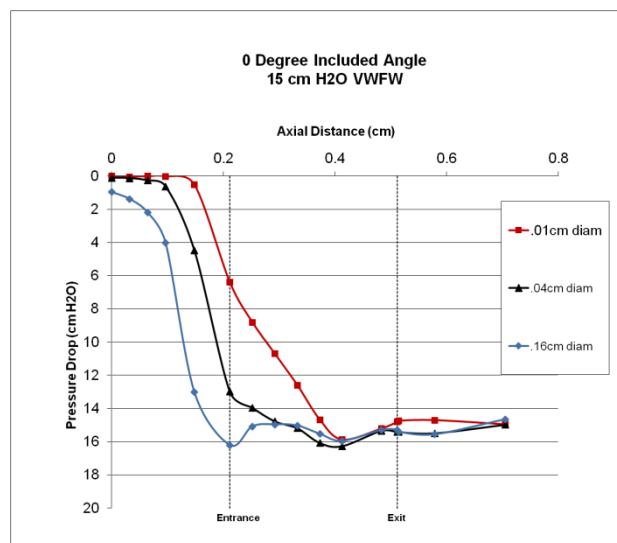

Figure 3.9 Comparison of pressure distributions for three glottal diameters for the symmetric uniform glottis for a transglottal pressure drop of 15 cm H_2O when flow is directed along the vertical wall with the pressure taps.

The pressures on the non flow wall side have significant differences from those on the flow wall, which were discussed above. The pressure distributions are shown in **Figures 3.10, 3.11, 3.12,** and **3.13.** The pressures tend to recover a little more upstream along the non flow wall than they do along the flow wall. Indeed, the intraglottal pressures tend to be greater than for the flow wall side, even extending higher than the pressure at the last downstream tap. It is noted that there is now the absence of the double dip in pressure for the 0.16 cm diameter condition. These pressure differences would be due to flow separation from the non flow wall, as this is most prominently noticed at the pressure taps 11, 12, 13, and 14 near the glottal exit. An interesting observation is that for the largest diameter of 0.16 cm, taps 12, 13, 14, and 15 all show positive pressures relative to that of tap 16. This is usually thought to be due to air circulating around the glottal exit corner back towards the vocal fold (and corner where tap 15 is) so that there is impact pressure, raising the pressure above the downstream value. Because this is a symmetric case, there is no difference between a full larynx and a hemilarynx.
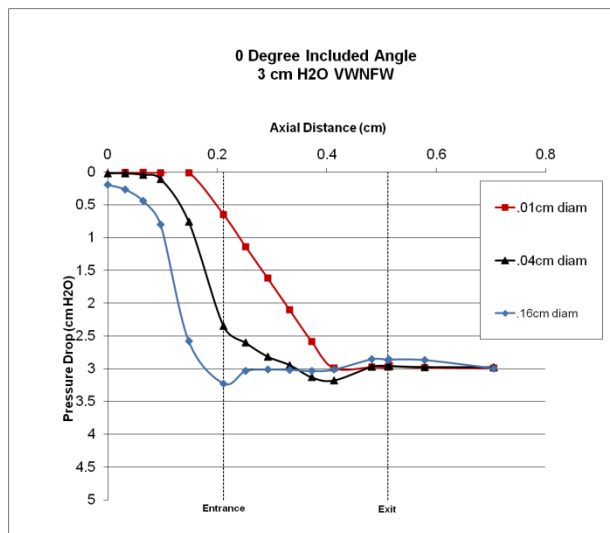
Figure 3.10 Comparison of pressure distributions for three glottal diameters for the symmetric uniform glottis for a transglottal pressure drop of 3 cm H_2O when flow is directed along the vertical wall opposing the wall with the pressure taps.
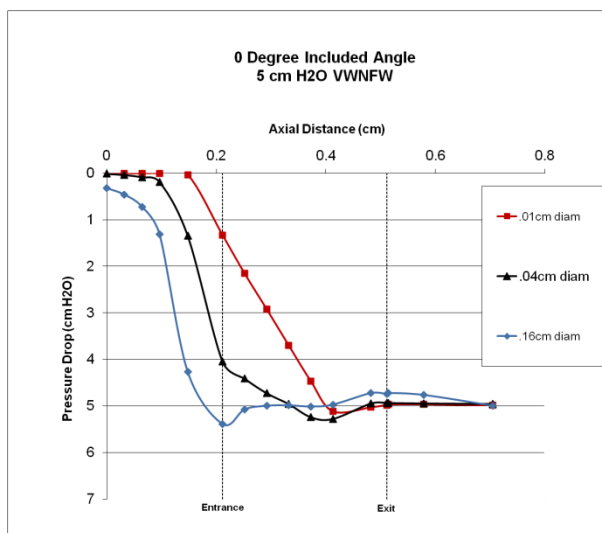

Figure 3.11 Comparison of pressure distributions for three glottal diameters for the symmetric uniform glottis for a transglottal pressure drop of 5 cm H_2O when flow is directed along the vertical wall opposing the wall with the pressure taps.

Figure 3.12 Comparison of pressure distributions for three glottal diameters for the symmetric uniform glottis for a transglottal pressure drop of 10 cm H_2O when flow is directed along the vertical wall opposing the wall with the pressure taps.
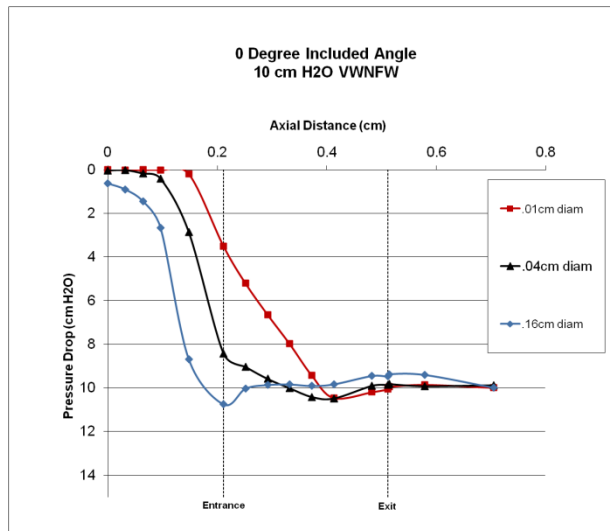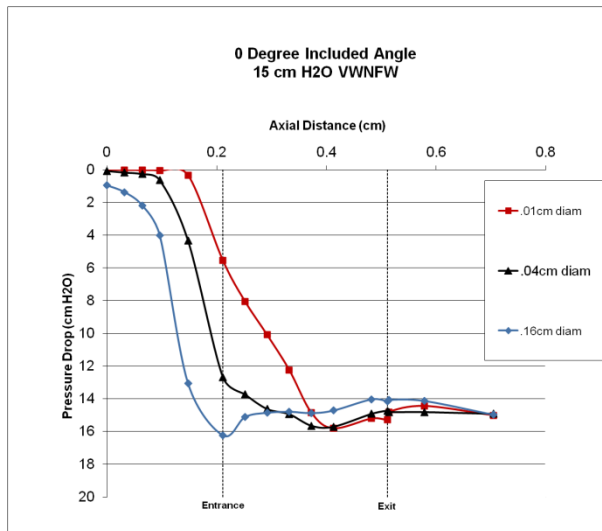

Figure 3.13 Comparison of pressure distributions for three glottal diameters for the symmetric uniform glottis for a transglottal pressure drop of 15 cm H_2O when flow is directed along the vertical wall opposing the wall with the pressure taps.

3.2 Converging Glottal Configurations

In order to produce a reasonable picture of what an oscillatory cycle may look like during phonation using only three different geometric configurations, first the uniform case was examined above. Next the -10 degrees converging glottal configuration is examined. The pressure distributions in comparison to the uniform case will look much different due to the continually narrowing diameter of the glottis. Flow wall versus non flow wall effects will be observed once again as well as comparisons across each of the glottal diameters measured. Thapa's previous measures of the -10 degree converging glottis at a glottal diameter of 0.04 cm will not be reported individually; however, his data were used in making the appropriate comparisons across the three glottal diameters for a hemilarynx.

3.2.1 Converging -10 Degree Glottis with 0.01 cm Diameter

For the -10 degree converging glottis, there are some key differences in the pressure distributions due to the bistablity of the fluid flow. Tap 8 of the -10 degree vocal fold piece was found to be clogged, and thus data collected from tap 8 of this vocal fold piece were omitted. First, the following two comparisons are made for the 0.01 cm glottal diameter: (a) the vertical wall as the flow wall while the slanted wall is the non flow wall, and (b) the slanted wall as the flow wall while the vertical wall is the non flow wall. To view the individual pressure distributions for each of the four flow runs conducted at different transglottal pressures, see Appendix C. Throughout each of the next few figures, the pressures occurring along the vertical wall (VW) will be represented with black solid lines, while pressures occurring along the slanted wall (SW) will be represented by red dashed lines. It is noted that for a convergent glottis, the pressures should decrease between the glottal entrance and near the glottal exit due to the reduction in cross sectional glottal area, as one would expect from the Bernoulli energy

equations. However, this does not mean that the pressures on the two walls should be equal, especially since the glottis is asymmetric relative to the tracheal axis, and there is bistability of the flow through and beyond the glottis. Another important note for the convergent cases is that the "flow wall" is the side the airflow moves past the glottal exit, which may affect the intraglottal pressures, but does not mean that the flow is separated from the convergent side within the glottis (since the glottis is converging). There may be differences in the air velocity near the walls but flow does not separate from the convergent side until it reaches the glottal exit, and then the flow separation will have an asymmetry along the axial distance, leaving the convergent side more upstream than the vertical wall.

Figure 3.14 shows pressure distributions when flow is first directed along the vertical wall. The pressures along the slanted wall are less than those along the vertical (flow) wall up to tap 11 (near the minimum pressure for the slanted non flow wall). The air particle velocities are most likely faster along the slanted (non flow) wall than along the vertical (flow) wall, thus lowering the pressures compared to the vertical (flow) wall. A primary difference observed in the figure is the location of the minimum in the pressure distribution. The minimum for the slanted (non flow) wall occurs near tap 11, where vocal fold (glottal exit) curvature begins, suggesting that that is where the fastest flow on the slanted side resides. However, the lowest pressure for the vertical (flow) wall is near tap 12, on the exit curved surface itself, strongly suggesting that the flow moves around that point relatively quickly as the airflow moves toward that side of the airway.
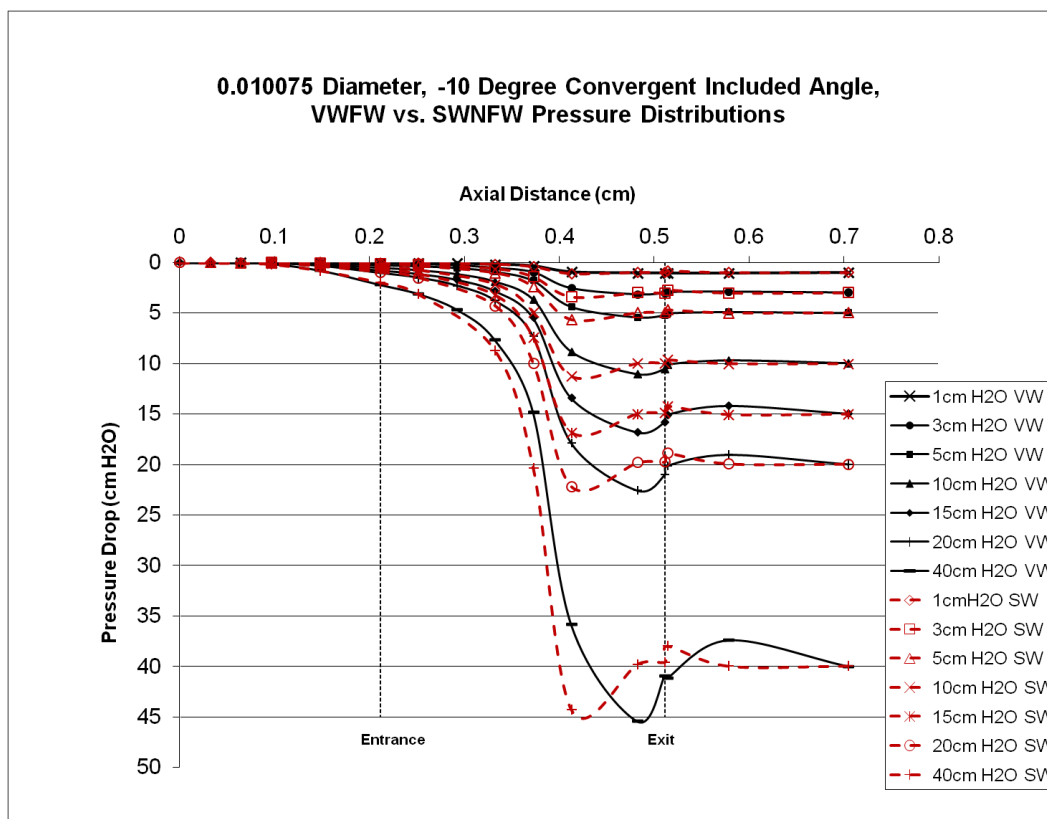
Figure 3.14 Comparison of the pressure distributions on the vertical wall as the flow wall (VWFW), solid curves, and on the slanted wall as the non flow wall (SWNFW), dashed curves, for a −10 degree converging glottal configuration at 0.01cm diameter for 7 different transglottal pressures.

Figure 3.15 shows the case for the same configuration (-10 degree converging), where the slanted wall is the flow wall, and the vertical wall is the non flow wall (the flow was forced to move in the airway past the glottis on the slanted wall side). The pressure distributions are somewhat similar to the previous case, where the slanted (flow) wall has lower pressures up to tap 11 and the vertical (non flow) wall has its minimum past that of the slanted wall, near tap 12. Again, this suggests that at a relatively small diameter of 0.01 cm, the bistable condition of the flow is relatively insignificant in affecting the intraglottal pressures, and the glottal asymmetry itself creates the differences in the pressure distributions. Here the pressures in the glottis are slightly higher on the vertical side, with a minimum pressure closer to the glottal exit, giving
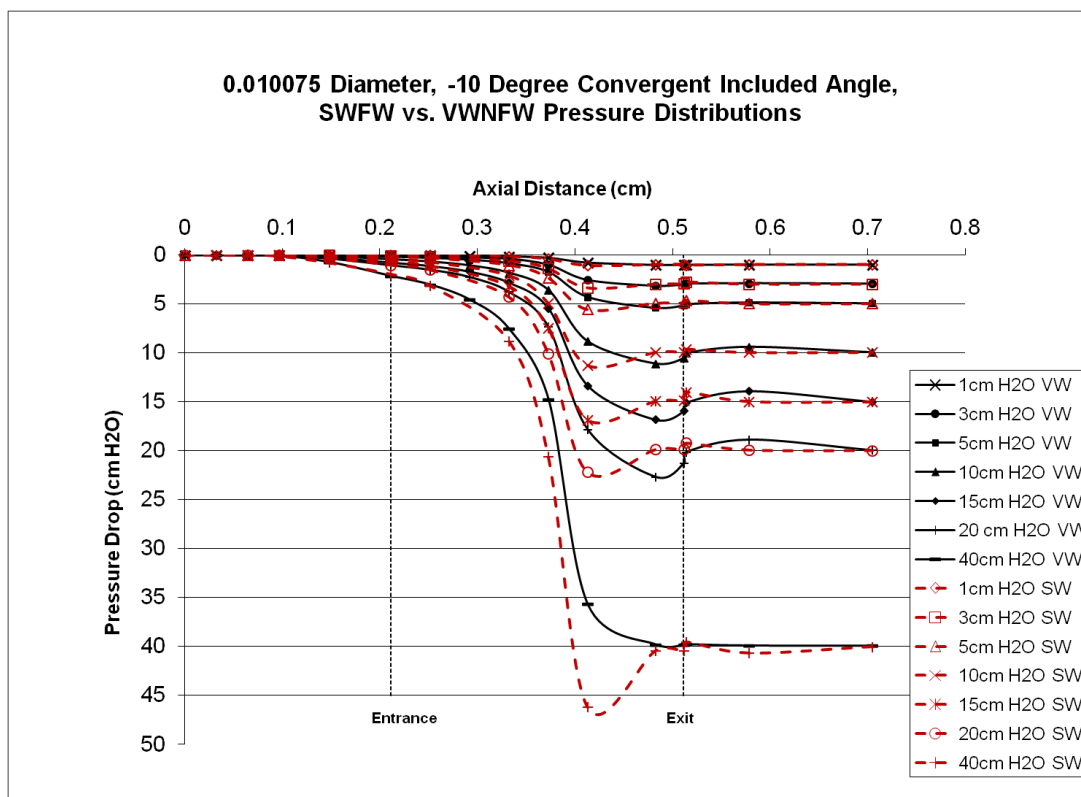
Figure 3.15 Comparison of the pressure distributions on the slanted wall as the flow wall (SWFW), dashed curves, and on the vertical wall as the non flow wall (VWNFW), solid curves, for a −10 degree converging glottal configuration at 0.01cm diameter for 7 different transglottal pressures.

greater outward pressures for most of the glottis and an inward pull closer to the glottal exit proper.

3.2.2 Converging -10 Degree Glottis with 0.16 cm Diameter

Figure 3.16 shows the pressure distributions when the flow is directed along the vertical wall, and the slanted wall is the non flow wall (to view individual pressure distributions, see Appendix C). In comparison to the 0.01cm -10 degree converging glottis, at a diameter of 0.16 cm the intraglottal pressures have lower pressure distributions within the glottis and reach the transglottal pressure value more upstream in the glottis. The interesting finding is that the intraglottal pressures are now higher on the slanted wall starting prior to the glottal entrance (that
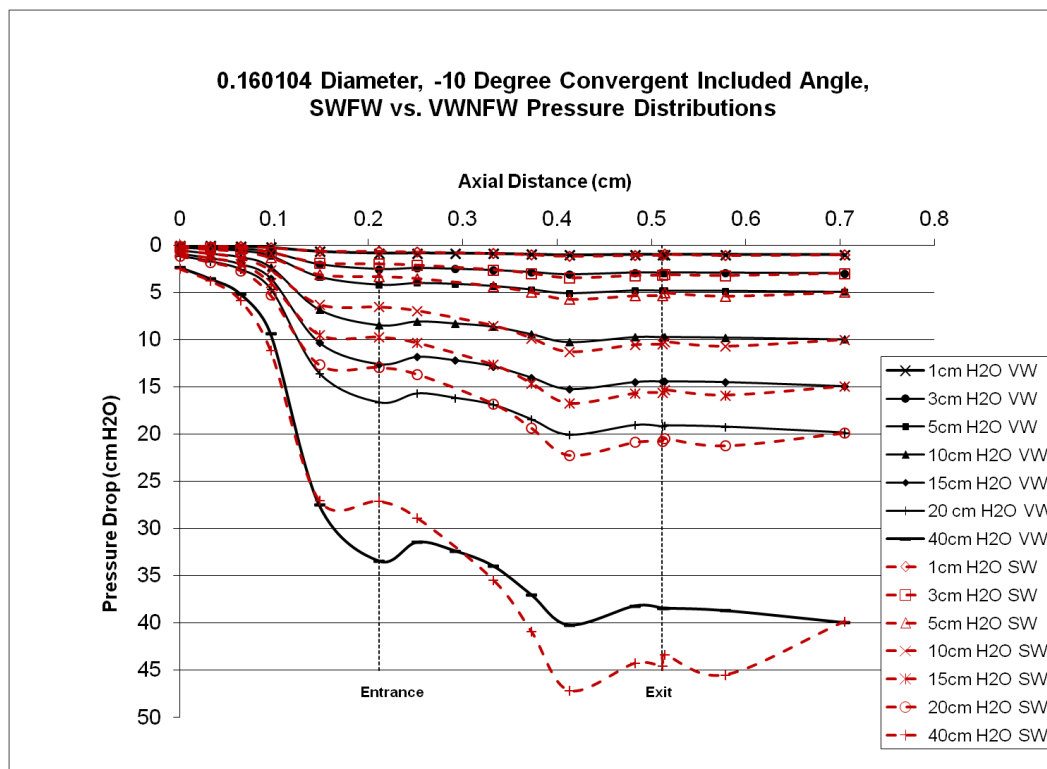
is, starting at tap 5) than on the vertical wall, whereas the opposite was true for the smaller

diameter 0.01 cm. The difference in pressures is approximately 25%. Thus, the asymmetry with

the largest diameter studied here creates very different pressure distributions. Therefore the

forcing functions on the two surfaces of the vocal folds are different, here pushing outward on

the slanted wall with more force than on the vertical wall. Both the vertical wall and the slanted

wall pressure distributions have similar shapes, although the pressures seem to have a slight peak

at tap 6 on the slanted wall and tap 7 on the vertical wall across each of the transglottal pressure

drops.

Figure 3.16 Comparison of the pressure distributions on the vertical wall as the flow wall (VWFW), solid curves, and on the slanted wall as the non flow wall (SWNFW), dashed curves, for a −10 degree converging glottal configuration at 0.16 cm diameter for 7 different transglottal pressures.

Figure 3.17 Comparison of the pressure distributions on the slanted wall as the flow wall (SWFW) and on the vertical wall as the non flow wall (VWNFW) for a −10 degree converging glottal configuration at 0.16 cm diameter for 7 different transglottal pressures.

When the flow wall is switched to the slanted wall for the larger diameter of 0.16 cm, the shapes of the pressure distributions remain similar, but as seen in **Figure 3.17**, a surprising finding is that the pressure distributions in the glottis for the vertical wall (VWNFW) are shifted upward, and the pressure distributions in the glottis on the slanted wall (SWFW) are moved downward by about 30%. This creates an overlap of the two pressure distributions of the two medial vocal fold surfaces. The changes in these pressure distributions are consequences of the bistable nature of the flow. The physical interpretation is that there will be more outward (positive, pushing) pressure force on the glottal entrance locations on the slanted wall, and then lower (negative, pulling) pressure forces in the glottis past the glottal entrance on the slanted

wall, setting up a force that essentially attempts to pivot the slanted wall to a greater convergence angle, whereas the effect is less on the vertical wall.

3.2.3 Comparison of Pressure Distributions across Glottal Diameters for the Converging

-10 Degree Glottis

In comparing the glottal diameters for the -10 degree converging glottal configuration, with one wall always vertical, there is a great deal of correspondence in the pressure distributions for each of the desired transglottal pressure runs. For the purpose of conciseness, the pressure distributions for a 10 cm H_2O pressure drop will be shown and the rest of the transglottal pressure runs can be found in Appendix C, as only slight variations occur. **Figures 3.18, 3.19, 3.20**, and **3.21** show the four cases in which the pressure distributions were measured based on flow bistability. The smallest diameter 0.01 cm case results in the largest intraglottal pressures over the upstream half of the glottis, and the deepest dip of pressure near tap 12 on the vertical wall. As diameter increases, the intraglottal pressures decrease and the lowest pressures occur near tap 11 at the beginning of the glottal exit rounding. That is, for both the 0.04 cm diameter and 0.16 diameter, the lowest pressures occur near tap 11, regardless of the wall or the flow direction..

In comparing the flow wall and non flow wall pressure distributions, there are pressure differences on the two sides of the glottis. Comparing **Figures 3.18 and 3.21**, where the flow is along the vertical wall, intraglottal pressures are higher on the convergent side and lower on the vertical side for all three diameters for about two-thirds of the glottis length, followed by a more downstream pressure dip for the vertical wall for the smallest diameter. For example, for the 0.16 cm diameter case, the pressure drop from the trachea at glottal entry is a little more than 8 cm H_2O on the vertical wall, but less pressure drop of about 6.5 cm H_2O on the slanted wall. Since

the measure is the pressure DROP from the trachea, the 6.5 cm H_2O drop is a higher actual pressure than the larger 8 cm H_2O pressure drop. For a transglottal pressure of 10 cm H_2O, a difference of about 1.5 cm H_2O is about 15%, which may give rise to a significant difference in driving pressure on the two sides of the glottis, with greater force on the convergent side. Comparing **Figures 3.19 and 3.20,** where the flow is along the slanted wall (that is, exiting toward the tunnel side on which the slanted wall resides), again the vertical wall has the higher pressures, and the pressures are quite similar to when the flow is along the vertical wall, with pressure differences and inferred driving force differences being quite similar. Thus, the asymmetry itself, rather than the direction of the flow, is determining the pressure differences between the vertical and slanted walls, and those differences are not negligible, where there is more outward driving force on the slanted wall than on the vertical wall.

3.3 Diverging Glottal Configurations

The diverging glottal configuration is the last glottal configuration which will be examined. The pressure distributions for both the uniform and -10 degree converging cases have already been shown, but to understand what may be occurring during one entire oscillation during phonation, a diverging glottal condition needs to be studied. The results of the +10 degree diverging case will now be presented similarly to the each of the previous glottal configurations.

In general, the pressure distributions in the diverging glottis have a minimum value near the glottal entry because the minimal diameter occurs at the glottal entrance. Only some pressure distributions will be shown here, but additional figures can be found in Appendix D.
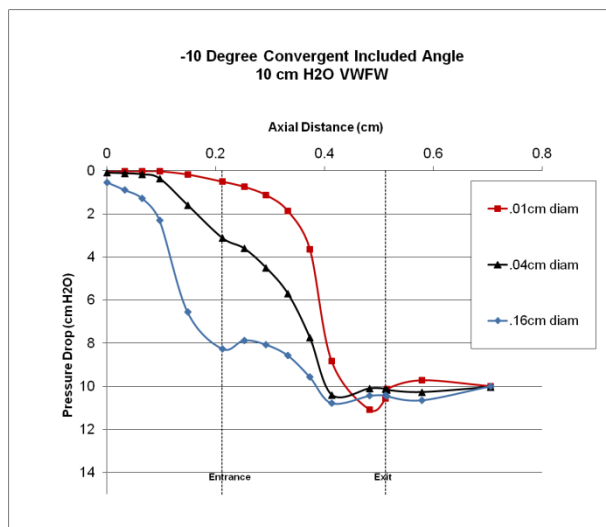
Figure 3.18 Comparison of the pressure distributions for three glottal diameters for a 10 cm H_2O transglottal pressure when the vertical wall was the flow wall (VWFW) with pressure taps for a -10 degree converging glottis.
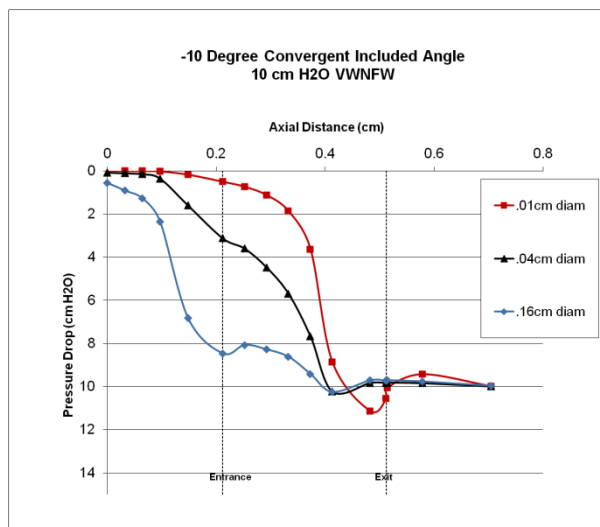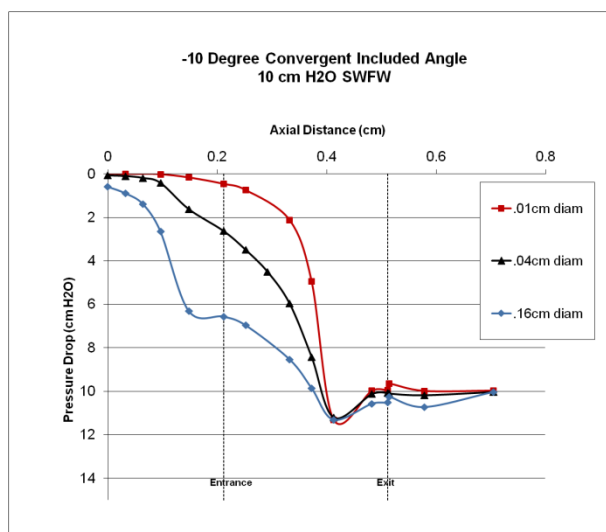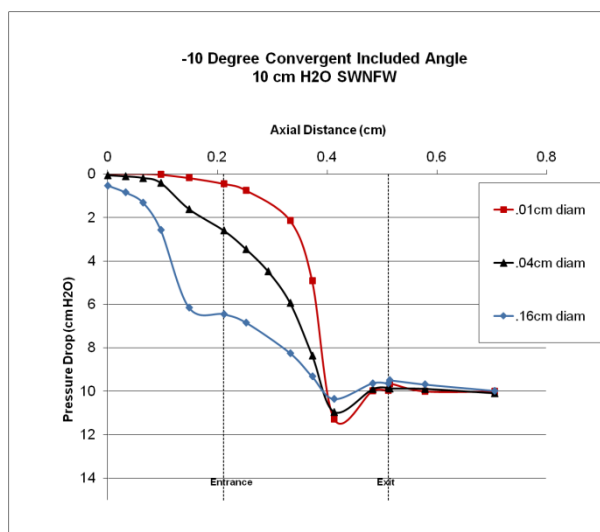
Figure 3.19 Comparison of the pressure distributions for three glottal diameters for a 10 cm H_2O transglottal pressure when the vertical wall was the non flow wall (VWNFW) with pressure taps for a -10 degree converging glottis.

Figure 3.20 Comparison of the pressure distributions for three glottal diameters for a 10 cm H_2O transglottal pressure when the slanted wall was the flow wall (SWFW) with pressure taps for a -10 degree converging glottis.

Figure 3.21 Comparison of the pressure distributions for three glottal diameters for a 10 cm H_2O transglottal pressure when the slanted wall was the non flow wall (SWNFW) with pressure taps for a -10 degree converging glottis.

3.3.1 Diverging +10 Degree Glottis with 0.01 cm Diameter

Similar to the converging glottis case, for the +10 degree diverging glottis the slanted wall seems to experience the greatest pressure drops overall. Unlike the -10 degree converging glottis, for which the lowest pressures are near the glottal exit, the lowest pressure values now occur near the glottal entrance where the minimal diameter is located. **Figure 3.22** shows the pressure distributions for the situation where the flow is directed along the vertical wall, and **Figure 3.23** shows the results when the flow is directed along the slanted wall. There the forms of the distributions for each transglottal pressure are quite similar, differing slightly at glottal entry. The largest variation between the two flow direction cases lays in the 40 cm H_2O pressure distribution for the case where the slanted wall is the flow wall. There two local minima appear, at the entrance (tap 6) and on the rounding of the glottal exit (tap 12). This may be the first sign of an effect of the flow bistability for a diameter as small as 0.01 cm in the data of this study. It is noted that the pressures at taps 13 and 14 are elevated in both figures on the divergent slanted wall, suggesting a possible air circulation moving onto those two taps (but only on the divergent side, not the vertical glottal wall side). This characteristic of the pressure distributions becomes more pronounced at larger transglottal pressure drops.
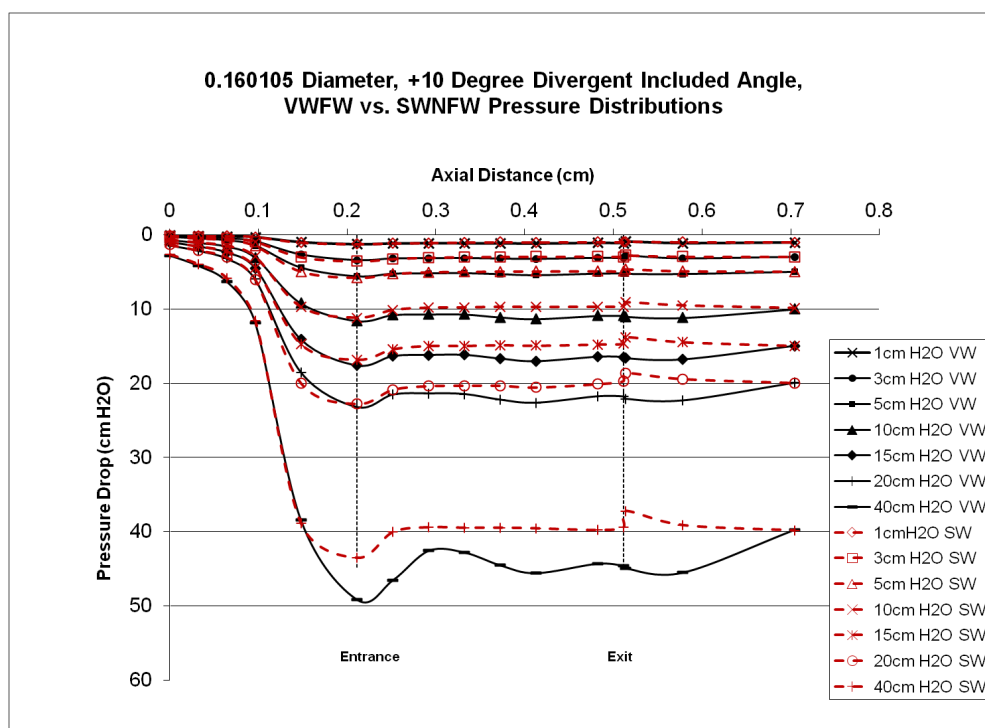
Figure 3.22 Comparison of the pressure distributions on the vertical wall as the flow wall and on the slanted wall as the non flow wall for a +10 degree diverging glottal configuration at 0.01 cm diameter for 7 different transglottal pressure drops.
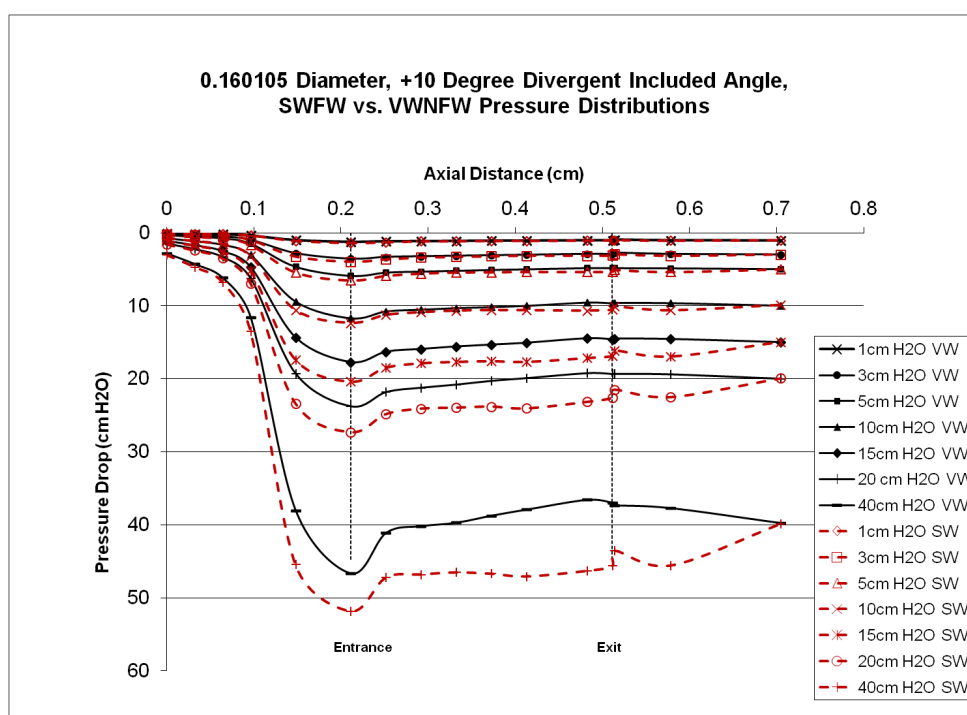

Figure 3.23 Comparison of the pressure distributions on the slanted wall as the flow wall and on the vertical wall as the non flow wall for a +10 degree diverging glottal configuration at 0.16 cm diameter for 7 different transglottal pressure drops.

3.3.2 Diverging +10 Degree Glottis with 0.16 cm Diameter

For the 0.16 cm diameter +10 degree diverging glottis, the pressure distributions show differences relative to the bistable conditions of the flow once again (**Figures 3.24 and 3.25**). This follows the continuing trend that larger glottal diameters create differences in the pressure distributions on the two sides of the glottis when the direction of the flow is shifted from one side to the other (bistability). When the flow is along the vertical wall, that wall has lower intraglottal pressures (**Figure 3.24**), and when the flow is along the divergent slanted wall, that wall has lower intraglottal pressures (**Figure 3.25**), and the differences are considerable– about 15% of the transglottal pressure**.** This appears to follow from the typical explanation that pressures are lower on the side with faster flows. Another important observation is that, for either the flow wall or non flow wall, the pressure distributions have very little variation within the glottis once the pressures have recovered around tap 7, and those pressures are close to the downstream

Figure 3.24 Comparison of the pressure distributions on the vertical wall as the flow wall and on the slanted wall as the non flow wall for a +10 degree diverging glottal configuration at 0.16 cm diameter for 7 different transglottal pressures.

pressure (atmospheric pressure). These results suggest that the divergent glottal angle is large enough that the flow separates from the slanted wall upstream in the glottis under either circumstance of flow direction. Also supporting this notion of an upstream flow separation is the observation that in both **Figure 3.24** and **Figure 3.25** the pressure distribution is flatter for the divergent side and tends to increase (called "pressure recovery") more so for the vertical wall. That is, the relatively flat distribution on the divergent wall is a consequence of this typical assumption often made for pressures downstream of a flow separation point in a diverging duct; however, here the duct is not symmetric, and the vertical side imposes novel characteristics on the flow, governing the pressures on the vertical wall. In addition, the more rounded pressure distribution near glottal entry for the slanted wall also may suggest flow separation upstream in the glottis.

Figure 3.25 Comparison of the pressure distributions on the slanted wall as the flow wall and on the vertical wall as the non flow wall for a +10 degree diverging glottal configuration at 0.16 cm diameter across 7 different transglottal pressures.

3.3.3 Comparison of Pressure Distributions across Glottal Diameters for the Diverging +10

Degree Glottis

Similar to the -10 degree converging case discussed above, only the 10 cm H_2O pressure

drop case will be reported here; the remaining transglottal pressure cases can be found in

Appendix D. As **Figures 3.26 to 3.29** indicate, an increase in the glottal diameter results in lower

pressures on the inferior vocal fold surface (taps 1-5). This is shown by the data for the 0.16 cm

case, which is lower than for the other two diameters. The highest subglottal pressures are for the

smallest diameter (0.01 cm). For the smallest diameter the pressure distributions are similar

across the conditions, with the interesting finding that the vertical wall has it lowest pressures at

tap 7 and the divergent slanted wall has its lowest pressures at tap 6 where the minimal diameter

is located. The effect of the asymmetry can be seen by comparing **Figure 3.26** with **Figure 3.28,**

where the pressure distributions are nearly alike for the 0.01 cm and 0.04 cm diameters, but for

the largest diameter 0.16 cm, the pressures are lower on the vertical flow wall (below the

downstream pressure at tap 16) and higher on the slanted divergent non flow wall (essentially

equal to the downstream pressure at tap 16). When the flow wall is the divergent wall, **Figures**

3.27 and 3.28 there is relatively little difference between the two glottal walls relative to the

pressure distributions. Thus, the flow bistability is important for the largest glottal diameter, but

less so for the smaller diameters, and the diameter itself is more important, so for the largest

diameter and not as important for the smaller diameters, for the +10 degree divergent glottis with
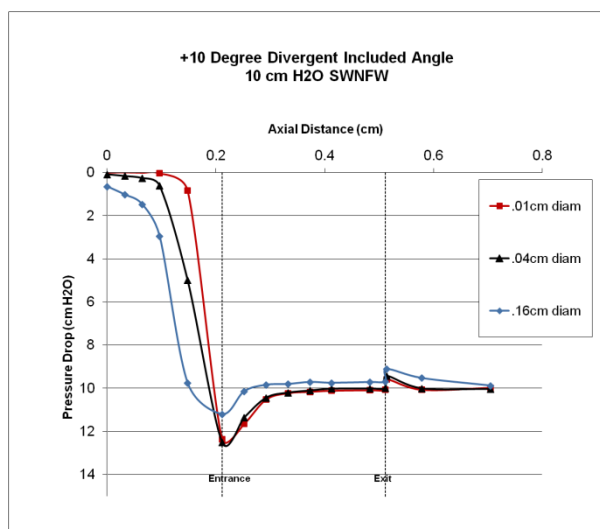
one wall vertical.
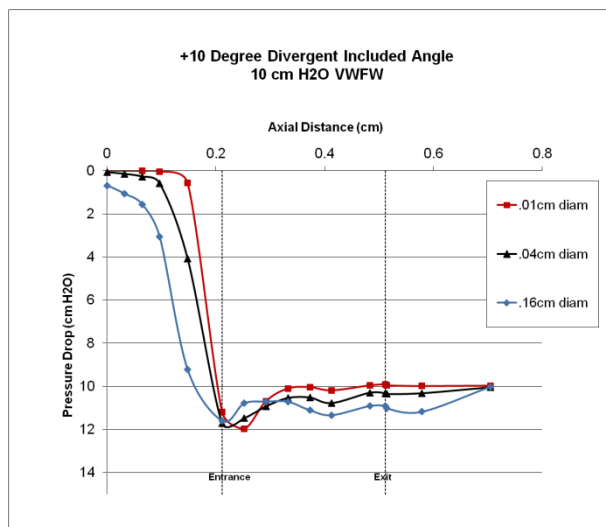
Figure 3.26 Comparison of the pressure distributions for three glottal diameters for a 10 cm H_2O transglottal pressure when the vertical wall was the flow wall (VWFW) for a +10 degree diverging glottis.
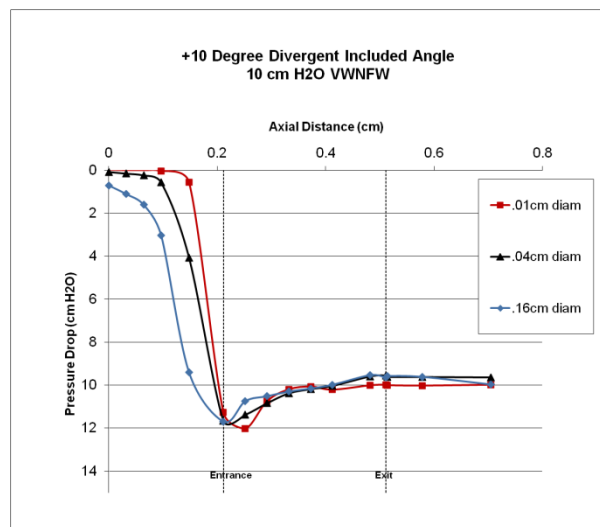
Figure 3.27 Comparison of the pressure distributions for three glottal diameters for a 10 cm H_2O transglottal pressure when the vertical wall was the non flow wall (VWNFW) for a +10 degree diverging glottis.
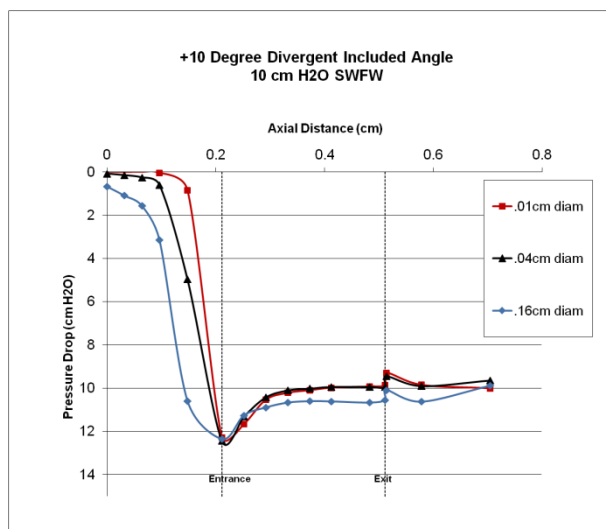
Figure 3.28 Comparison of the pressure distributions for three glottal diameters for a 10 cm H_2O transglottal pressure when the slanted wall was the flow wall (SWFW) for a +10 degree diverging glottis.

Figure 3.29 Comparison of the pressure distributions for three glottal diameters for a 10 cm H_2O transglottal pressure when the slanted wall was the non flow wall (SWNFW) for a +10 degree diverging glottis.

CHAPTER 4. DISCUSSION

4.1 Pressures and Flows

In this study, the hemilarynx condition has been described (that is, with one side always vertical), the data collection procedures using Plexiglas model M5 have been discussed, and data from the 0.01 cm, 0.04 cm, and 0.16 cm glottal diameter cases have been reported for a 0 degree uniform case, the -10 degree converging case, and the +10 degree diverging case for diameters of 0.01 cm and 0.16 cm. It is now important to review the implications that the corresponding data may suggest in regards to the asymmetric forces present within the hemilarynx condition. Several comparisons of the pressure distributions for each glottal angle used (0, -10, +10 degrees) at each individual glottal diameter (0.01 cm, 0.04 cm, 0.16 cm) are thus necessary to provide insight into the pressure patterns that arise during phonation in a hemilarynx.

With respect to the role that glottal diameter plays in determining the airflows, it is clear that in order to produce the same transglottal pressure drops within the model, larger glottal diameters demand larger volume flows than smaller glottal diameters (because larger diameters tend to offer less flow resistance). **Figure 4.1** is a pressure versus flow graph, where each of the glottal angles is shown at each of the glottal diameters, and the flow values are the average of the flow wall and non flow wall runs for the same glottal geometry. The figure shows that the flows were greater for the larger diameters at all three glottal angles, indicating less flow resistance at larger glottal diameter. In addition, the uniform glottis produced the smallest flows for the same transglottal pressures for the 0.01 cm and 0.04 cm diameters, but not for the largest diameter used, where it appears that the uniform duct produces slightly less flow resistance than the convergent and divergent cases (these data are consistent with those in Fulcher *et al.*, 2006). The divergent and convergent cases of this study (remembering that the configuration is

Transglottal Pressure vs. Volume Flow
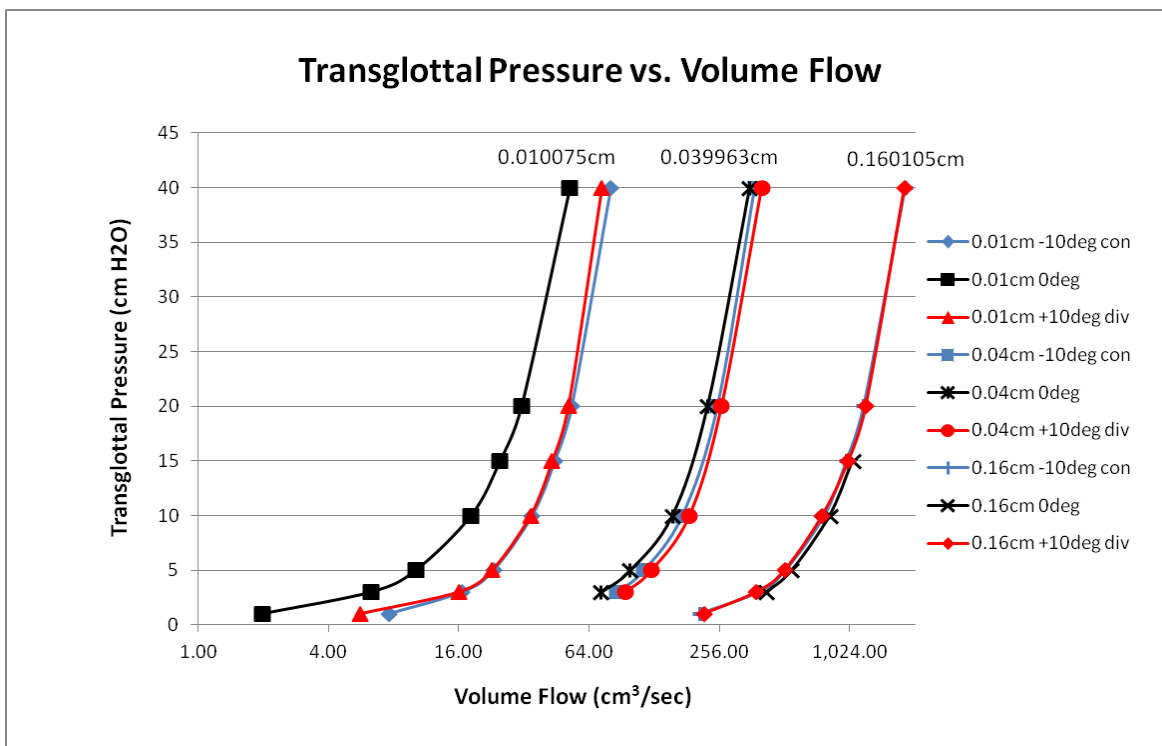
Figure 4.1 Pressure versus flow relationships for the three glottal angles at three glottal diameters.

asymmetrical with one vertical wall) show about the same flows (and therefore the same flow resistance) for each of the three diameters taken separately, whereas for the symmetric glottis at +10 and -10 degrees, the flow resistance is less for the divergent glottis (Fulcher *et al.*, 2006; Scherer & Fulcher 2016). Thus, the asymmetry of having a vertical glottal wall alters the flow resistance compared to the symmetric glottis of the same angle, changing expectations about the flow resistance difference between -10 and +10 degrees.

Relative to the bistability of the flow, does bistability of the flow affect the intraglottal pressures? There is negligible difference in the pressure distributions for the 0.01 cm diameter for the uniform case, and thus bistability has little effect for this case. For the -10 degree convergent case for a diameter of 0.01 cm (**Figures 3.14 and 3.15**), the convergent glottal side had slightly lower intraglottal pressures and the negative pressure dip near glottal exit further

from the glottal exit. Thus, for the convergent angle, there was slightly less outward pressure on the convergent wall than on the vertical wall, which seems counterintuitive (and thus computational work for that configuration is necessary in order to obtain a better understanding of this phenomenon). However, relative to bistability, a comparison between **Figures 3.14 and 3.15** indicates negligible differences in the pressure distributions, and thus the differences are not due to bistability but due to configuration asymmetry. Similarly for the +10 degree divergent glottis, for the relatively narrow 0.01 cm diameter, the slight differences in the pressure distributions on the vertical wall and the divergent wall are about the same for both flow directions, and again bistability has little effect. The primary effect is the asymmetric configuration. Bistability may have little effect due to the relatively smaller flows (and lower Reynolds numbers) such that the flow remains laminar within the glottis when the diameter is 0.01 cm (the highest Reynolds number across all 0.01 cm conditions was only 450).

Effects of bistability were present for the other two diameters, 0.04 cm and 0.16 cm. For the 0.04 cm convergent case, the asymmetry resulted in lower intraglottal pressures on the vertical wall when flow was along that wall (**Figures 3.18 and 3.21**), and also lower pressures on the vertical wall when it was the non flow wall (**Figures 3.19 and 3.20**), again suggesting that bistability occurred, but that it had relatively little effect, whereas the asymmetry produced the primary effect of altering the intraglottal pressures. For the largest diameter, 0.16 cm, and the convergent case, the results were quite similar, with one variation: the pressures were always lower on the vertical wall side except for the downstream half of the glottis when the flow wall was the divergent side (**Figures 3.18 – 3.21)**. For the divergent cases, the pressure distributions on the two glottal sides for the diameter of 0.04 cm were nearly identical regardless of the directionality of the flow (**Figures 3.26-3.29)**, suggesting that for this asymmetric configuration

the 0.04 cm diameter condition does not create significant pressure differences within the glottis despite the asymmetry and bistability. However, for the larger diameter of 0.16 cm and the divergent glottis, the bistability created pressure distribution *reversals*, where for the condition of flow along the vertical wall, the pressures along that wall were lower than along the divergent wall (by 15% or more of the transglottal pressure), and when the flow was along the divergent wall, THAT wall had the lower pressures, and the differences (of about 20-30% of the transglottal pressure) were throughout the glottis (**Figures 3.24-3.29**).

It is known that there is indeed a bistable condition of the flow for a 0.04 cm diameter glottis at most glottal angles (Thapa 2005). This condition is also observed in the 0.16 cm diameters of the present study. This is reasonable since as the glottal diameter increases, the volume flows increase as well, with greater inertial forces throughout the glottis. It is therefore inferred that between the glottal diameters 0.01 cm and 0.04 cm there is a location where a bistable condition of the fluid flow begins to be present at particular glottal angles.

In order to examine the relationships among the different diameters in regards to flows, it is important to examine the differences in the pressure distributions at each respective glottal diameter. Following the example of Chapter 3, the 10 cm H_2O transglottal pressure drops will be used to make the necessary geometrical comparisons. The first situation to compare for each of the glottal diameters is the vertical wall as the flow wall. **Figure 4.2** shows each of the pressure distributions for the three glottal angles in the 0.01 cm diameter case while flow is directed along the vertical wall. At the glottal entrance, the greatest differences in pressure are present as a consequence of the geometry of each glottal angle. The pressure distributions therefore reach the proximity of the supraglottal pressure more upstream based on the location of the minimal average diameter of the glottis, which changes location axially based on the glottal angle. This

trend is also noticeable in **Figure 4.3** for the 0.04 cm diameter case and in **Figure 4.4** for the
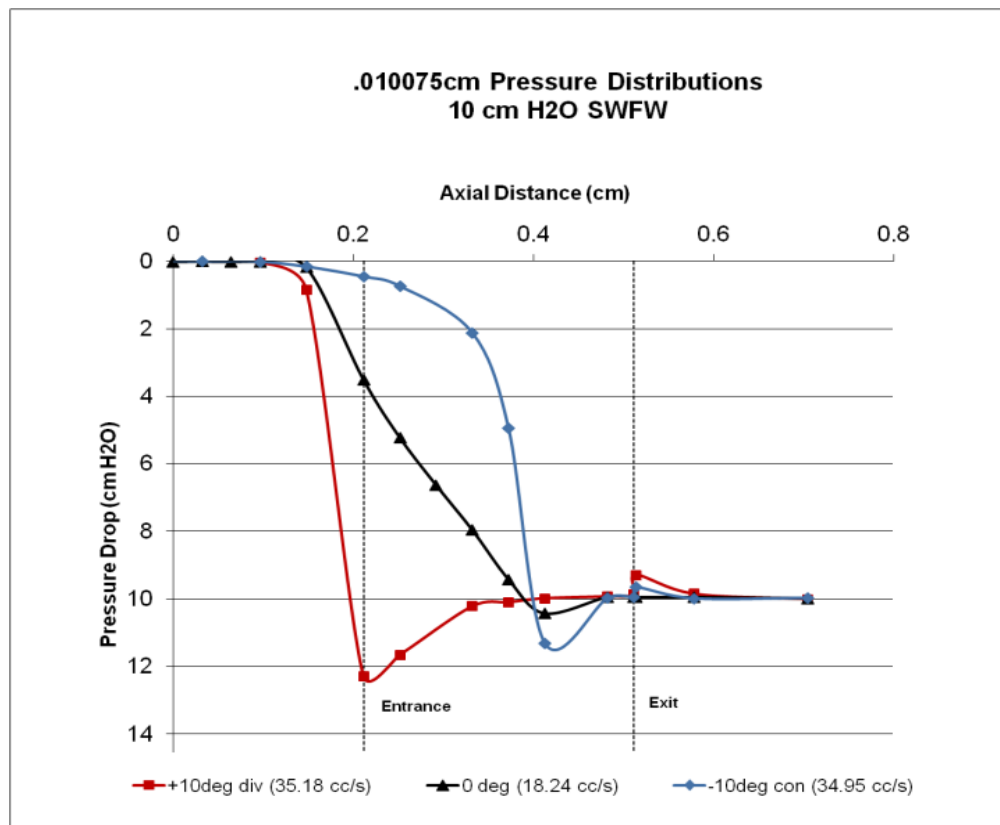
0.16 cm diameter case.
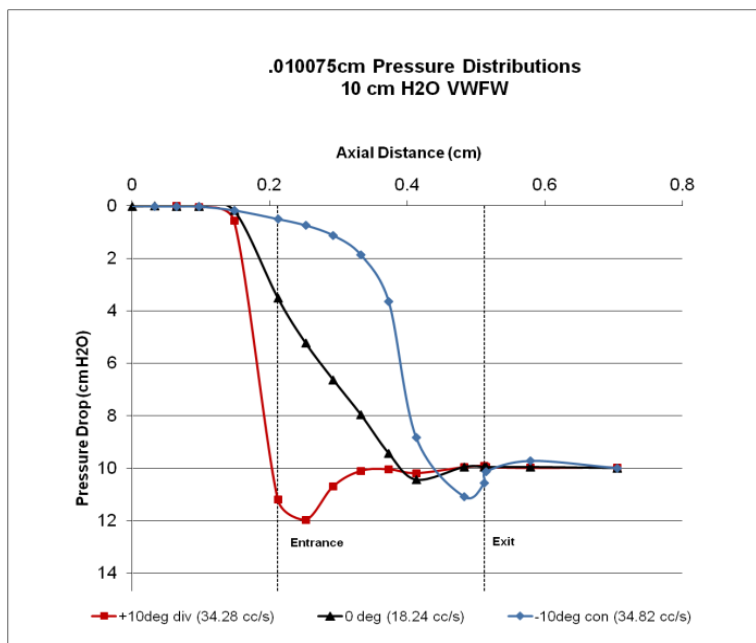
Figure 4.2 Comparison of the glottal angles when the VW is the FW at the 0.01 cm diameter.
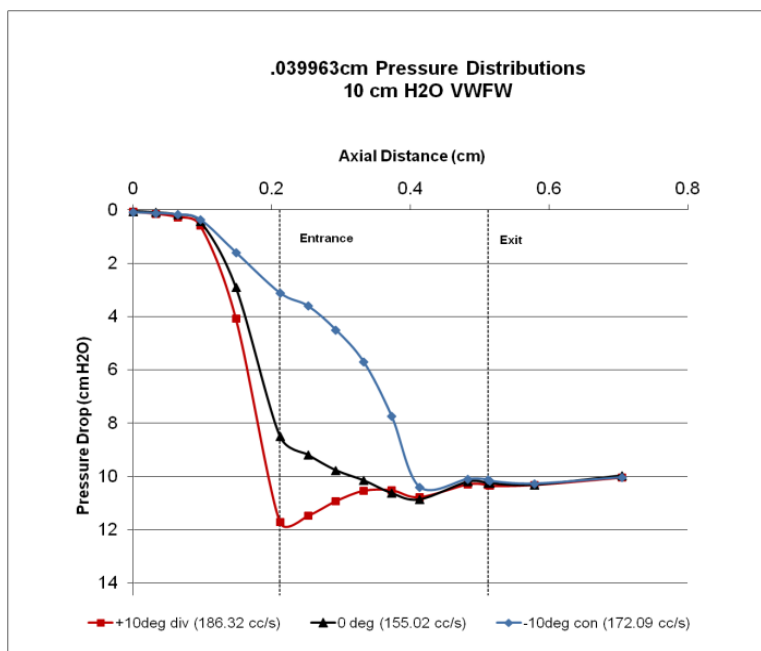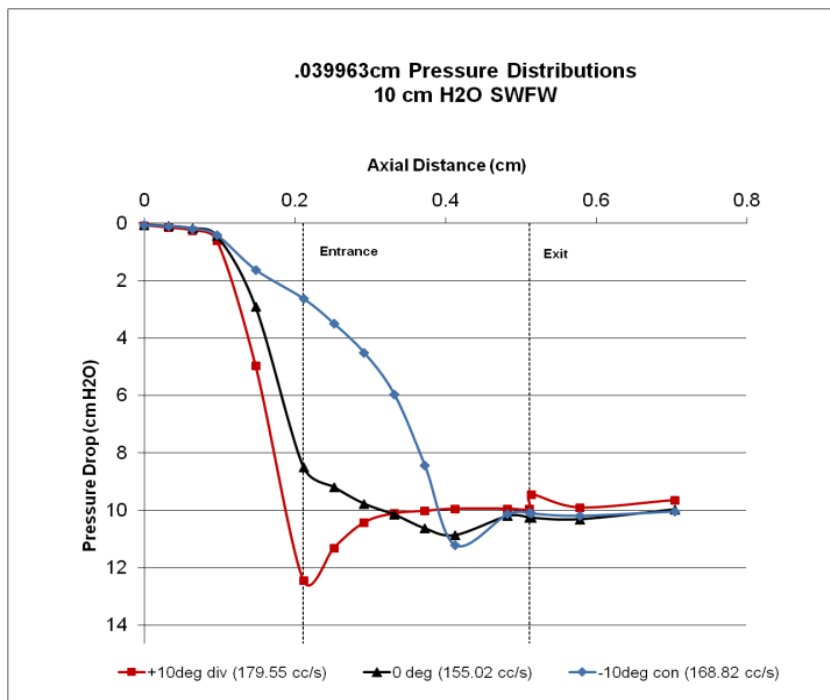

Figure 4.3 Comparison of the glottal angles when the VW is the FW at the 0.04 cm diameter.
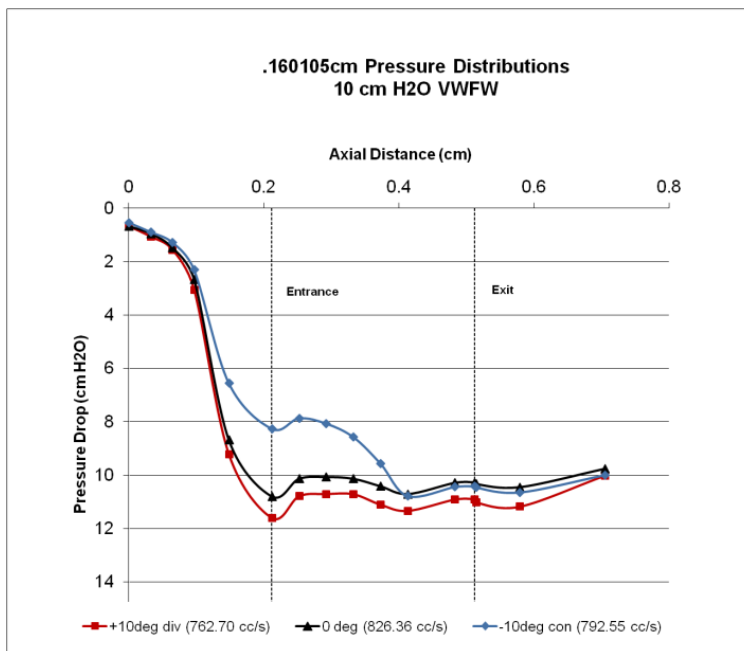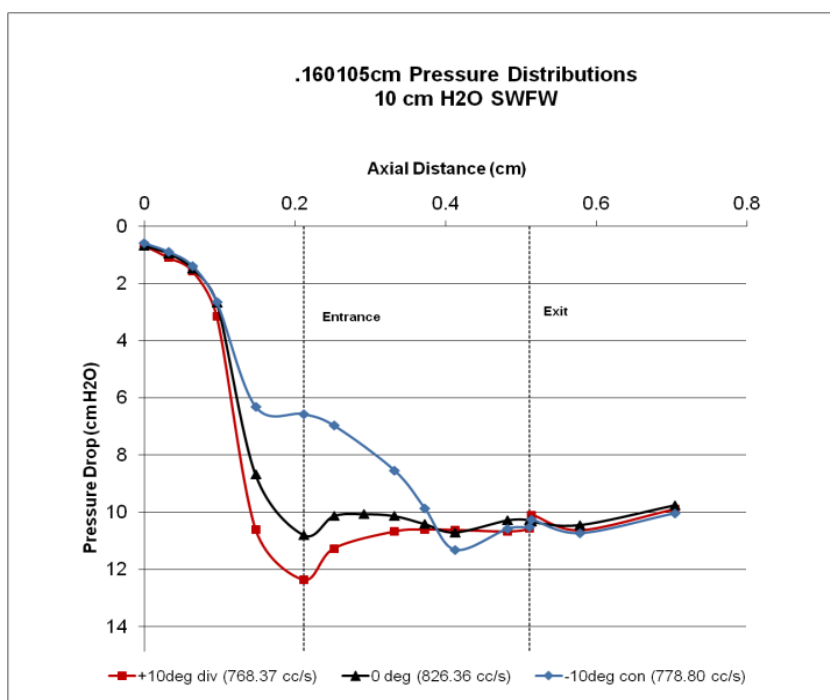
Figure 4.4 Comparison of the glottal angles when the VW is the FW at the 0.16 cm diameter.

In comparison of the three figures, it appears that as the glottal diameter increases, the pressure distributions also reach the proximity of the supraglottal pressure at shorter axial distances. This general behavior of the pressure distributions makes sense, since as the glottal diameter increases, the ratio of the glottal cross-sectional area to the cross-sectional area of the wind tunnel decreases. The slight change of glottal angle will in turn affect the pressure distributions less at larger diameters because in relation to the length of the glottis, the change in cross-sectional area at different locations inside the glottis is less of a proportional change. To again point out key differences between the vocal fold walls, **Figures 4.5**, **4.6**, and **4.7** show the glottal angles at each of the glottal diameters when the slanted wall is the flow wall. When comparing the three figures where flow is directed along the vertical wall with the three figures where flow is directed along the slanted wall, the largest differences can be seen at the 0.16 cm diameter. At this particular glottal diameter, the -10 degree converging case shows clear differences between the vertical wall and the slanted wall at the glottal entrance. Specifically at

pressure tap 6, the vertical wall experiences a larger pressure drop, suggesting that there is a

faster fluid flow by this tap. At pressure tap 6 on the slanted wall, there instead seems to be a

plateau from tap 5 to tap 6, suggesting that the flow is impacting the surface at the entrance.

Following this point the pressures gradually increase throughout the remainder of the glottis as

the flow is funneled in by this wall.

Figure 4.5 Comparison of the glottal angles when the SW is the FW at the 0.01 cm
diameter.

Figure 4.6 Comparison of the glottal angles when the SW is the FW at the 0.04cm diameter.

Figure 4.7 Comparison of the glottal angles when the SW is the FW at the 0.16 cm diameter.

4.2 Full Larynx and Hemilarynx Comparison

One of the key questions of this study is what differences are present in the asymmetric forces existing between a healthy regular larynx and a hemilarynx. Reports have been made previously in regards to Titze's hypothesis of functional similarity that the pressures found in a hemilarynx parallel the pressures one would find in a full larynx, but at half the flows (Titze 1993). Fulcher *et al.* were able to determine that there is indeed a functional similarity between both a full larynx and a hemilarynx using data obtained by Thapa (2005) and the computational package FLUENT (Fulcher *et al*. 2010). Instead of reporting the same functional similarity reported in the past for the new hemilarynx data at the smaller 0.01 cm diameter and the larger 0.16 cm diameter, the asymmetric hemilarynx will be compared to a full larynx of the same size diameter. The volume flows should therefore be roughly the same in each case, rather than being half of the value.

Figures 4.8, **4.9**, **4.10**, and **4.11** show full larynx versus hemilarynx comparisons of four pressure distributions for each of the following: -10 degree converging glottis at 0.01 cm diameter, +10 degree diverging glottis at 0.01 cm diameter, -10 degree converging glottis at 0.16 cm diameter, and +10 degree diverging glottis at 0.16 cm diameter. For each of these figures, the full larynx data (Scherer unpublished data 2012) presented was that on the flow wall. To make appropriate comparisons to a hemilarynx, the pressures along the slanted wall were used, representing the existing vocal fold tissue. The pressure values used were also those when flow was directed along the slanted wall.

First, examining the 0.01cm diameter cases, there are only very small differences in the diverging case. In the converging case, however, there is a noticeable shift in location within the glottis where the greatest pressure drop occurs. For the full larynx, the greatest pressure drop is

located at tap 11, but for the hemilarynx, the greatest pressure drop is located at tap 12, closer to the glottal exit. Although this is only a slight difference in the magnitudes of the pressure minima, it does show an important difference in the asymmetric forces for a full larynx and a hemilarynx present during vocal fold oscillation. In the figures for the 0.16 cm diameter case, there are several interesting differences in the pressure distributions. First, in the -10 degree converging case, the pressures at tap 6 (glottal entrance) seem to be lower in the full larynx than in the hemilarynx. This could suggest that instead of the opposing wall having a mirrored shape, by bringing the glottal angle of the opposing wall closer to the midline, the flow at glottal entrance actually favors the vertical wall. This could be due to viscous effects of some kind, where the flow tends to create an adhesion to the vertical wall first, but then later favors the slanted wall.

Second, it can be seen that the pressures for the hemilarynx are not very different from those of the full symmetric larynx (except for the 0.16 cm diameter divergent case at the highest transglottal pressure, where the hemilarynx pressures are lower). Because of the small number of transglottal pressure drops at which data were collected, this raises a question about the 0.16 cm diameter hemilarynx. Would the pressure differences between the full larynx and the hemilarynx increase at larger transglottal pressure drops and larger diameters? It certainly seems as though this could be the case; however, the only way of answering this question would be to collect a more complete set of data.
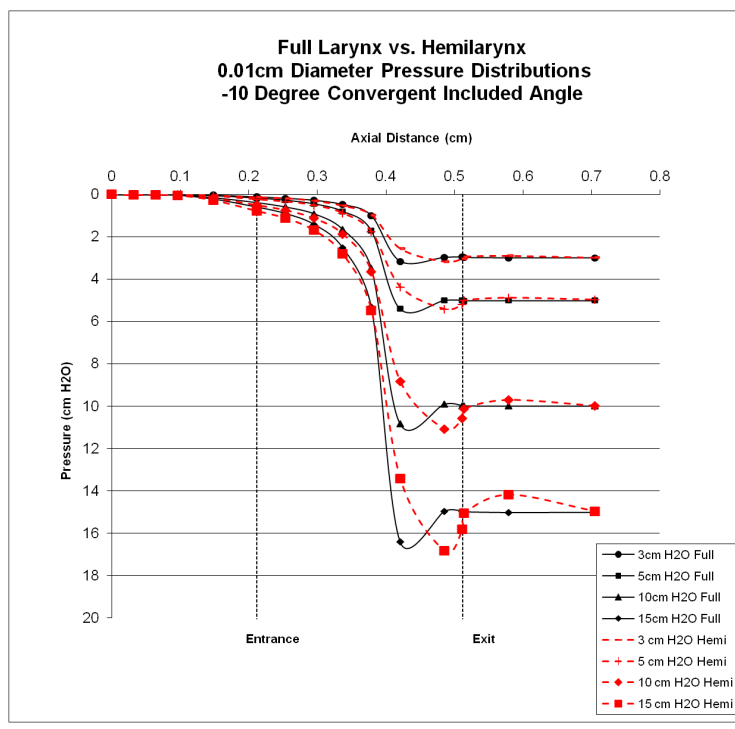
Figure 4.8 Full larynx and hemilarynx comparisons of -10 degree convergent pressure distributions at 0.01 cm.
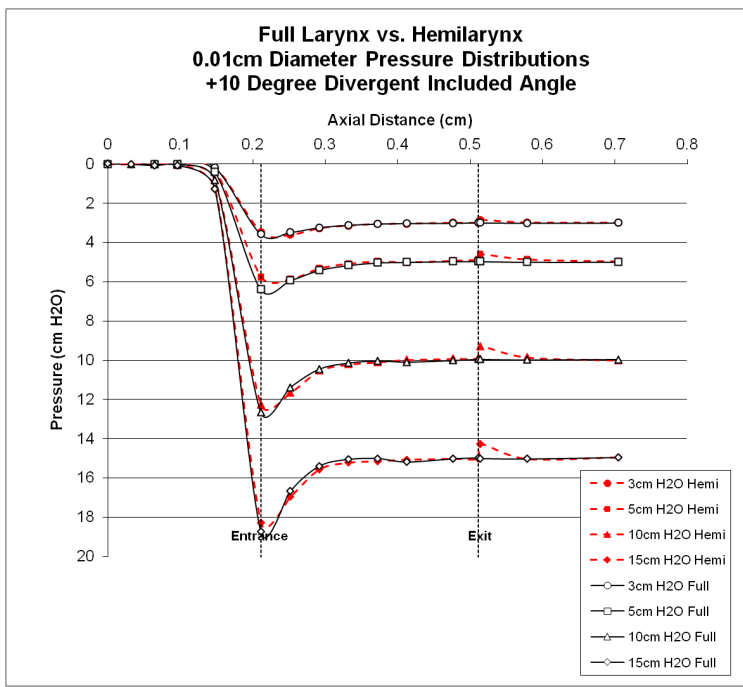
Figure 4.9 Full larynx and hemilarynx comparisons of +10 degree divergent pressure distributions at 0.01 cm.
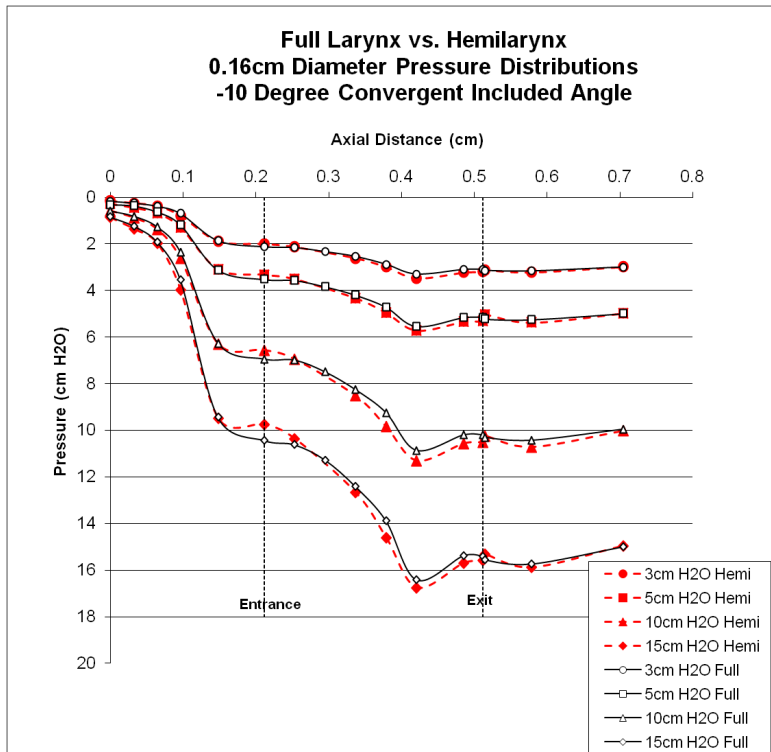
Figure 4.10 Full larynx and hemilarynx comparisons of -10 degree convergent pressure distributions at 0.16 cm.
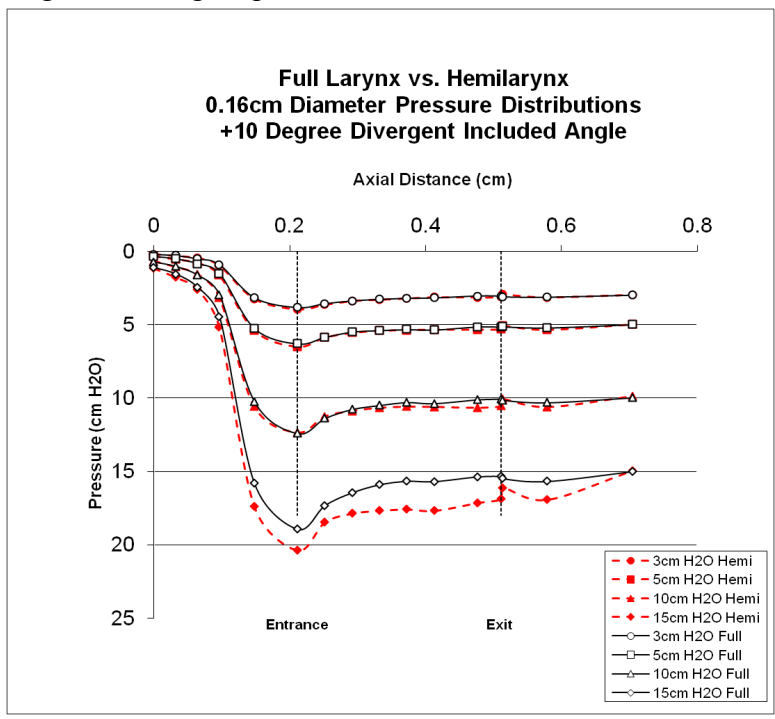
Figure 4.11 Full larynx and hemilarynx comparisons of +10 degree divergent pressure distributions at 0.16 cm.

CHAPTER 5. CONCLUSIONS

The goal of using a "hemilarynx" configuration in a physical model was to mimic (to a first approximation) the larynx of an individual for whom one vocal fold has been removed and has been replaced by a vertical side, where the other vocal fold is healthy and can vibrate with relatively normal variation of motion and contour. The more general goal with the glottal configurations used in this study was to research the pressure differences upon the two glottal sides for a wide range of asymmetric glottal configurations. It is noted that the three angles (zero, -10, +10 degrees) and three glottal diameters (0.01, 0.04, 0.16 cm) used in this study are considered to be rather typically within the vibratory pattern of most cycles of normal phonation, as well as for the hemilarynx situation. The asymmetry with a vertical wall will be present within certain vibratory patterns where obliquity of the glottis (that is, where the midline of the glottis is not vertical) prevails. Thus, this study continues the area of research of asymmetric pressures for asymmetric glottal shapes in order to determine the asymmetric driving forces upon the two vocal folds. This then continues to address the problem of how to mechanically understand the driving forces on the vocal folds and the resulting vibratory motion when the data presented here (and in other studies) are implemented into multimass models of phonation.

From studying the pressure and flow relationships using model M5 in this study, pressure distributions were produced under constant flow conditions for three glottal diameters and three glottal angles. The following conclusions can be drawn:

1. Strong replication of data using the physical model M5 was possible, suggesting that carful use of the model results in duplication of results over time.

2. The larger the glottal diameter, the less flow resistance is present within the model, and the greater the fluid flows required to reach the desired transglottal pressures.

3. Bistability of the fluid flow has less effect on the pressure distributions measured in a hemilarynx than the asymmetry of the glottis does, especially at smaller glottal diameters.

4. For the small diameter (0.01 cm), pressures measured along the convergent flow wall are lower than on the vertical wall, but similar on both sides for the divergent glottis.

5. For the larger (0.16 cm) glottal diameter for the convergent glottis, where bistability is an important factor, the pressures are lower (20% of the transglottal pressure) on the vertical wall when the vertical wall is the flow wall, but higher upstream then lower downstream in the glottis when the flow is along the slanted convergent wall.

6. For the larger (0.16 cm) glottal diameter for the divergent glottis, again where bistability is important, lower pressures (15% of the transglottal pressure) are on the vertical wall when it is the flow wall, and lower pressures (25% of the transglottal pressure) are on the slanted wall when it is the flow wall.

7. Pressures in the symmetric full larynx of the same diameters and angle tend to be similar to the pressures in the hemilarynx cases of this study, with minor variations.

It is noted that one important application of the data presented here is to estimate the dynamic pressures in an excised larynx setup where there are pressure taps built into the vertical wall opposite the vibrating larynx (as in Alipour & Scherer, 2001), and the pressures on the vertical wall are estimates of the pressures on the dynamic vocal fold. The study here suggests that the pressures will be approximately correct when the diameters are small, but up to 25% or so incorrect for larger diameters. For larger diameters it is fortunate that recoil forces will be greater than aerodynamic forces, and thus poorer pressure estimates will not play such an important role.

A primary goal is to incorporate the pressures of this study into a larger table ("lookup table") within a multimass model of phonation to determine the vibratory effects of the

asymmetric pressures during asymmetric vibratory motion. An important question to answer is

"Do the pressures within asymmetric configurations tend to force greater symmetry of motion or

enhance the asymmetric motion"? Such questions require further study of more glottal

configurations.

REFERENCES

Alipour, F., Scherer, R. C. (**2000**). "Dynamic glottal pressures in an excised hemilarynx model," J. Voice **14** (4), 443-454.

Alipour, F., Scherer, R. C. (**2002**). "Pressure and velocity profiles in a static mechanical hemilarynx model," J. Acoust. Soc. Am. **112,** 2996-3003.

Fulcher, L. P., Scherer, R. C., Zhai G., and Zhu Z., (**2006**). "Analytic representation of volume flow as a function of geometry and pressure in a static physical model of the glottis," J. of Voice, 20/4, 489-512.

Fulcher, L. P., Scherer, R. C., De Witt, K. J., Thapa, P., Bo, Y., Kucinschi, B. R., (**2010**). "Pressure Distributions in a Static Physical Model of the Hemilarynx: Measurements and Computations," J. Voice **24**, 2-20

Ishizaka, K., and Flanagan, J. L. (**1972**). "Synthesis of vocal sounds from a two mass model of the vocal folds," Bell Sys. Tech. J. **51**, 1233-1268.

Ishizaka, K., and Matsudaira, M. (**1972**). "Fluid mechanical considerations of vocal cord vibration," SCRL Monograph Number 8.

Jiang, J., and Titze, I. R. (**1993**). "A methodological study of hemilaryngeal phonation," Laryngoscope **103,** 872-882.

Scherer, R. C. and Fulcher, L. P., (**2016**). "Divergent or convergent glottal angles: Which give greater flow?", 10th International Conference on Voice Physiology and Mechanics, Vinq Del Mar, Chile, March 14-17.

Scherer, R. C., Shinwari, D., De Witt, K., Zhang, C., Kucinschi, B. R., and Afjeh, A. (**2002**). "Intraglottal pressure distributions for a symmetric and oblique glottis with uniform duct (L)," J. Acoust. Soc. Am**. 112**, 1253-1256.

Scherer, R. C., Shinwari, D., De Witt, K., Zhang, C., Kucinschi, B., and Afjeh, A. (**2001**).

"Intraglottal pressure profiles for a symmetric and oblique glottis with a divergence

angle of 10 degrees," J. Acoust. Soc. Am. **109**, 1616-1630.

Thapa, P. (**2005**). "Pressure Distributions in a Static Hemilarynx Model," Masters Thesis.

Bowling Green State University.

Titze, I. R. (**1993**). "Current topics in voice production mechanisms," Acta Otolaryngol

(Stockh.), **113**, 421-427.

van den Berg, J., Zantema, J. T., and Doornenbal, P. (**1957**). "On the air resistance and the

Bernoulli effect of the human larynx," J. Acoust. Soc. Am. **29**, 626-631.

APPENDIX A. CALIBRATION OF THE PRESSURE TRANSDUCERS

This appendix supplies calibration figures for each of the Validyne pressure transducers

DP103-10 and MP45-16, at each of the signal conditioners gain settings. The figures below show

comparisons between the new calibration equations and the previous calibrations from 2011

made by Jason Whitfield (Whitfield 2011).
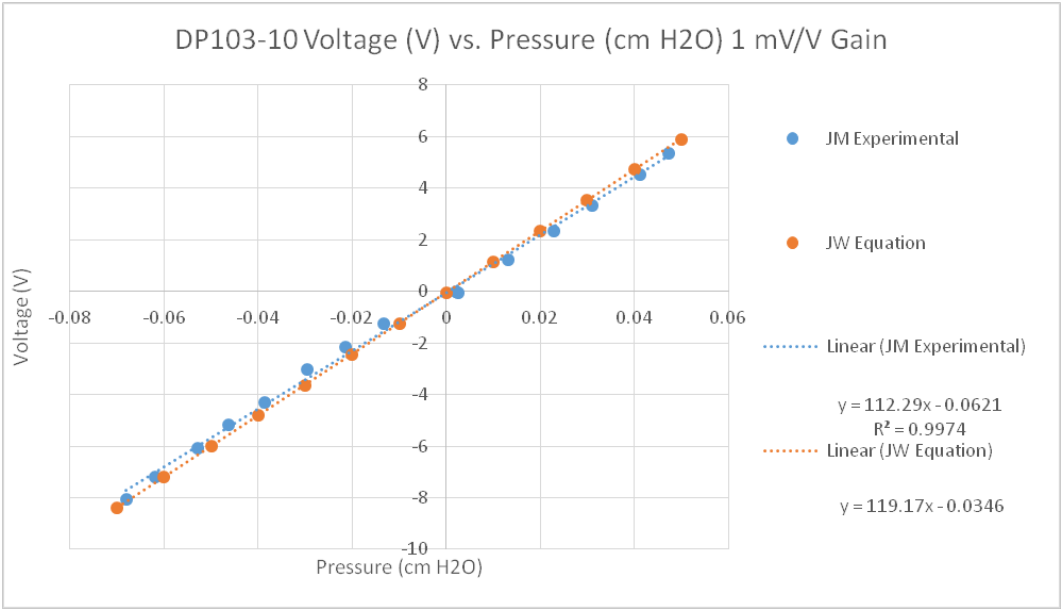
Figure A1 1 mV/V gain calibration for DP103-10.
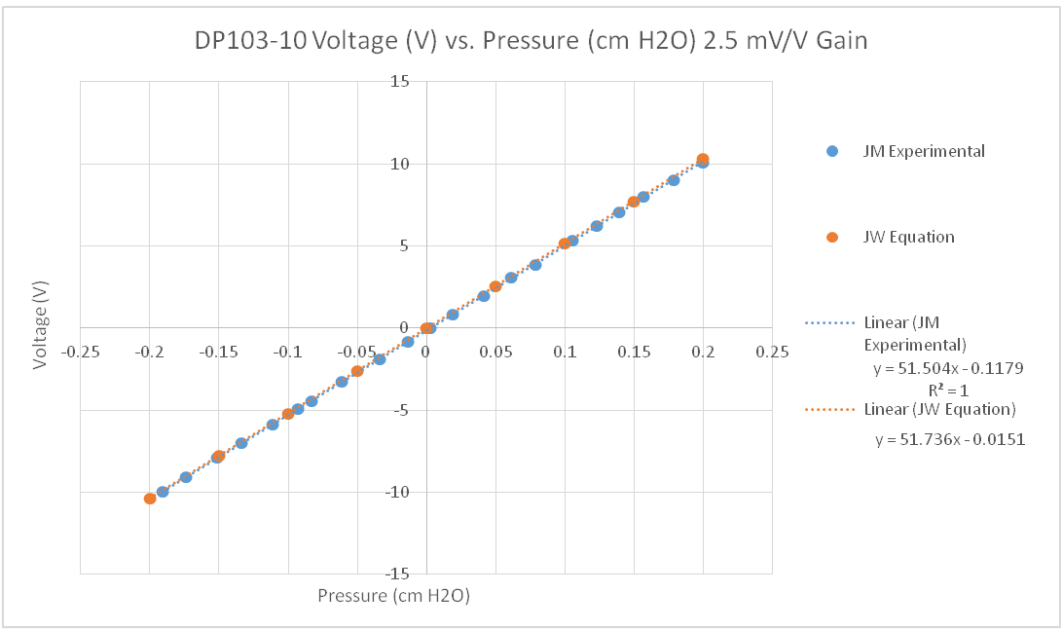
Figure A2 2.5 mV/V gain calibration for DP103-10.
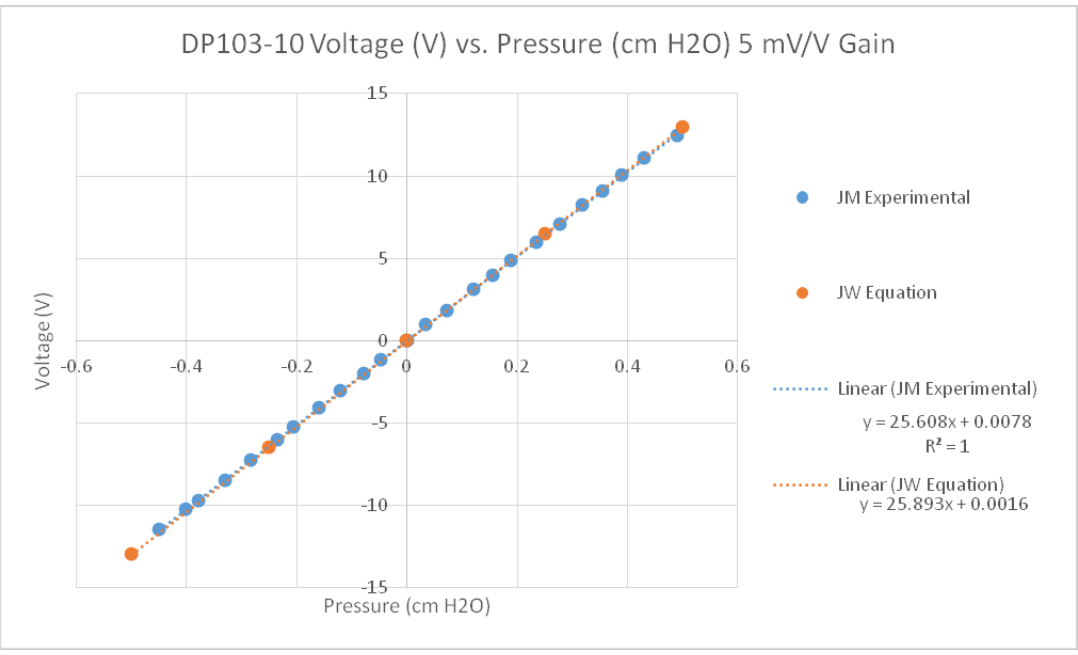
Figure A3 5 mV/V gain calibration for DP103-10.
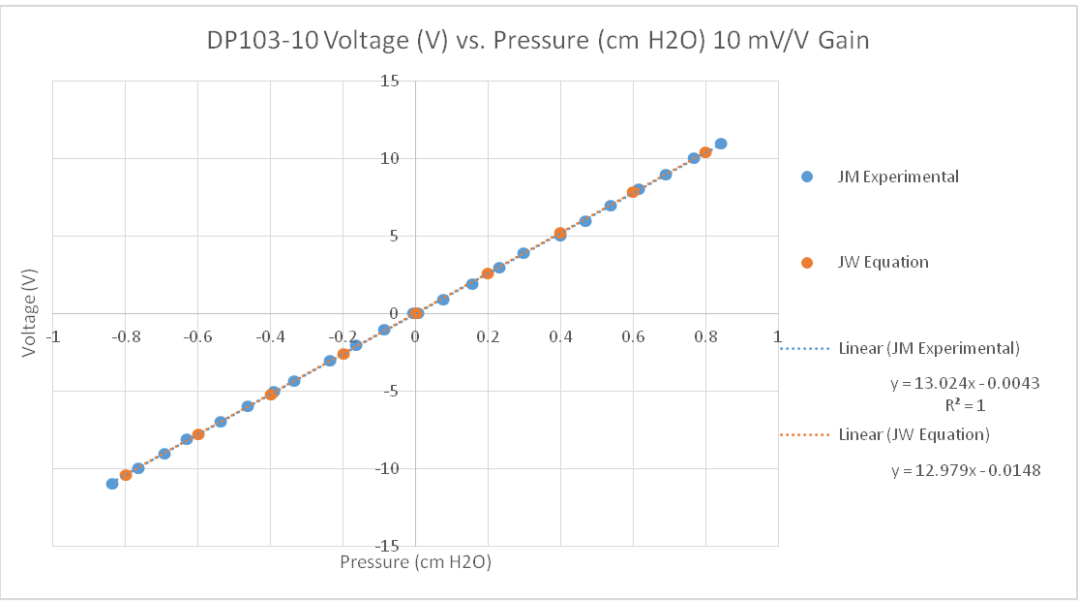
Figure A4 10 mV/V gain calibration for DP103-10.
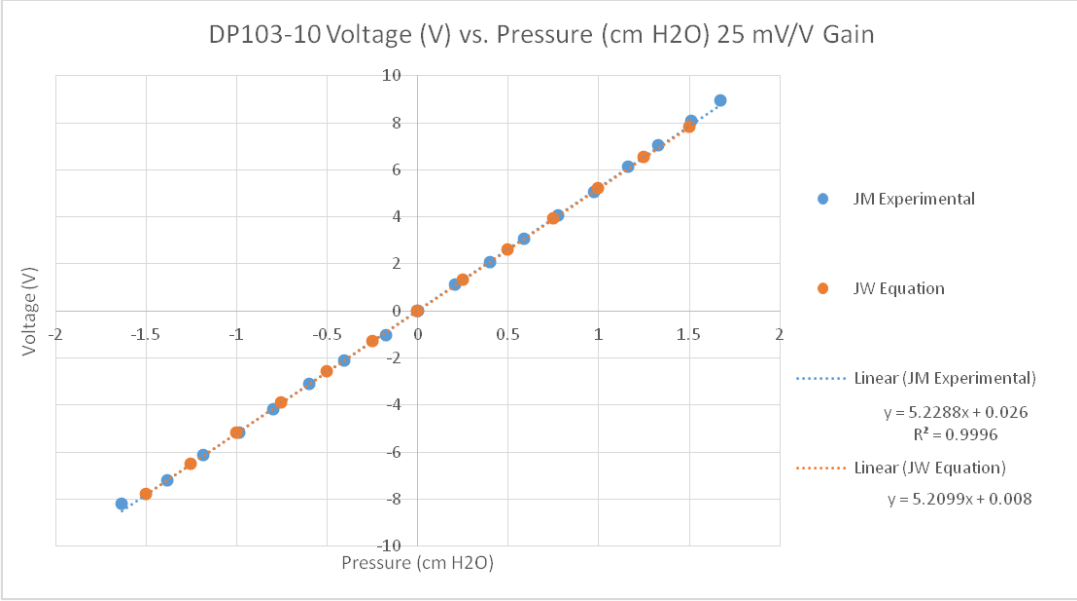
Figure A5 25 mV/V gain calibration for DP103-10.
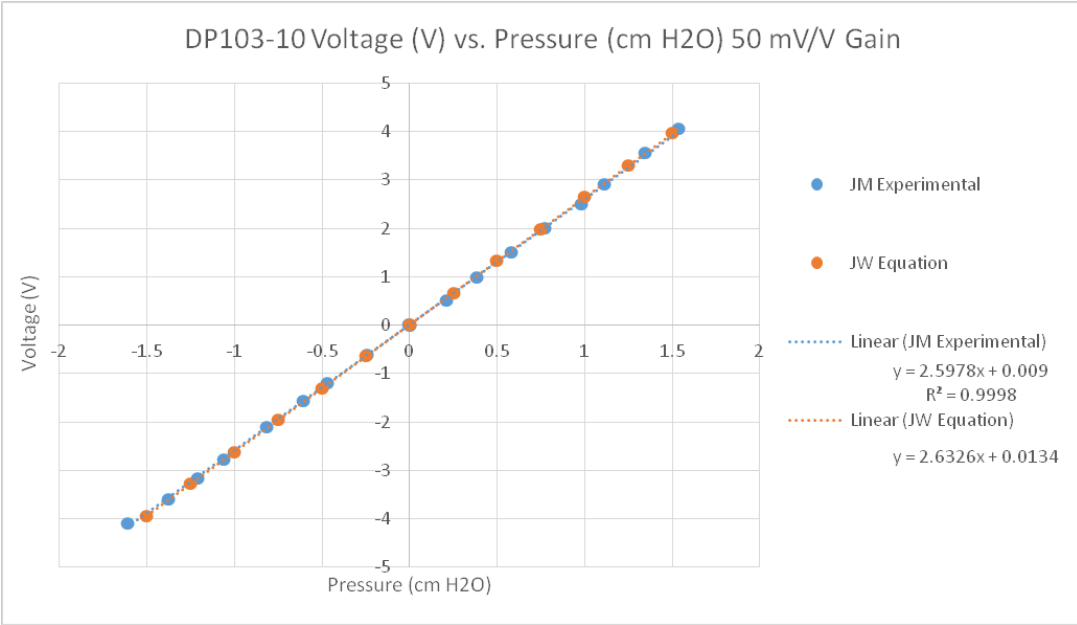
Figure A6 50 mV/V gain calibration for DP103-10.
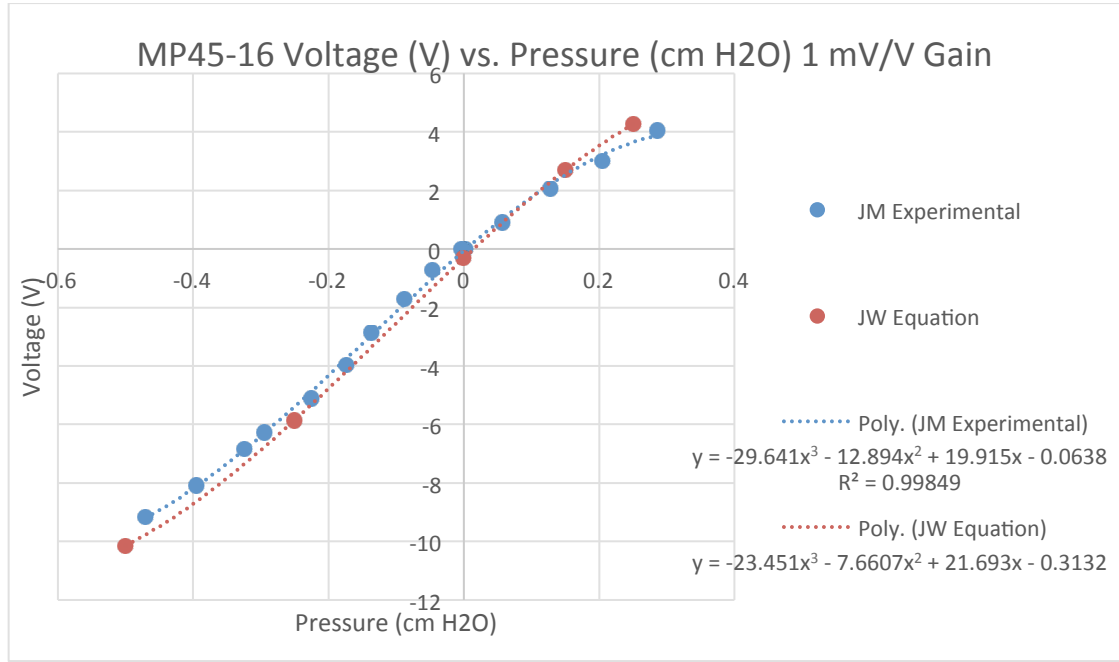
Figure A7 1 mV/V gain calibration for MP45-16.
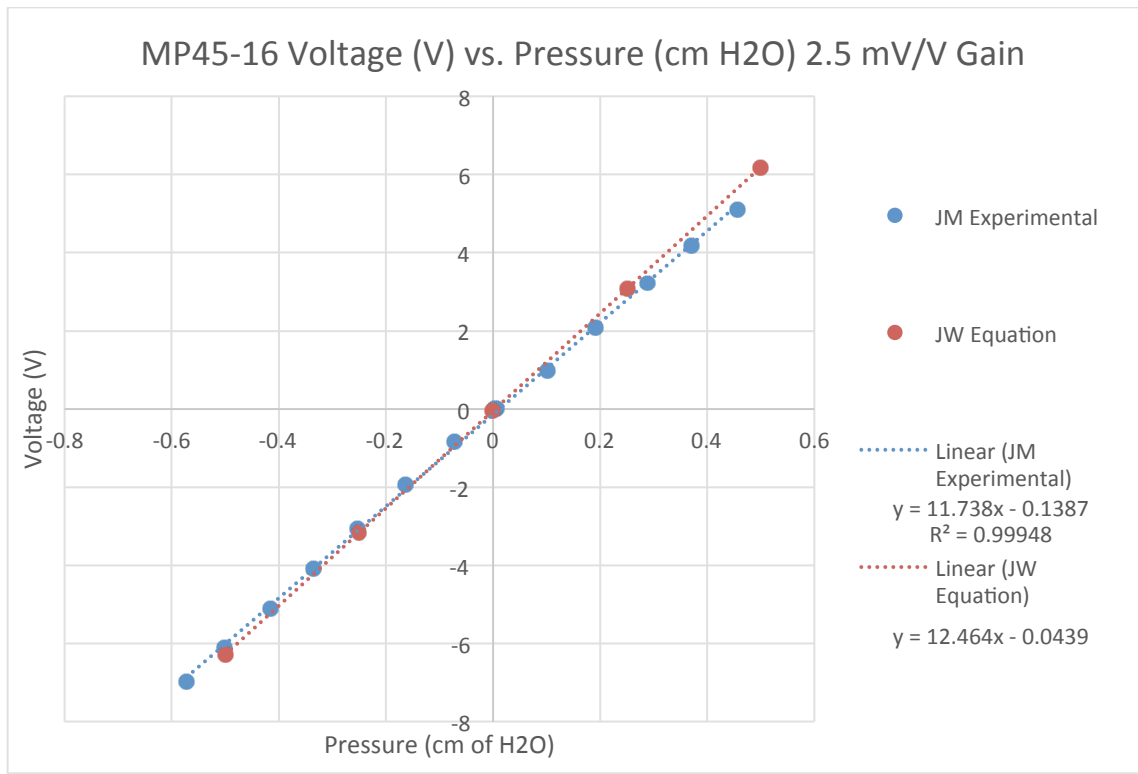
Figure A8 2.5 mV/V gain calibration for MP45-16.
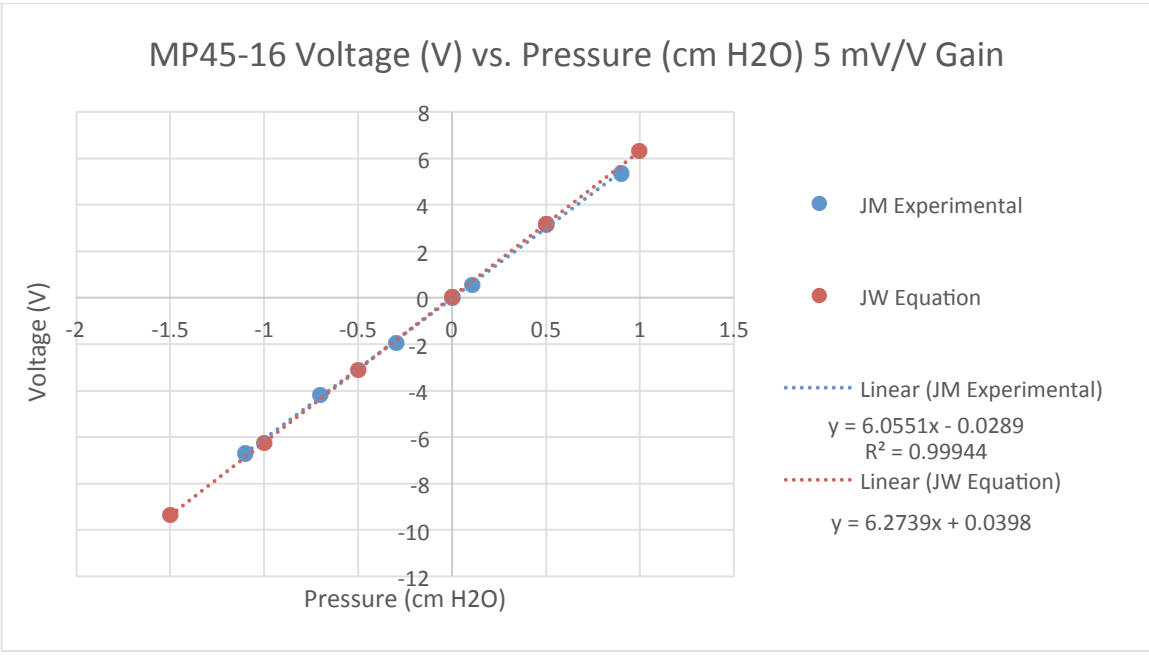
Figure A9 5 mV/V gain calibration for MP45-16.
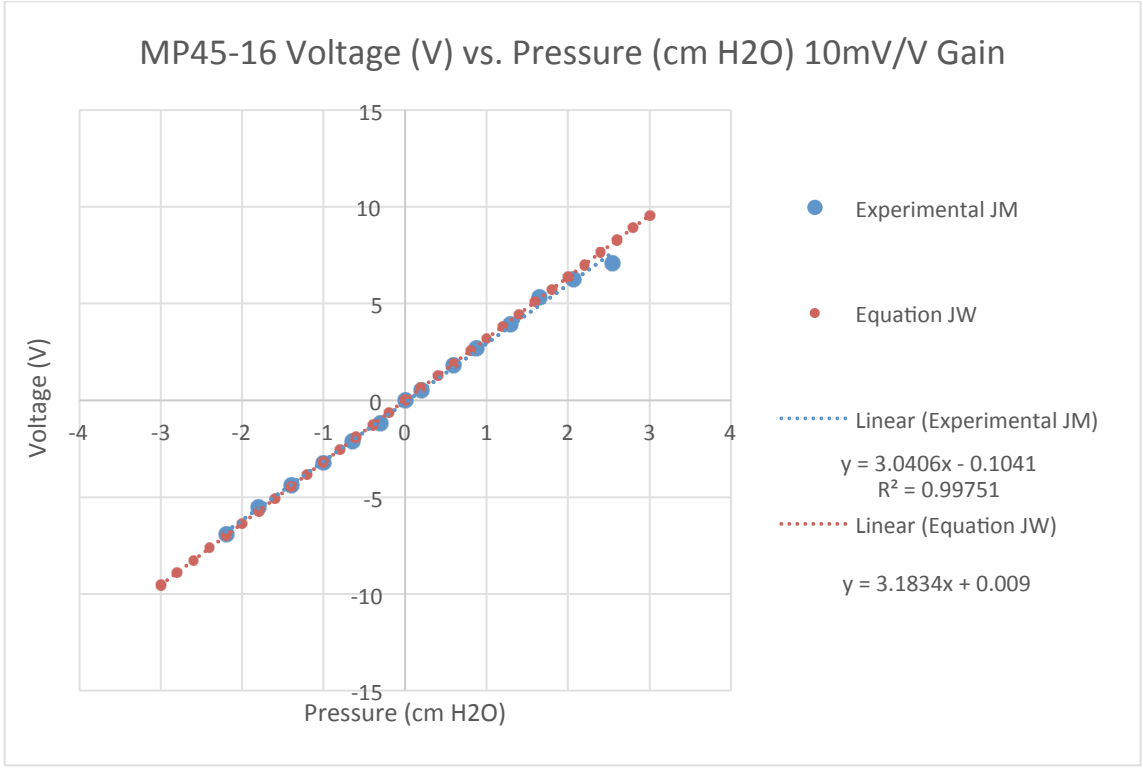
Figure A10 10 mV/V gain calibration for MP45-16.
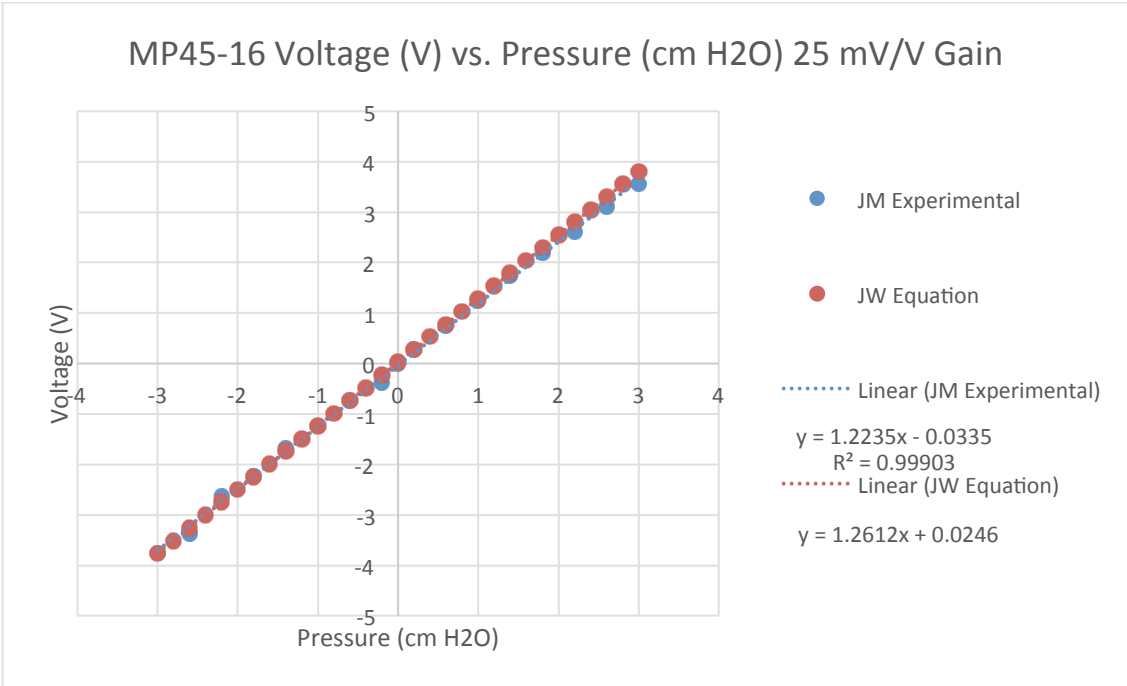
Figure A11 25 mV/V gain calibration for MP45-16.
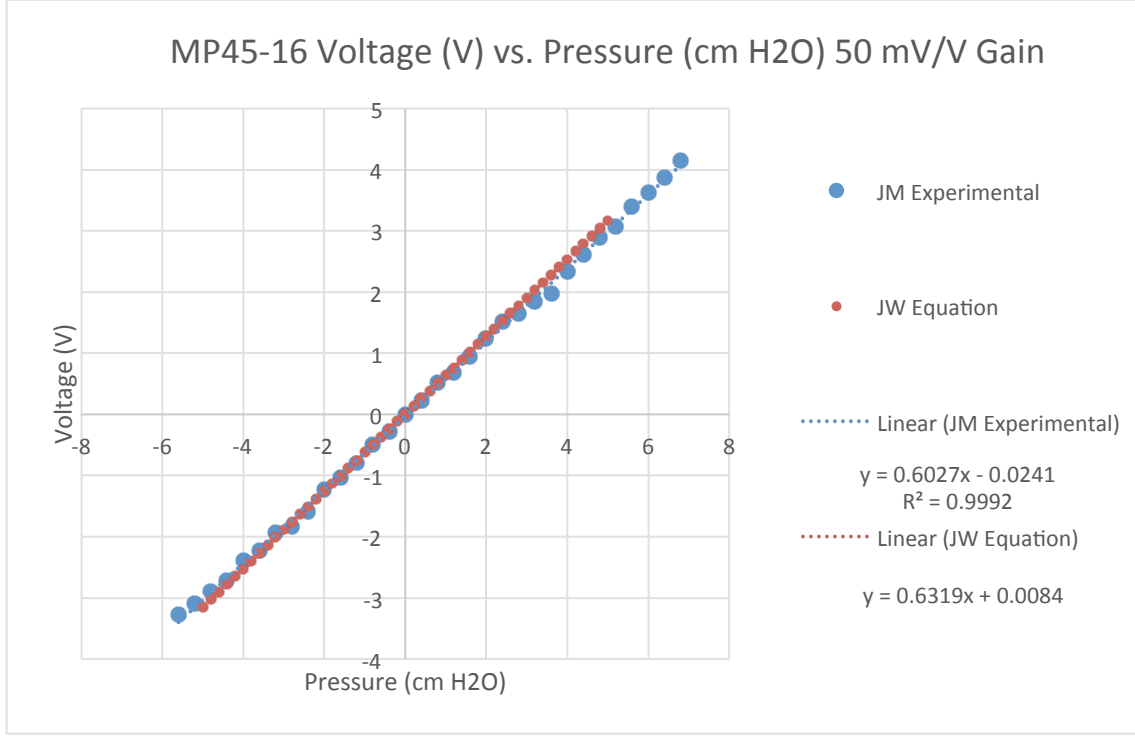
Figure A12 50 mV/V gain calibration for MP45-16.

APPENDIX B. CALIBRATION OF THE PNEUMOTACHS

This appendix shows calibrations of the Rudolph 370-2630 and Model 4813 pneumotachs using the Gilmont #5 and #6 flowmeters with steel floats. Each calibration is dated, however cleaning of the wind screens was not necessarily conducted before every single calibration.
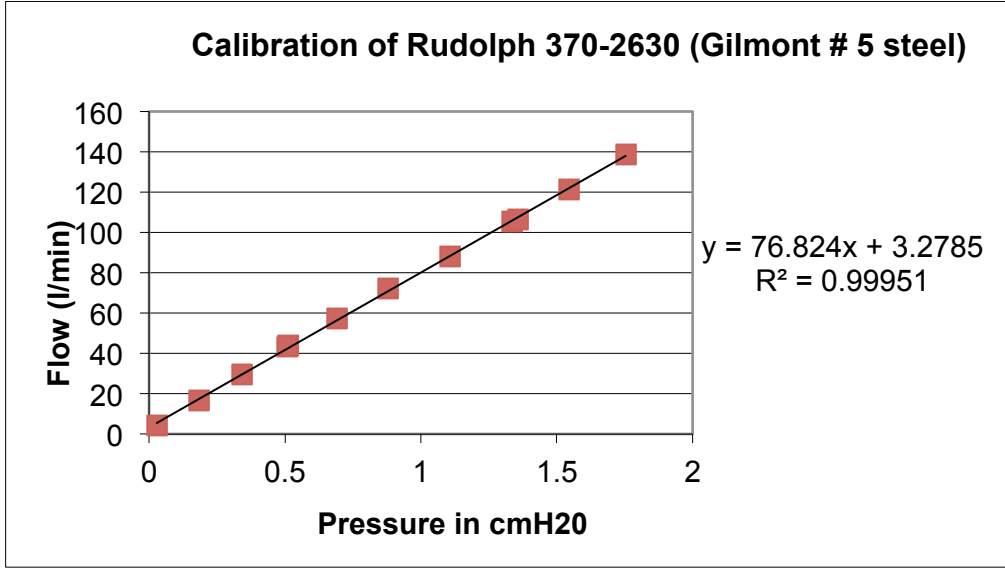
Figure B1 January 6th, 2016 calibration of Rudolph 370-2630 pneumotach.
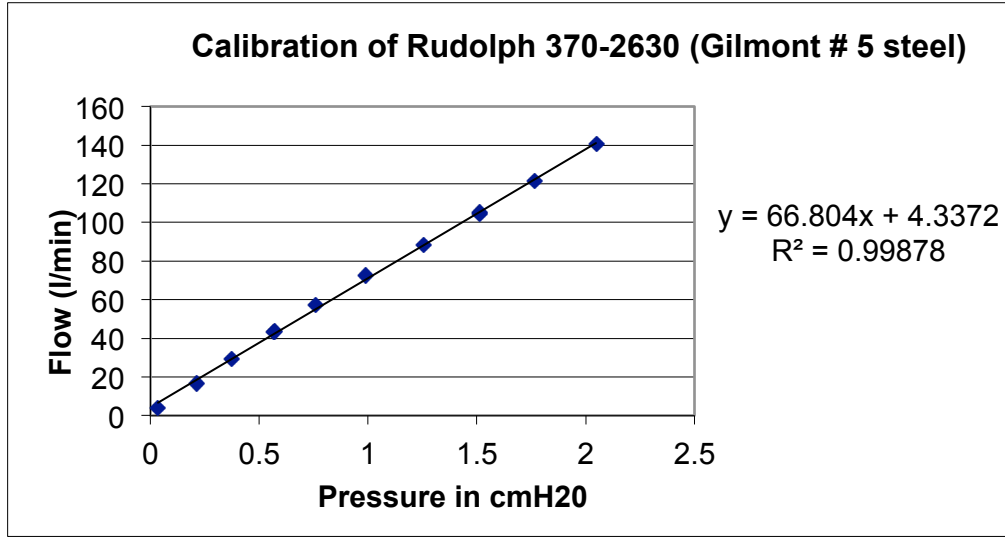
Figure B2 February 9th, 2016 calibration of Rudolph 370-2630 pneumotach.
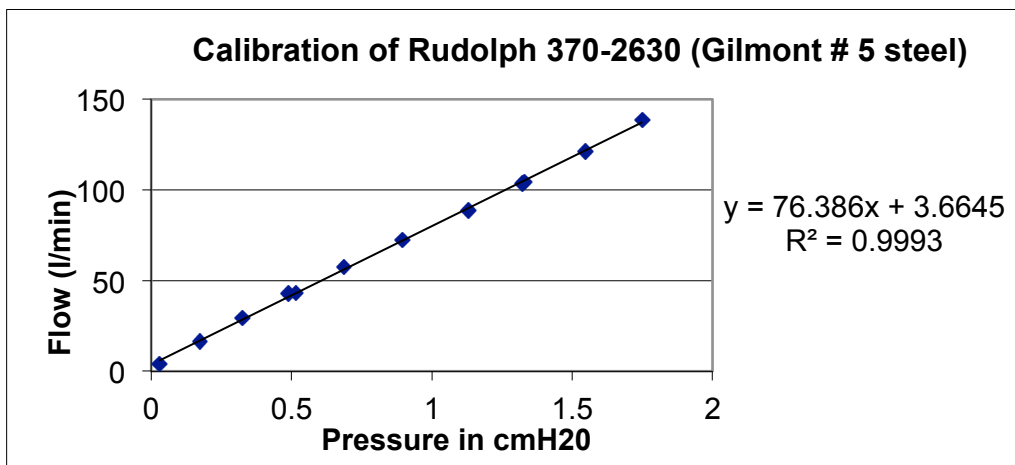
Figure B3 February 24th, 2016 calibration of Rudolph 370-2630 pneumotach.
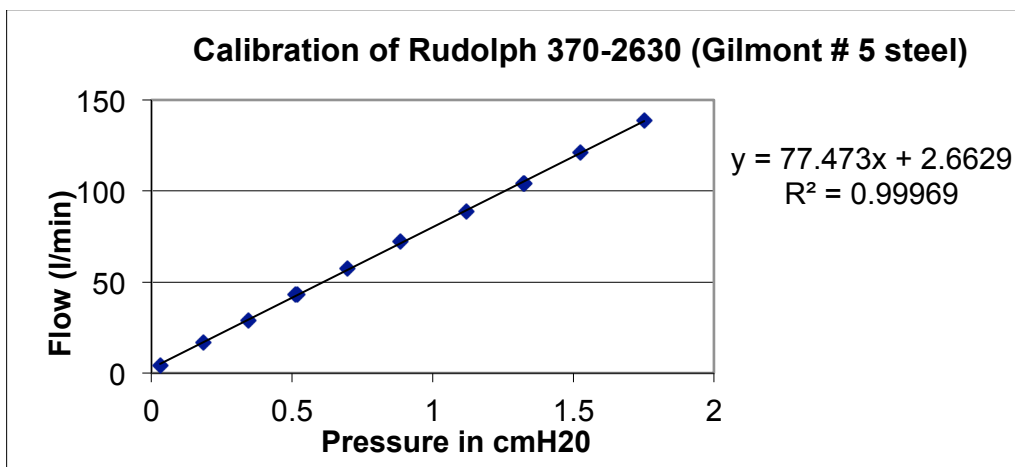
Figure B4 March 3rd, 2016 calibration of Rudolph 370-2630 pneumotach.
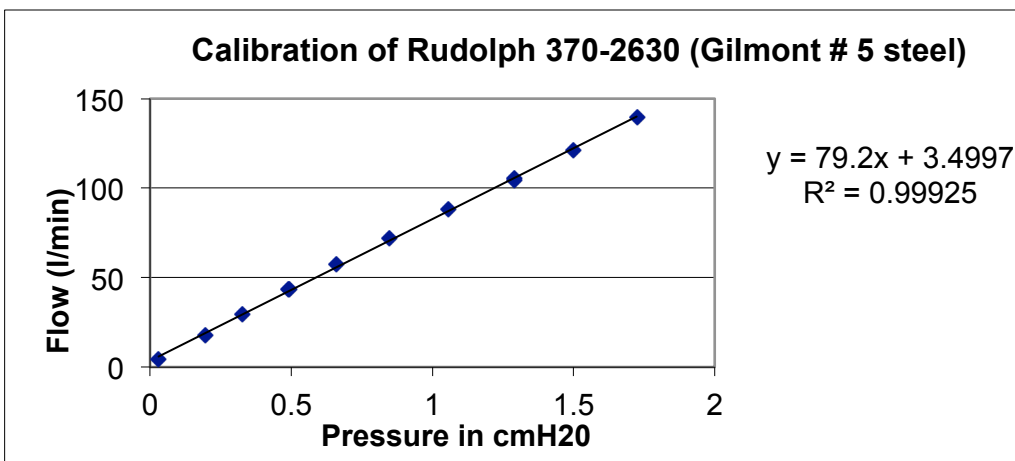
Figure B5 March 30th, 2016 calibration of Rudolph 370-2630 pneumotach.
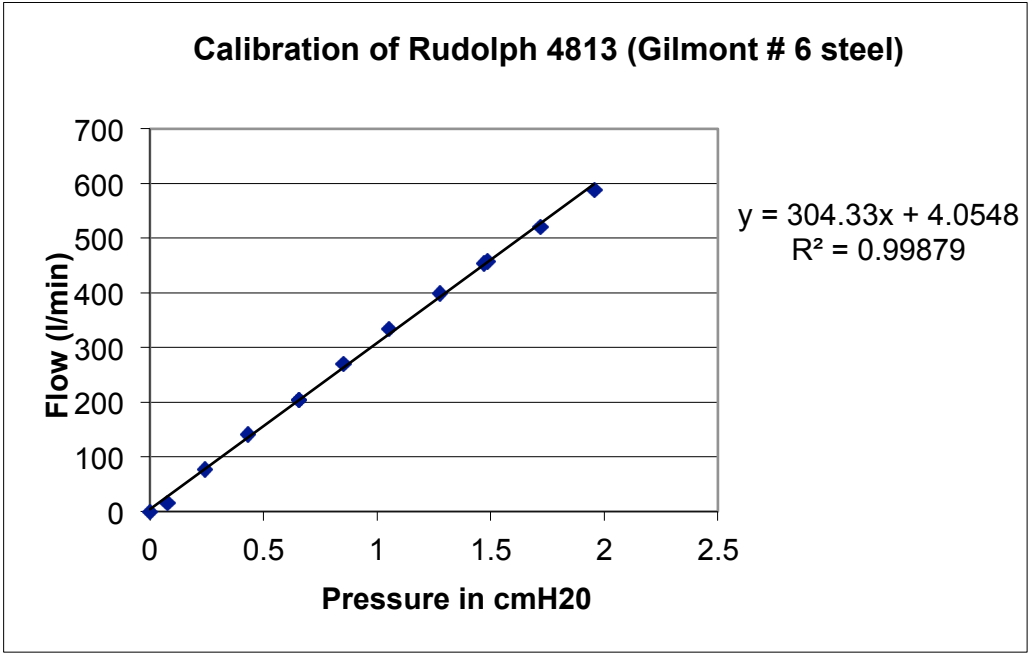
Figure B6 January 11th, 2016 calibration of Rudolph 4813 pneumotach.
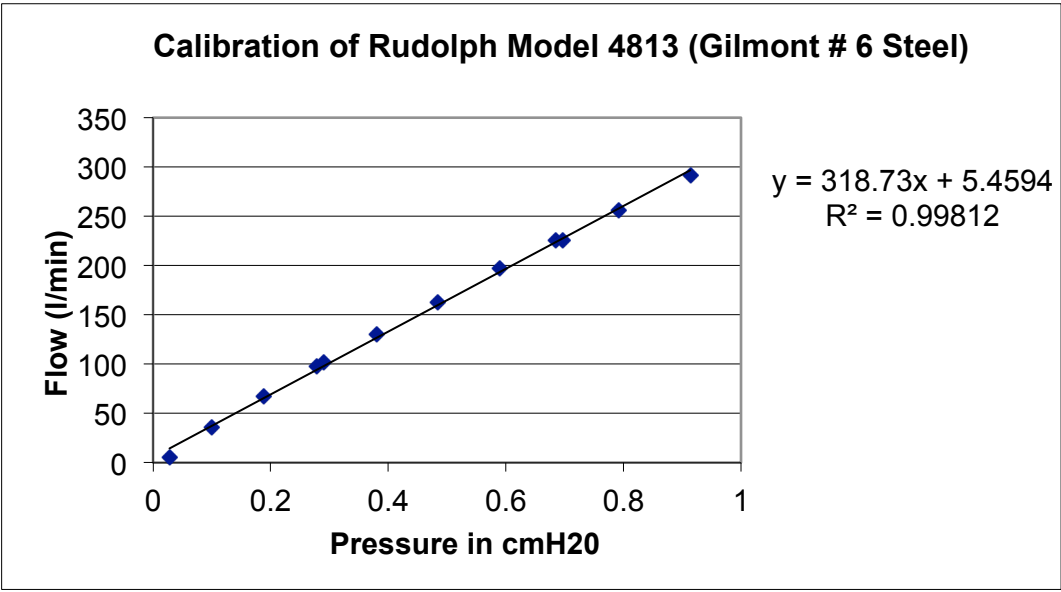
Figure B7 March 30th, 2016 calibration of Rudolph 4813 pneumotach.

APPENDIX C. CONVERGING -10 GLOTTIS DISTRIBUTIONS

In this Appendix, each of the pressure distribution families for the flow wall and non flow wall cases are shown individually for the converging -10 degree glottis. This serves the purpose of allowing the reader to view the pressures present on one wall to better show differences and similarities between each of the transglottal pressures.
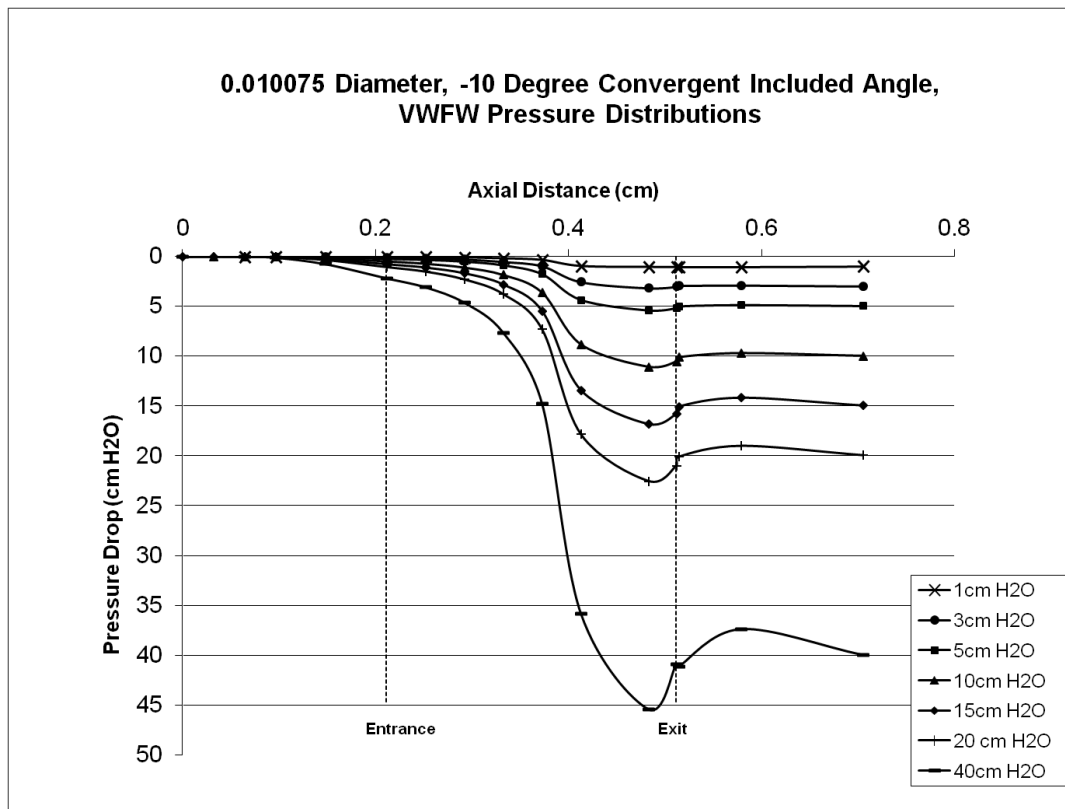
Figure C1 Pressure distributions for 0.01 cm converging glottis for 7 transglottal pressures when flow is directed along the vertical wall.
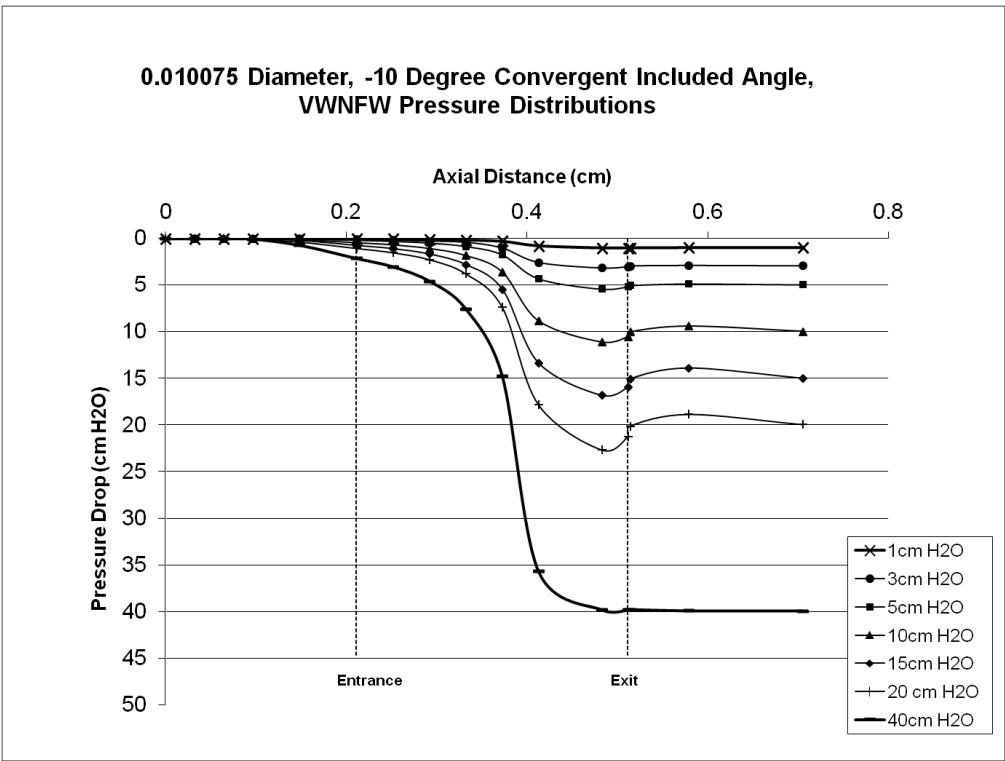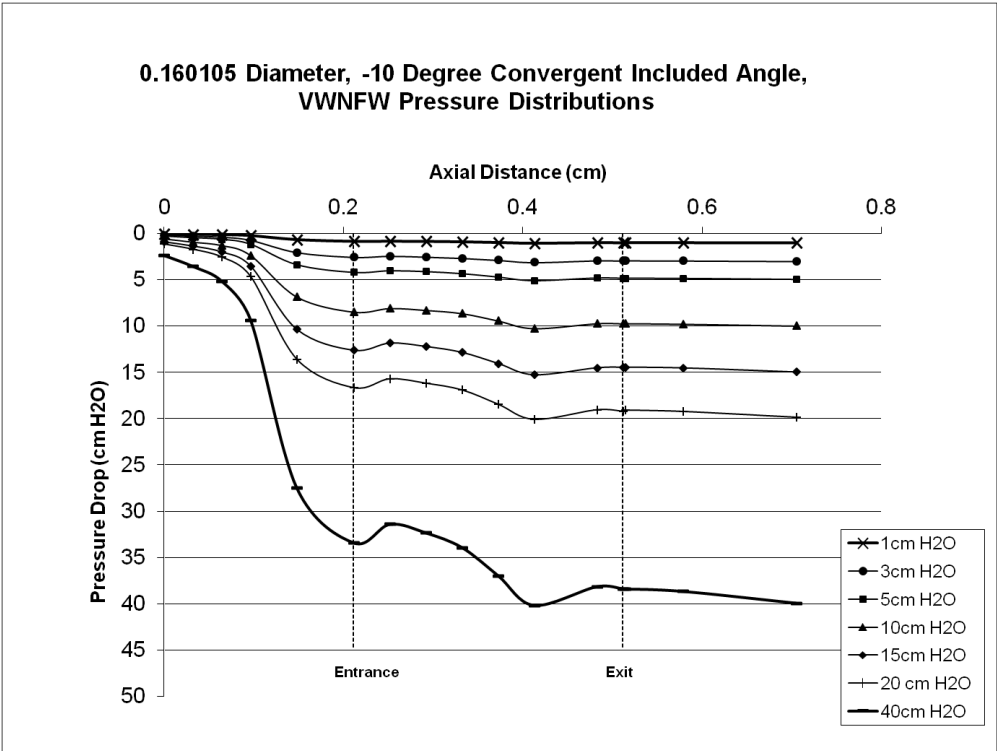
Figure C2 Pressure distributions for 0.01 cm converging glottis for 7 transglottal pressures when flow is directed away from the vertical wall.
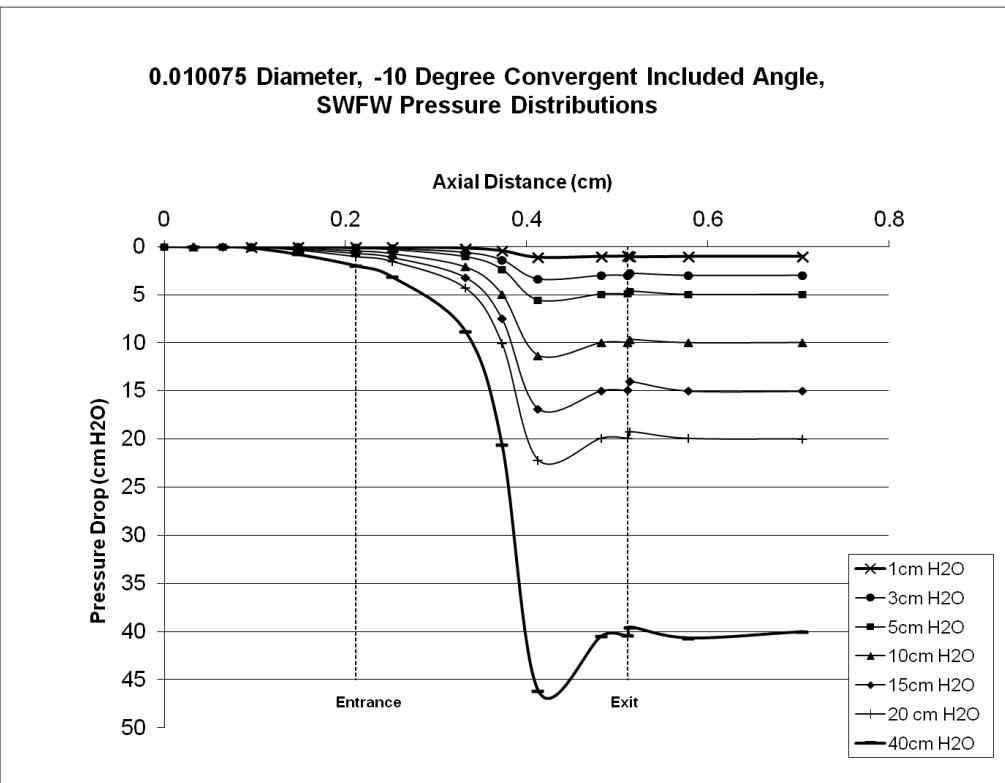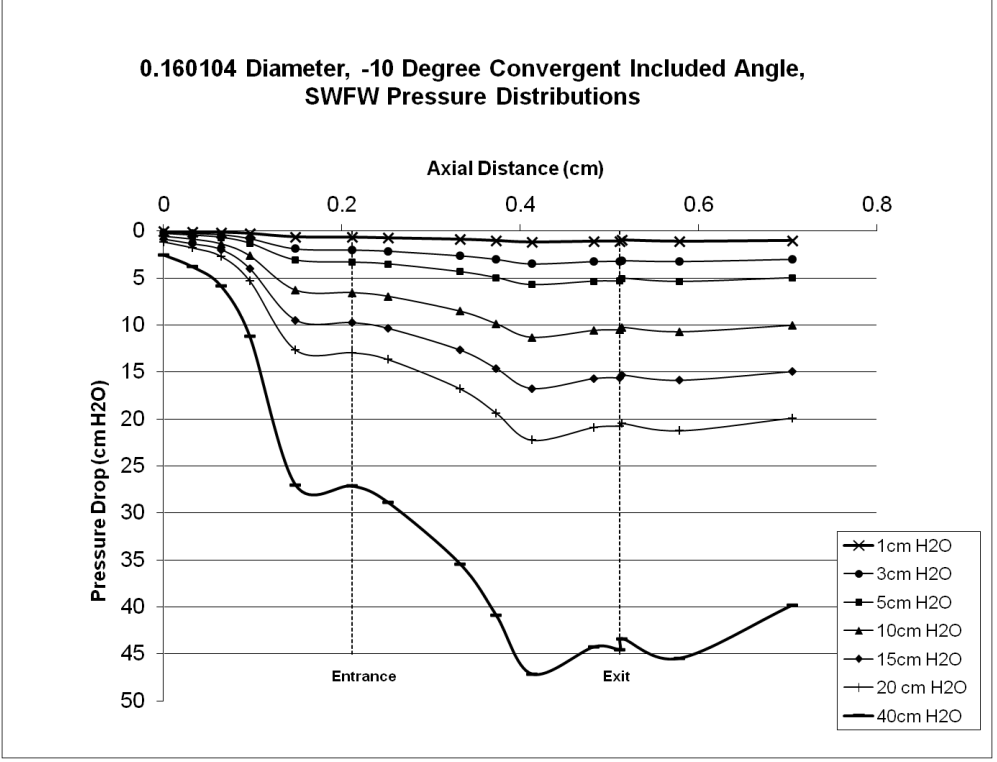

Figure C3 Pressure distributions for 0.01 cm converging glottis for 7 transglottal pressures when flow is directed along the slanted wall.
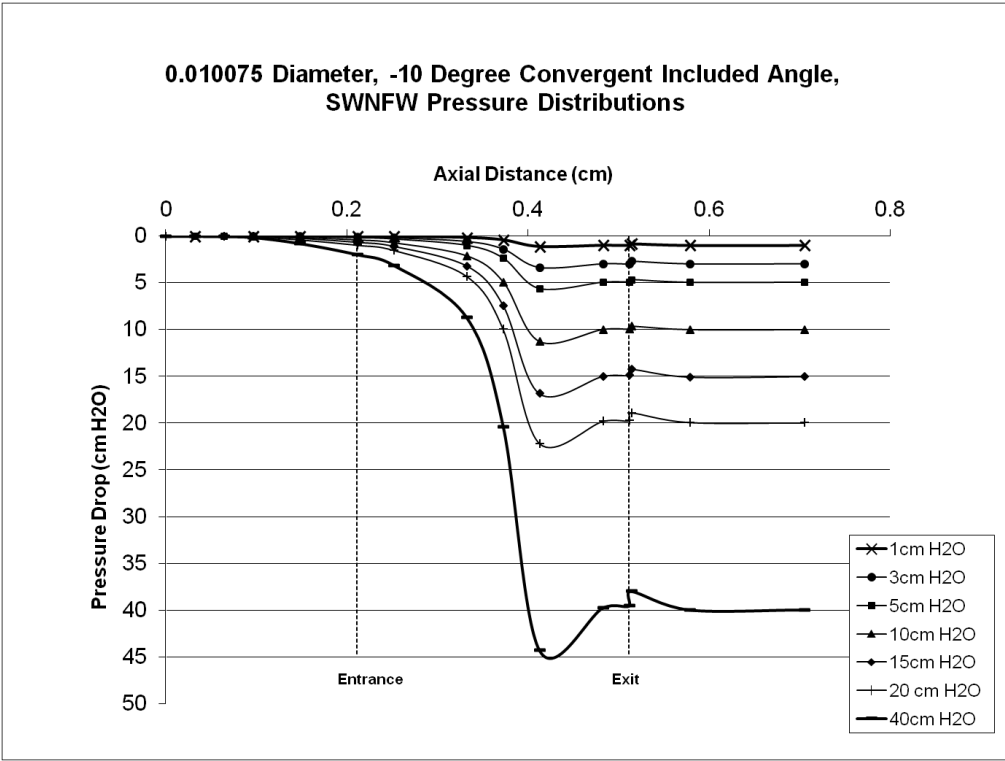
Figure C4 Pressure distributions for 0.01 cm converging glottis for 7 transglottal pressures when flow is directed away from the slanted wall.
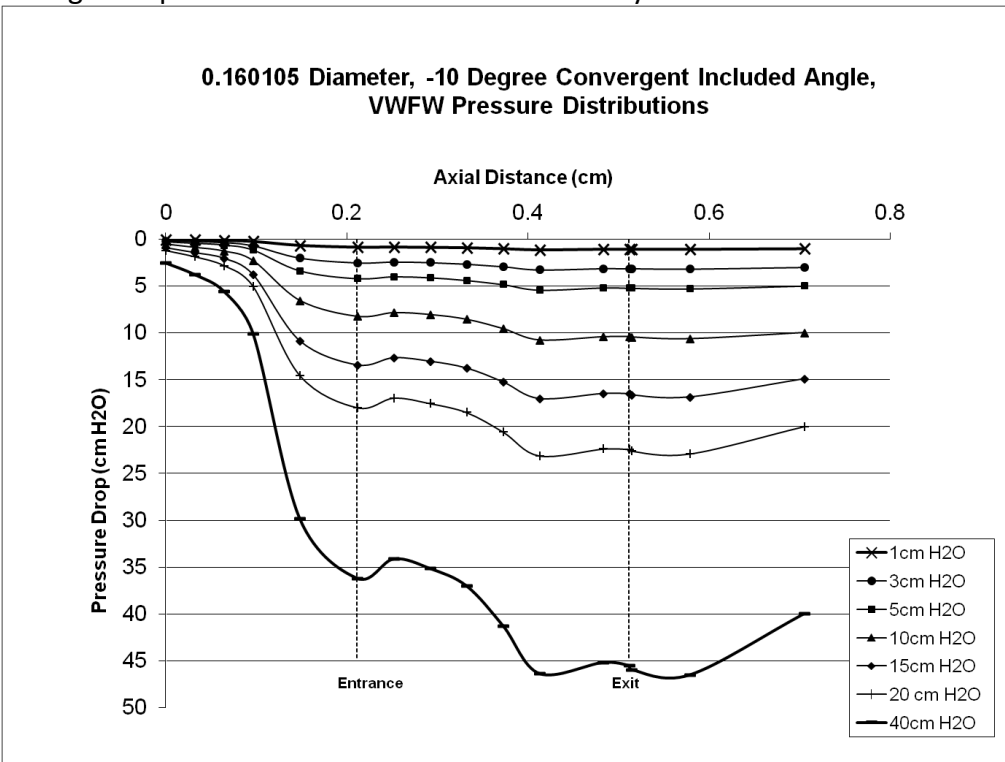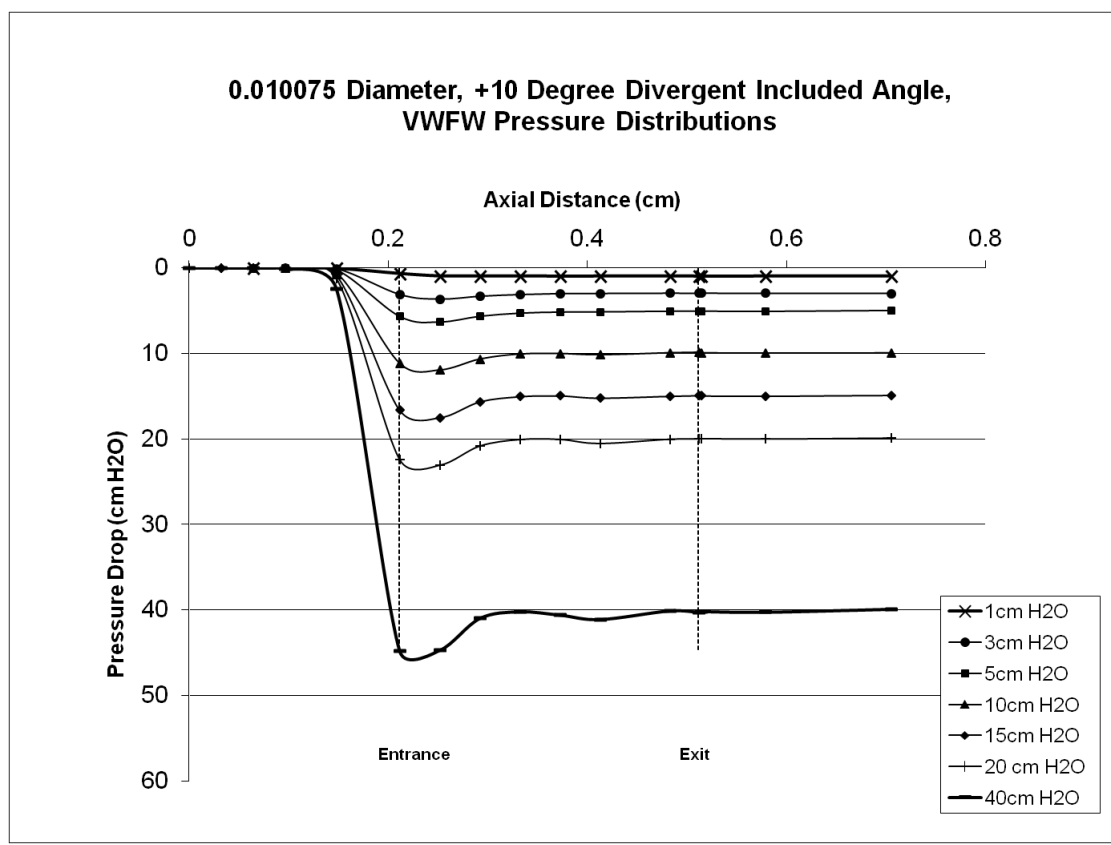

Figure C5 Pressure distributions for 0.16 cm converging glottis for 7 transglottal pressures when flow is directed along the vertical wall.
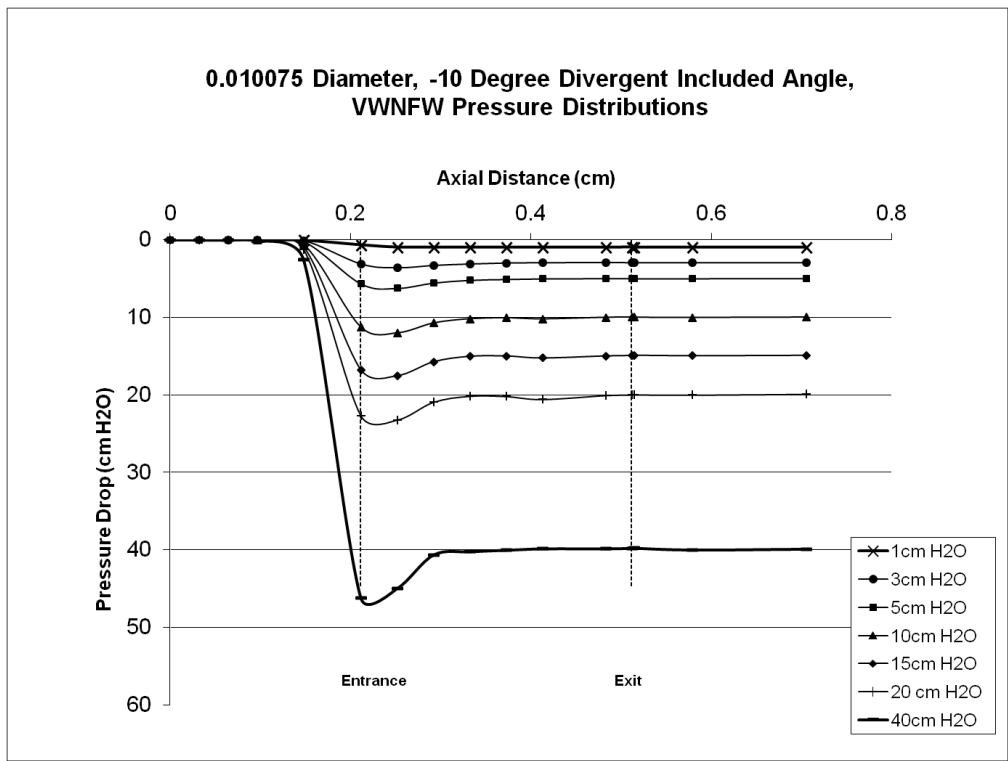
Figure C6 Pressure distributions for 0.16 cm converging glottis for 7 transglottal pressures when flow is directed away from the vertical wall.
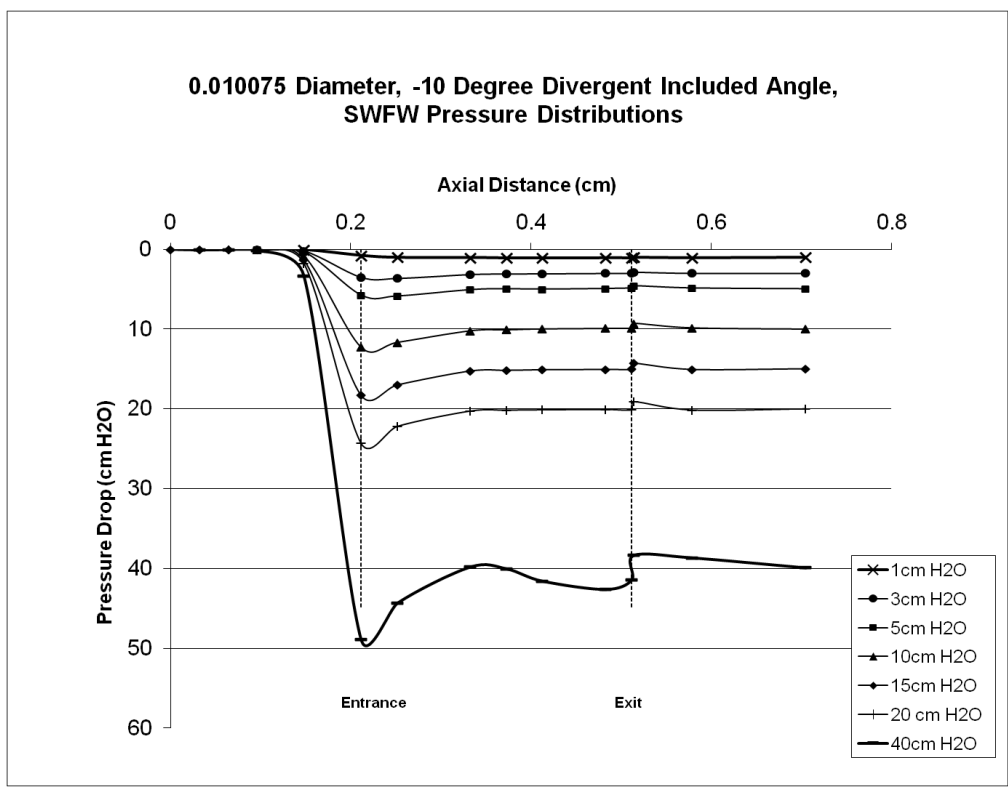

Figure C7 Pressure distributions for 0.16 cm converging glottis for 7 transglottal pressures when flow is directed along the slanted wall.

Figure C8 Pressure distributions for 0.16 cm converging glottis for 7 transglottal pressures when flow is directed away from the slanted wall.

APPENDIX D. DIVERGING +10 GLOTTIS CONFIGURATIONS

In this Appendix, each of the pressure distribution families for the flow wall and non flow wall cases are shown individually for the diverging +10 degree glottis. This serves the purpose of allowing the reader to view the pressures present on one wall to better show differences and similarities between each of the transglottal pressures.

Figure D1 Pressure distributions for 0.01 cm diverging glottis for 7 transglottal pressures when flow is directed along the vertical wall.

Figure D2 Pressure distributions for 0.01 cm diverging glottis for 7 transglottal pressures when flow is directed away from the vertical wall.

Figure D3 Pressure distributions for 0.01 cm diverging glottis for 7 transglottal pressures when flow is directed along the slanted wall.
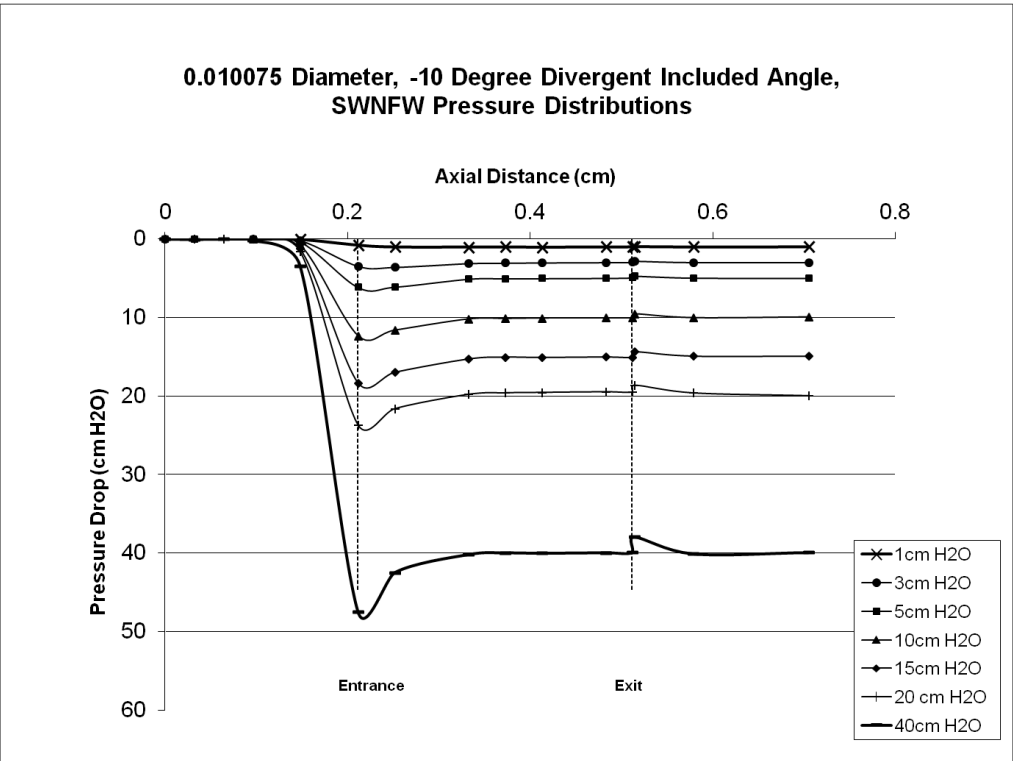
Figure D4 Pressure distributions for 0.01 cm diverging glottis for 7 transglottal pressures when flow is directed away from the slanted wall.
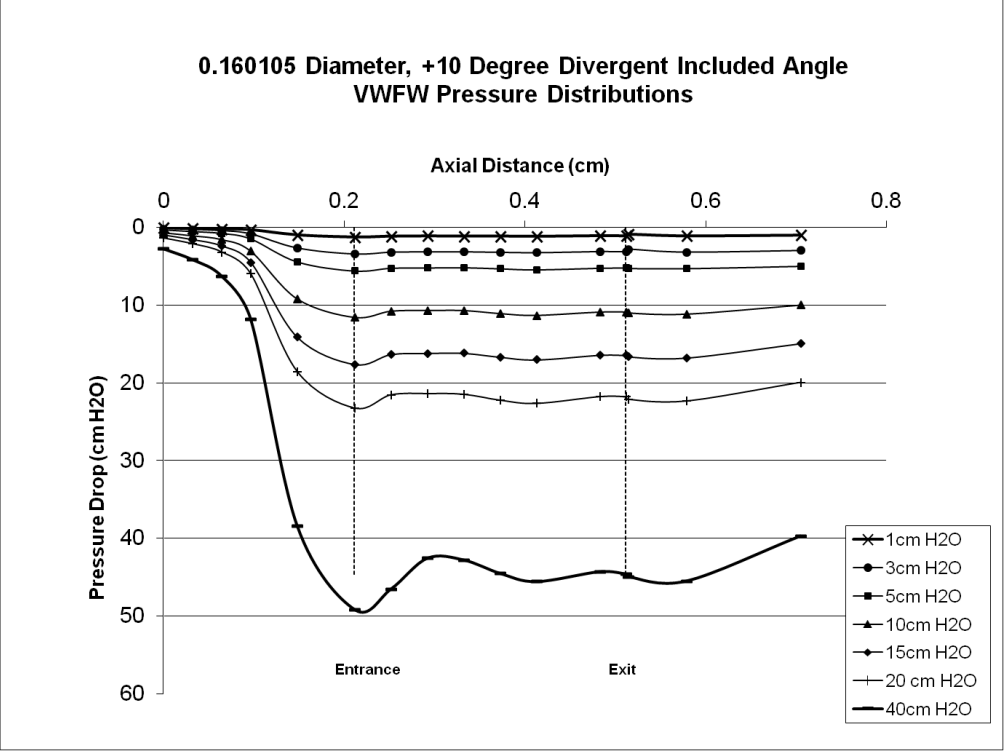

Figure D5 Pressure distributions for 0.16 cm diverging glottis for 7 transglottal pressures when flow is directed along the vertical wall.
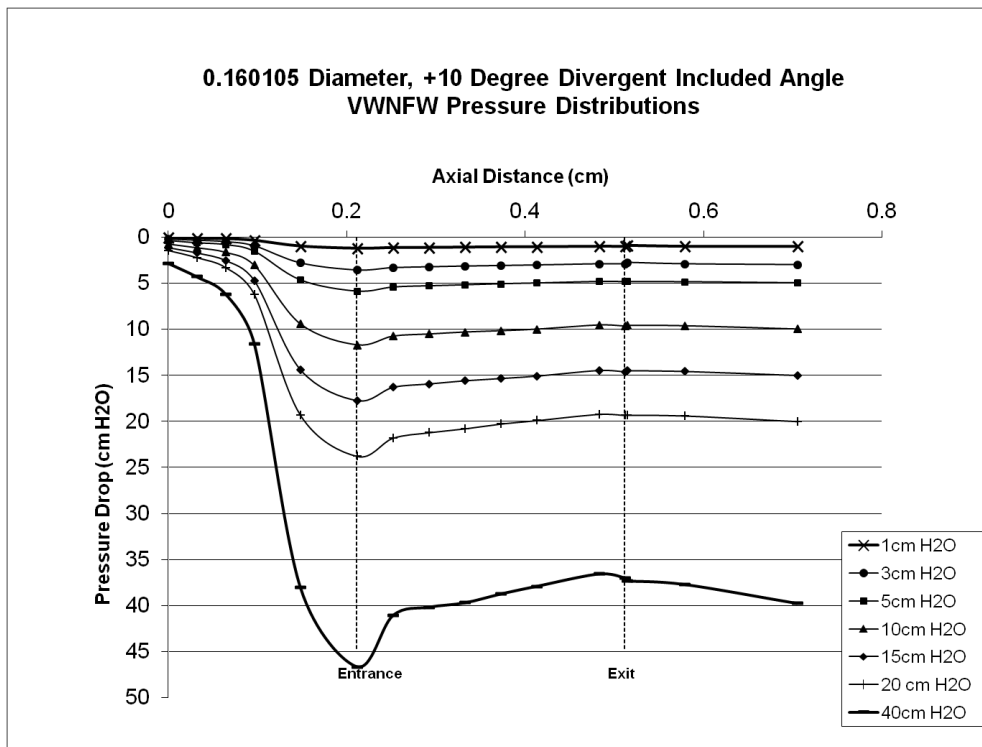
Figure D6 Pressure distributions for 0.16 cm converging glottis for 7 transglottal pressures when flow is directed away from the vertical wall.
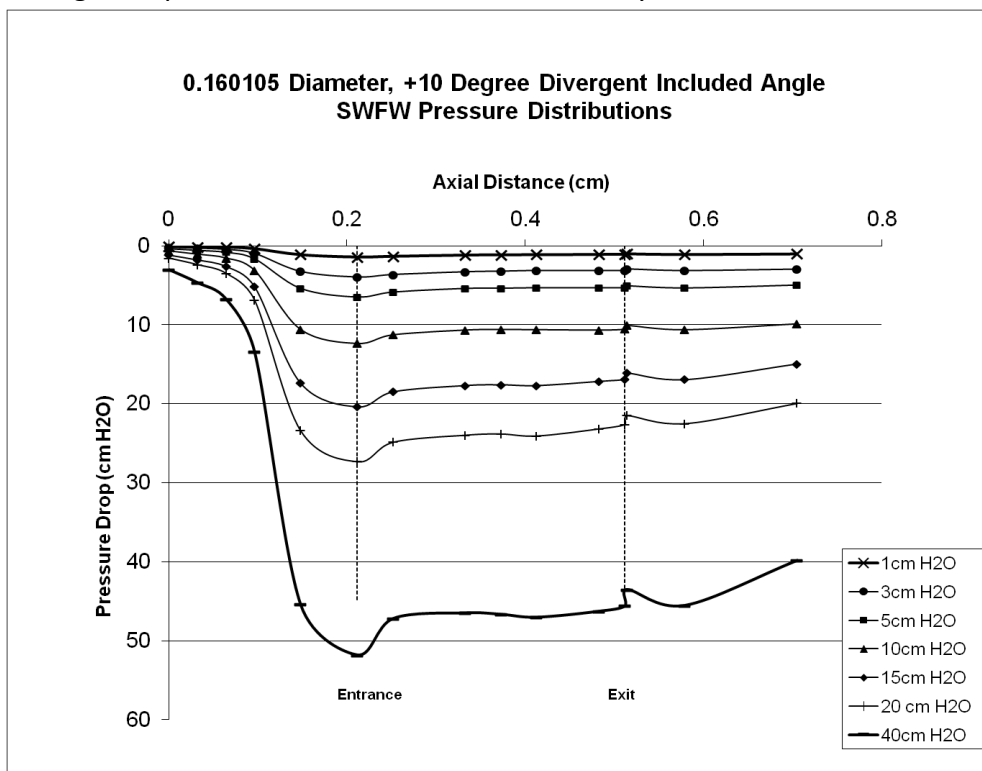

Figure D7 Pressure distributions for 0.16 cm diverging glottis for 7 transglottal pressures when flow is directed along the slanted wall.
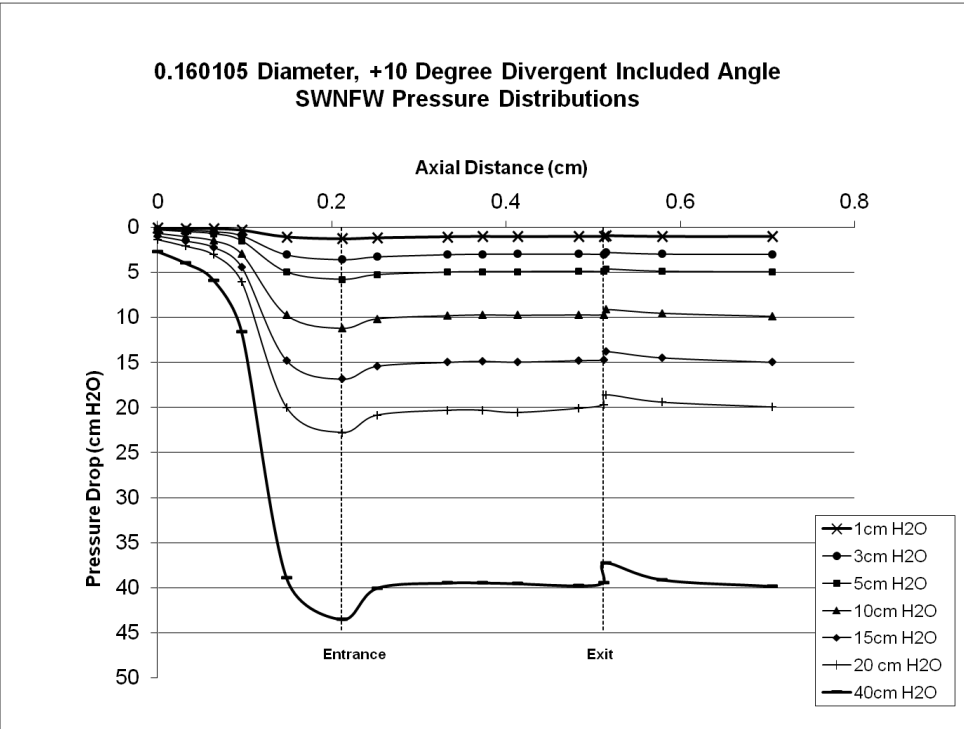
Figure D8 Pressure distributions for 0.16 cm diverging glottis for 7
transglottal pressures when flow is directed away from the slanted wall.